



Norwegian University of
Science and Technology

Structural Analysis of the Gripper Connection during Monopile Installation

Nishat Al Nahian

Marine Technology

Submission date: June 2016

Supervisor: Zhen Gao, IMT

Norwegian University of Science and Technology
Department of Marine Technology



**NORWEGIAN UNIVERSITY OF SCIENCE AND TECHNOLOGY
DEPARTMENT OF MARINE TECHNOLOGY**

MASTER OF SCIENCE THESIS IN MARINE TECHNOLOGY

ON

**STRUCTURAL ANALYSIS OF THE GRIPPER CONNECTION
DURING MONOPILE INSTALLATION**

NISHAT-AL-NAHIAN

10th, JUNE, 2016

SUPERVISOR: PROFESSOR ZHEN GAO

CO-SUPERVISORS: LIN LI AND WILSON GUACHAMIN ACERO

Thesis Outline

MSC THESIS IN MARINE TECHNOLOGY

SPRING 2016

FOR

STUD.TECHN. Nishat Al Nahian

Structural Analysis of the Gripper Connection during Monopile Installation

Background:

Transportation and installation of offshore wind turbine components are important aspects for reducing the life-cycle cost of offshore wind farms. Most of the offshore wind farms today are located in relatively shallow waters (10-30 m of water depths), with monopile as the mostly-used foundation.

Installation of monopile at the offshore sites are based on crane operations using a jack-up installation vessel or a floating installation vessel. The monopile is normally lifted off from the same installation vessel or a barge, lowered through the wave splash zone onto the sea bed, and then hammered into the soil. During the initial hammering process, the monopile is restricted by a gripper which is connected to the installation vessel in order to keep the verticality. The gripper device contains three-four hydraulic cylinders which are typically in compression. Monopile foundations are normally welded circumferentially piece by piece and the outer surface of the monopile at the welding path might not be smooth. This geometrical discontinuity may introduce large dynamic axial forces in the hydraulic cylinder of the gripper when the monopile was hammered down to the sea bed. This may cause damages in the gripper device. In addition, as compared to jack-up installation vessels, floating installation vessels can be deployed more efficiently. However, a floating installation vessel may have large wind- and wave-induced motions and this might induce large forces between the monopile and the gripper in particular during the initial hammering process.

The purpose of this study is to investigate the magnitude of the contact force between the hydraulic cylinder and the monopile and the stress level in the hydraulic cylinder during the initial hammering process using ABAQUS.

The student will be provided the design of the gripper device and the coupled global model of the floating installation vessel, the monopile and the gripper in Simo.

Assignment:

The following tasks should be addressed in the thesis work:

1. Literature review on general procedures and critical phases for monopile foundation installation, global response analysis of floating structures under wave loads, numerical modeling of soil-pile interaction and structural contact problem and numerical analysis.
2. With the given information about the soil conditions, establish the simplified soil model in Simo based on the API procedure, and with the given global model of the floating installation vessel and the monopile, perform dynamic response analysis of the complete system during the initial hammering process. Estimate the gripper loads under such conditions.
3. Investigate the design, the material properties and the mechanical properties of the hydraulic cylinder in the gripper device and the geometry of the circumference welds. Establish in ABAQUS a numerical model of one hydraulic cylinder and part of the monopile and define the contact between them. Properly define the boundary conditions for the model. Perform a mesh convergence study.
4. Perform first a static analysis with the applied axial force on the hydraulic cylinder. Perform a dynamic analysis considering a constant vertical speed of the monopile, identify the critical locations with high stresses, and investigate the characteristics of the stress time series.
5. Perform a sensitivity study on the following model parameters, the vertical speed of the monopile, the geometry of the welds, the axial stiffness induced by the hydraulic fluid and the material properties of the cylinder.
6. Report and conclude on the investigation.

In the thesis, the candidate shall present his personal contribution to the resolution of the problem within the scope of the thesis work.

Theories and conclusions should be based on mathematical derivations and/or logic reasoning identifying the various steps in the deduction.

The candidate should utilize the existing possibilities for obtaining relevant literature.

The thesis should be organized in a rational manner to give a clear exposition of results, assessments, and conclusions. The text should be brief and to the point, with a clear language. Telegraphic language should be avoided.

The thesis shall contain the following elements: A text defining the scope, preface, list of contents, summary, main body of thesis, conclusions with recommendations for further work, list of symbols and acronyms, reference and (optional) appendices. All figures, tables and equations shall be enumerated.

The supervisor may require that the candidate, in an early stage of the work, present a written plan for the completion of the work. The plan should include a budget for the use of computer and laboratory resources that will be charged to the department. Overruns shall be reported to the supervisor.

The original contribution of the candidate and material taken from other sources shall be clearly defined. Work from other sources shall be properly referenced using an acknowledged referencing system.

The thesis shall be submitted in two copies as well as an electronic copy on a CD:

- Signed by the candidate
- The text defining the scope included
- In bound volume(s)
- Drawings and/or computer prints which cannot be bound should be organized in a separate folder.

Zhen Gao

Lin Li

Wilson I. Guachamin Acero

Supervisors

Deadline: 10.6.2016

Preface

This report presents the work done by NISHAT-AL-NAHIAN for the Master Thesis, in order to obtain the MSc in Marine Technology degree with Marine Structure specialization from Norwegian University of Engineering and Technology. The work was carried out during spring 2016, in Trondheim. My supervisor was Prof. Zhen Gao and co-supervisors were PhD candidate Lin Li and Wilson Guachamin Acero.

The main scope of this thesis is to investigate the extent of the contact force between the hydraulic cylinder and the Monopile and the stress level in the hydraulic cylinder during the initial hammering period using ABAQUS. For the global analysis; design of the gripper device, HLV-MP coupled model, the monopile and the gripper model were provided in SIMO. From the SIMO model, global response force of the gripper is calculated and presented based on the previous work done by Lin Li. Later local analysis of the gripper system is done with ABAQUS then the results and findings are presented here.

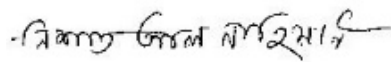
In the fall of 2015, I worked on the topic, soil-pile reaction during the initial hammering process for the Project at NTNU. Though my thesis topic is quite different from my previous project work but I enjoyed the challenges and learned a lot from my supervisors.

Acknowledgements

I would like to express my earnest gratitude to my advisor Professor Zhen Gao for the continuous support of my thesis work, for his patience, inspiration, and vast knowledge. He was exceptionally helpful and very kind to me and his guidance helped me all the time of study and writing of this thesis report.

Also, I would like to thank wholeheartedly Lin Li and Wilson Guachamin Acero for their kind support, instructions and guidance. Without their help, it would have been very difficult for me to complete the project within the stipulated time.

Finally, I would like to give special thanks to my family for their continuous support.



NISHAT-AL-NAHIAN

NTNU, Trondheim

6th June 2016

Abstract

Offshore wind energy market is increasing rapidly due to the very high demand for the green energy worldwide. At present, the most dominated structure for the offshore wind turbine is a monopile structure which is getting bigger in diameter and length day by day to support larger turbine. As a result, the new challenges like installation, maintenance and risks issues are arising during the installation of the monopile. In this thesis, MP initial hammering (shallow penetration) procedure with a heavy Lifting Vessel(HLV) and dynamic response of the coupled HLV-MP system has been presented. Modelling of the soil-pile system is also discussed elaborately. Later from the dynamic response of the gripper, local analysis of the gripper system is done by Abaqus. A simplified model of the gripper system is established and the effects of MP welding seam parameter, MP speed, roller size, boundary condition, spring stiffness on the critical component of the gripper system have been presented.

Table of Contents

THESIS OUTLINE	III
PREFACE	VI
ACKNOWLEDGEMENTS	VII
ABSTRACT	VIII
LIST OF FIGURES	XI
LIST OF TABLES	XIII
LIST OF SYMBOLS	XIV
ACRONYM	XV
1. INTRODUCTION	1
1.1 GENERAL	1
1.2 BACKGROUND AND MOTIVATION	3
1.3 OBJECTIVES	4
1.4 METHOD	5
2. OFFSHORE MONOPILE INSTALLATION	6
2.1 LIFTING AND LOWERING OPERATION	6
2.2 MONOPILE HAMMERING OPERATION	8
2.3 CRITICAL EVENTS AND POSSIBLE FAILURE MODES	10
2.4 FINDING ALLOWABLE SEA STATE	11
2.5 THEORY AND METHODOLOGY FOR NUMERICAL MODELLING AND ANALYSIS	12
2.5.1 <i>Overview of the Global model</i>	12
2.5.2 <i>Time domain simulation</i>	12
2.5.3 <i>Modelling of gripper device</i>	13
2.6 SOIL-MP INTERACTION	13
2.6.1 <i>Static p-y generation</i>	15
2.6.2 <i>Soil-MP Model for Global Analysis</i>	26
2.7 DYNAMIC RESPONSE OF HLW-MP SYSTEM AT DIFFERENT PENETRATION	30
3. GRIPPER- MONOPILE CONTACT PROBLEM	37
3.1 PROBLEM STATEMENT	37
3.1.1 <i>Basic Layout of the Gripper Monopile System</i>	40
3.1.2 <i>Simplified Model</i>	42
3.2 FUNDAMENTAL THEORY	43
3.3 NUMERICAL MODELLING	45
3.3.1 <i>Properties of the Cylinder and Arm</i>	45
3.4 ABAQUS MODELLING	46
3.4.1 <i>Modelling</i>	46
3.4.2 <i>Material Assignment</i>	48
3.4.3 <i>Assembly</i>	49

3.4.4 Interaction	51
3.4.5 Step.....	53
3.4.6 Boundary Condition.....	54
3.4.7 Meshing.....	56
4. ANALYSIS AND RESULT	58
4.1 STATIC ANALYSIS	58
4.1.1 Result.....	59
4.2 DYNAMIC ANALYSIS.....	61
5. CONCLUSION AND RECOMMENDATION	76
6. LIMITATION AND FUTURE WORK	78
7. LIST OF REFERENCES.....	79
8. APPENDICES	81
8.1 APPENDIX 01: GOVERNING DIFFERENTIAL EQUATION FOR Laterally Loaded PILE PROBLEM	81
8.2 APPENDIX 02: RESPONSE SPECTRA OF THE HLV-MP SYSTEM	85
8.3 APPENDIX 03: STIFFNESS CALCULATION OF THE SQUARE ARM.....	92
8.4 APPENDIX 04: DYNAMIC, EXPLICIT ANALYSIS (STABLE TIME INCREMENT CALCULATION)	94
8.5 APPENDIX 05: COUPLING.....	97
8.6 APPENDIX 06: SHOWCASE OF THE ABAQUS ANALYSIS	99

List of Figures

Figure 1: Component of a MP foundation (EWEA,2009).....	2
Figure 2: MP installation with gripper and Hammer on top.....	2
Figure 3: Flowchart (the method of this thesis)	5
Figure 4: Monopile Lifting And Lowering Arrangement, (L.Li, 2014).....	7
Figure 5: Set up for MP Hammering procedure (L.Li 2015).....	8
Figure 6: Axial Pile Load Transfer-Displacement (T-z) curves(API)	19
Figure 7: MP Tip-Load Displacement(Q-z) Curve(API)	21
Figure 8 Variation of coefficient C1,C2 and C3 with ϕ' (API)	25
Figure 9: Soil-MO interaction model [Lin Li, 2015].....	27
Figure 10: Figure shows P-y,T-z and Q-z curve	29
Figure 11: Global model for HLV-MP-Soil responses.....	31
Figure 12: Response spectra of the hydraulic cylinder force for two different wave peak period conditions at different MP penetration depth (pene)	33
Figure 13: Response spectra of the hydraulic cylinder force for different significant Wave height at different MP penetration depth (pene)	36
Figure 14: Typical Gripper device configuration.....	37
Figure 15: Top view of Gripper (roller) monopile system and side view of monopile with welding seam.....	38
Figure 16: Monopile wall and roller contact and when roller hit the welding seam.....	39
Figure 17: Basic layout of the gripper system during initial hammering.	40
Figure 18: Details of Section A and C.....	41
Figure 19: Welding details, section B	41
Figure 20: A Simplified model for Abaqus.	42
Figure 21: Cylinder model	47
Figure 22: Piston model.....	47
Figure 23: MP wall Model.....	48
Figure 24: Plastic properties of steel from the elastic limit.....	49
Figure 25: Assembly.....	50
Figure 26: Details of the MP-Roller assembly.....	50
Figure 27: Example of the structural coupling on piston back surface.....	52
Figure 28: Spring, represents the arm	53
Figure 29: BC, Cylinder_mid indicated by red colour and Symmetric BC of Piston and Cylinder	55
Figure 30: Boundary condition of MP and Piston.....	55
Figure 31: Local and global Mesh at cylinder and Piston.	57
Figure 32: Mesh at MP	57
Figure 33: Pressure applied on the piston face.	59
Figure 34: Static analysis	60
Figure 35: Displacement (mm)	60

Figure 36: Reference elements for result extraction, Seal(cylinder), piston and roller.....	62
Figure 37: Displacement of MP(m) vs Mises(Pa) stress at seal, piston and roller	64
Figure 38: MP movement and roller position (units in mm)	65
Figure 39: Max stress(Pa) at Piston for elastic vs elastic plastic material, MP speed 0.4 m/s	66
Figure 40: comparison of Mises stress for different welding capping at MP speed 0.8 m/s..	67
Figure 41: Comparison of stress at seal with different roller size	68
Figure 42: Sliding off the forward spring due to boundary condition	69
Figure 43: Displacement vs Stress, at Seal, Cylinder and Roller for Fixed BC at K1	71
Figure 44: Calculation of forces on both of the spring	72
Figure 45: Displacement vs stress for 20 and 10 mm capping with fixed BC of K1	73
Figure 46: Change of roller stress with the change of spring stiffness K2	74
Figure 47: Change of stress at seal due to the change of Stiffness of the spring K1	76
Figure 48: Laterally Loaded Soil-Pile system.....	82
Figure 49 : Response spectra of HLV,MP,Gripper and cylinder force at Hs=1.5m, Dir=150, Tp=5s	88
Figure 50: Response spectra of HLV,MP,Gripper and cylinder force at Hs=1.5m, Dir=150, Tp=10s	91
Figure 51: Kinematic coupling constraint.[19].....	97
Figure 52: Distributing coupling constraint.[19].....	97
Figure 53: Contact surface.....	100
Figure 54: Interaction	101
Figure 55: Stress at seal and Piston(roller size:70mm,roller BC at K1, capping 20 mm, speed 0.4 m/s)	102
Figure 56: Stress at seal and Piston(roller size:70mm,fixed BC at K1, capping 10 mm, speed 0.4 m/s)	103
Figure 57: Stress at seal and Piston(roller size:70mm,roller BC at K1, capping 10 mm, speed 0.4 m/s, one tenth stiffness of K2)	104
Figure 58: Stress at roller (roller size:70mm,Fixed BC at K1, capping 10 mm, speed 0.4 m/s)	107

List of Tables

Table 1: Main particulars of the MP hammering system [2]	9
Table 2: Soil properties [9]	28
Table 3: Standard deviation of the contact forces on one hydraulic cylinder at different penetration and wave conditions from 3-hour time-domain simulation	32
Table 4: Properties of the gripper system	45
Table 5: Interaction formulation	51
Table 6: Boundary conditions and load description	54
Table 7: Element size Vs Max Stress	58
Table 8: Max stress changes at roller with the change of spring stiffness K2	74
Table 9: Change of seal stress with the change of spring stiffness K2	75
Table 10: Change of piston stress with the change of spring stiffness K2	75
Table 11: Elastic Beam Relationship	82
Table 12: table for calculation minimum stable time incrementation.	95

List of Symbols

Symbol	Explanation
M	mass matrix
x	rigid body motion vector of the body with 6 DOFs
A	frequency depended on added mass matrix
D_1	linear damping matrix
D_2	hydrostatic restoring matrix
K	hydrostatic restoring matrix
h	retardation function
F_{ext}	external force vector
$q_{WA}^{(1)}$	first order excitation force
$q_{WA}^{(2)}$	second order excitation force
F_{moor}	mooring line forces of HLV
F_{cpl}	the coupling forces between the HLV and MP
F_{soil}	soil reaction force
P	lateral soil resistance
p_u	ultimate lateral soil resistance
S_u	undrained shear strength of soil.
ϕ'	effective internal friction angle
p_o'	effective overburden pressure in stress units
δW	(R, S, C, I) are the virtual work done by internal stresses, external (b and q) and inertial forces
Ω	Volume of element
$'b$	Body force at time
q_i	Contact forces (also a type of surface forces)
\bar{q}	Surface forces (i.e. pressure, other distributed loads)
a	Acceleration of body
$\delta u^2, \delta u^1$	Infinitesimal displacements of bodies 2 and 1 respectively
N_i^2	Normal vector for the contact forces
H_s	Significant wave height
Dir	Direction
T_p	Peak period

Acronym

<i>MP</i>	<i>Monopile</i>
<i>HLV</i>	<i>Heavy Lift Floating Vessel</i>
<i>DOF</i>	<i>Degree of freedom</i>
<i>API</i>	<i>American Petroleum Institute</i>
<i>STD</i>	<i>Standard deviation</i>
<i>NTNU</i>	<i>Norwegian University of Engineering and Technology</i>
<i>SIMA</i>	<i>Simulation and Engineering Analysis</i>
<i>FEA</i>	<i>Finite Element Analysis</i>
<i>EWEA</i>	<i>European Wind Energy Association</i>
<i>AWS</i>	<i>American Welding Society</i>
<i>IACS</i>	<i>International Association of Classification Societies</i>

1. Introduction

1.1 General

The Europe has initiated the sustainable development policy to meet the Increasing energy demand and for the sake of green future. Moreover, Sustainable energy development and sustainable development are the main focus for the global development all around the world. The sustainable energy development promotes a gradual transition from conventional energy sources (coal, oil, gas etc.) towards renewable energy sources like wind power, hydropower, and solar power. Wind energy is one of the sources which is intensively developed in the last few decades. Recently the wind turbine industry is moving towards offshore from onshore due to stronger winds, bigger wind turbine size and more available area. For that reason, new challenges like higher investment cost, maintenance issue are arising which are not optimally solved.

The principal components of a Wind turbine include turbines, towers, foundations, electric collection and transmission systems, and other balance of plant items. Four basic types of foundations have been used in offshore wind farms: monopiles, jackets, tripods and gravity foundation. Foundations are prefabricated onshore in one piece, carried offshore by barge or towed, launched at sea, and set on the bottom by a crane or derrick barge.

Monopiles(MP) are the most commonly used foundations in the water depth up to 40m and in this study we have only focused on the MP foundations. Monopiles are large diameter, thick walled, steel tubular that are driven (hammered) or drilled (or both) into the seabed (Figure 1). Outer diameters usually range from 4 to 6 m and 40 to 50% of the length is inserted into the seabed. Design codes and standards specify the thickness and the depth the piling is driven depends on the design load, soil conditions, water depth, and environmental conditions. Pile driving is more efficient and less expensive than drilling.

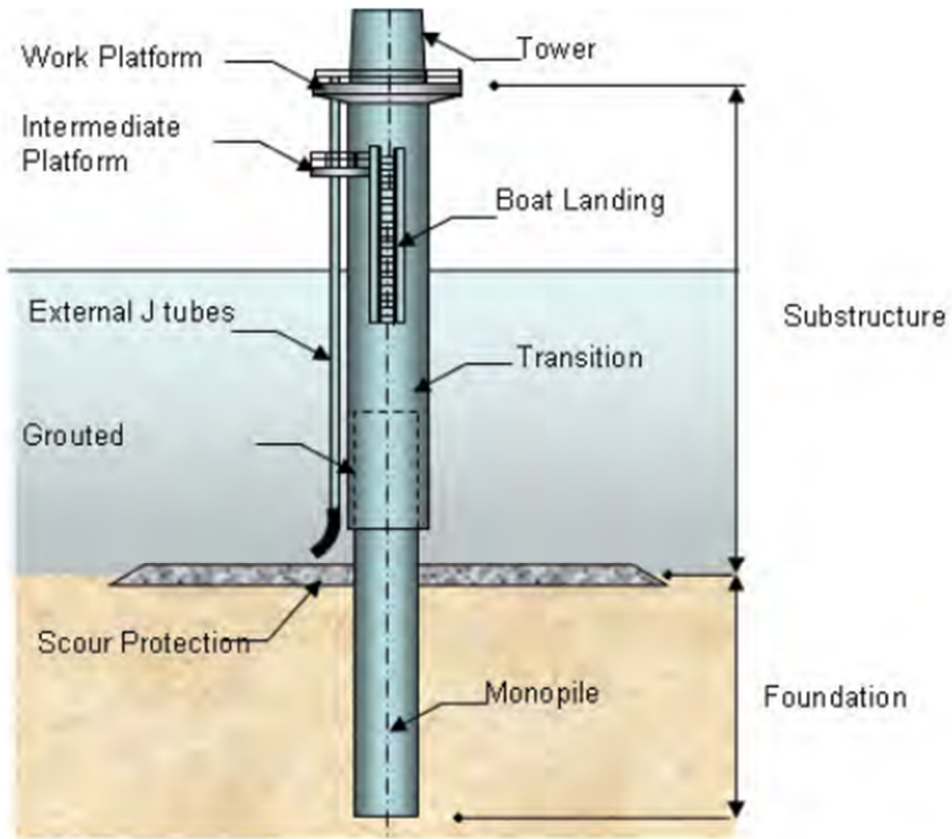


Figure 1: Component of a MP foundation (EWEA,2009)



Figure 2: MP installation with gripper and Hammer on top.

1.2 Background and Motivation

A jack-up installation vessel or a floating installation vessel, equipped with a crane is typically used to install MP at the offshore sites. The monopile is normally lifted off from the same installation vessel or a barge, lowered through the wave splash zone onto the seabed, and then hammered into the soil. During installation of monopiles, an often critical activity is the initial hammering phase where the MP and gripper are connected.

The gripper device contains three-four hydraulic cylinders which are typically in compression. Monopile foundations are normally welded circumferentially piece by piece and the outer surface of the monopile at the welding path might not be smooth. This geometrical discontinuity may introduce large dynamic axial forces in the hydraulic cylinder of the gripper when the monopile was hammered down to the sea bed. As a result, hydraulic systems used to connect both structures can suffer leakage or structural failure. Thus, it is important to investigate the parameters that limit this operation by following a systematic approach.

Few publications are published regarding MP installation. Previous studies were focused on proposing new installation methods, developing more accurate numerical models and assessments of allowable sea states. Lin li showed the MP lowering procedure with shielding effect to reduce the responses [2]. She also described the criteria to find the allowable sea states during the MP installation [1]. But no work was found that deals with the local analysis of the MP-grippers system though this is very important limiting criteria for offshore installation. So, in this thesis MP installation procedures have been discussed and responses from the global analysis have been presented based on the previous works. Later, gripper system has been modelled and analysis has been done by Abaqus (FEA).

1.3 Objectives

The purposes of this thesis are to study the MP installation procedure and local analysis of the gripper hydraulic system. So the main objectives of this thesis are described below:

1. Studying the MP initial Hammering process
 - Describing Hammering procedure
 - Identifying the limiting parameter
 - Soil-Pile interaction modelling
 - Overview of the global model
2. Performing the global analysis
3. Numerical modelling of the MP-gripper system
4. Finite Element Analysis(FEA) of the MP-gripper connection
5. Sensitivity study of the Key modelling parameters
6. Identifying potential failure modes of the MP gripper system

1.4 Method

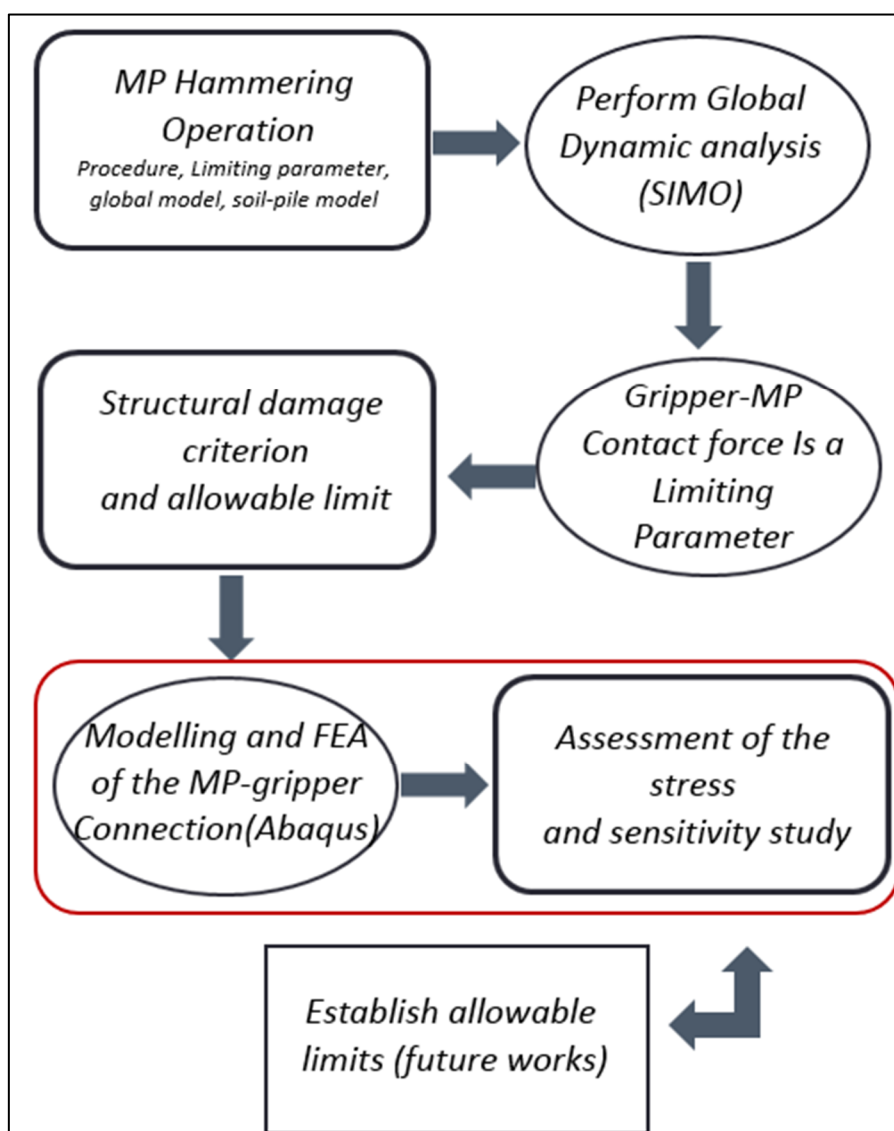


Figure 3: Flowchart (the method of this thesis)

MP hammering operation including procedure, limiting parameters and global model are discussed briefly and soil-pile interaction model is discussed elaborately based on the previous literature. The global analysis is done based on the paper published by Lin Li [2]. From the global analysis, response spectra of the gripper are presented and the contact force is identified as a limiting parameter. Then structural damage criteria for the gripper unit are discussed and a numerical model of the hydraulic gripper system is established. Later an Abaqus model is created where modelling steps are presented. Finally, results are presented and discussed from the Abaqus analysis.

2. Offshore Monopile Installation

The installation of monopile is generally comprised of the following steps:

1. Positioning the monopile vertically by using crane from a horizontal position.
2. Lowering the monopile down through the wave zone to the seabed. The monopile should be precisely landed at the designed point on the seabed.
3. Driving the monopile into the seabed with a hydraulic hammer.

When the MP arrive at the site then the MP is upended from a transportation vessel and lower through the water until it stands vertically on the seabed. Normally HLV or jack up rig is used to carry out the installation process though the characteristic response and motions are quite different. For HLV installation, soil, MP and HLV are coupled together, where wave excitation force, gripper force and soil pile reaction forces work together and additional force added with those terms due to the motion of the HLV itself. But when we use Jack up OWT, then the motion of the jack up due to the wave excitation is negligible. Thus, the motion of the HLV affects the response of the installation system so it is more convenient to work in harsh weather with jack up than HLV. However, jack up OWT has some limitation like it's application is limited to a maximum water depth around 45 m and the lowering of the jack up OWT is time-consuming and requires low sea states. Hence, for offshore MP installation, it is more expedient to use HLV than jack up OWT due to the flexibility of the operation but the challenges are higher for load transfer operation. [1,2]

2.1 Lifting and Lowering Operation

The following picture figure 4, is an ideal setup for the first two steps of MP installation. The system includes two rigid bodies, the floating installation vessel and the monopile. A hook is generally used to connect the lift wire and the sling that attached the monopile. The gripper is used to hold the monopile in one position which controls the horizontal movement of the monopile during the lowering of monopile and also during the hammering process. The gripper device is rigidly connected with the vessel but some damping devices are used inside the gripper to allow some movement which reduces the chance of local stress development.

As the diameter of the monopile is small compared with wavelength and the ratio of wave height to structure diameter is low also, so according to DNV-GL recommendation the inertia force is the governing device force on the monopile. Morison's formula is normally used to find the wave force per unit length on each strip of a vertical moving cylinder. [2]

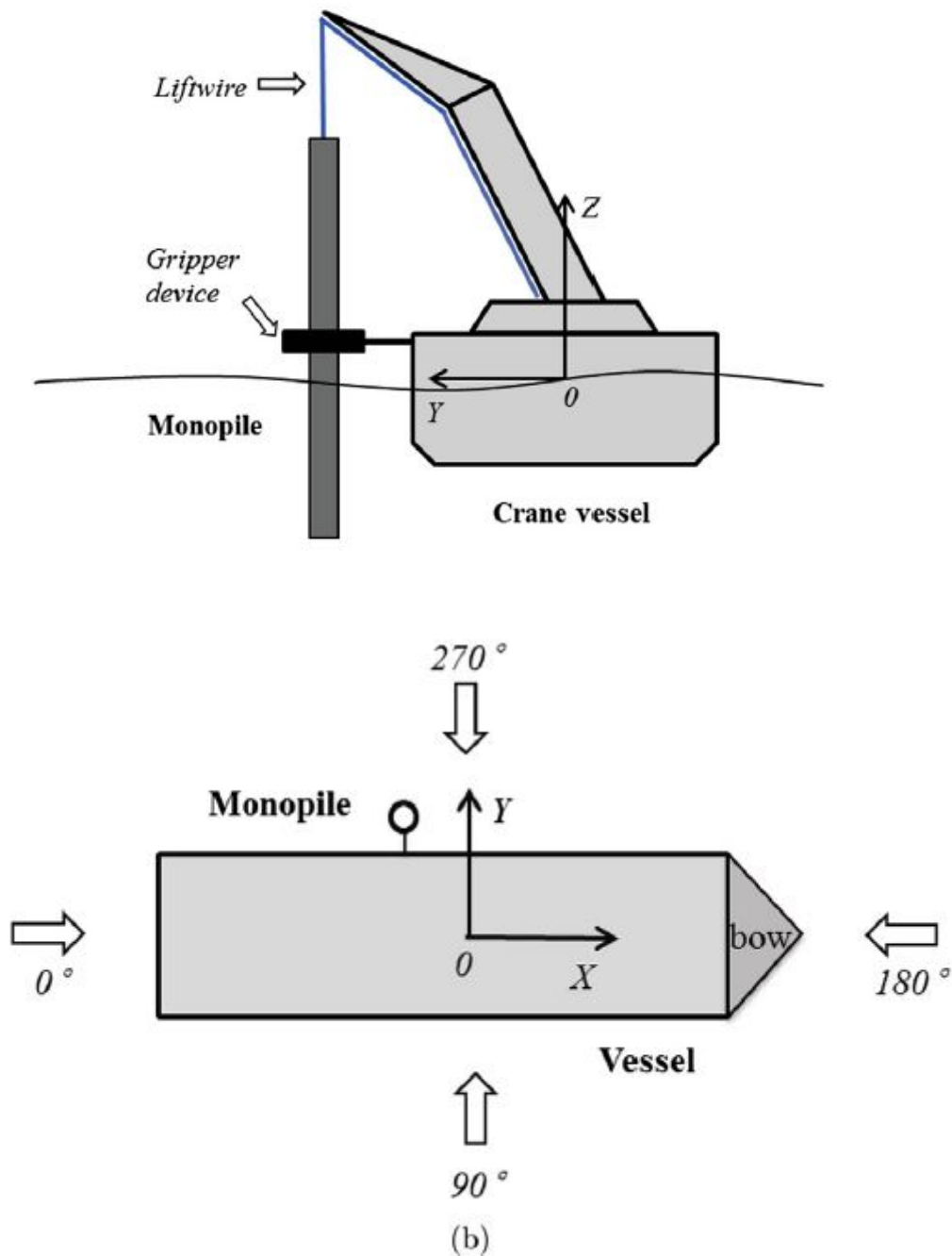


Figure 4: Monopile Lifting And Lowering Arrangement, (L.Li, 2014)

2.2 Monopile Hammering Operation

After lowering of the monopile, the next step is to drive the monopile into the seabed with a hammer on top. Figure 5, elucidate the set up for hammering operation. The system consists of a HLV, MP foundation, hammer and the gripper device. After the lowering operation to the seabed, the MP is supported vertically by the soil and laterally by the gripper device. The setup is still the same as MP lowering step, between gripper and monopile but there will be no lifting wire attached on the top of the MP instead the hammer is placed on top of the MP which increases its initial self-penetration. The common design of the gripper device includes several hydraulic cylinders. By varying the stroke length of the cylinders, the gripper is able to correct the mean inclination of the MP during the initial hammering process.

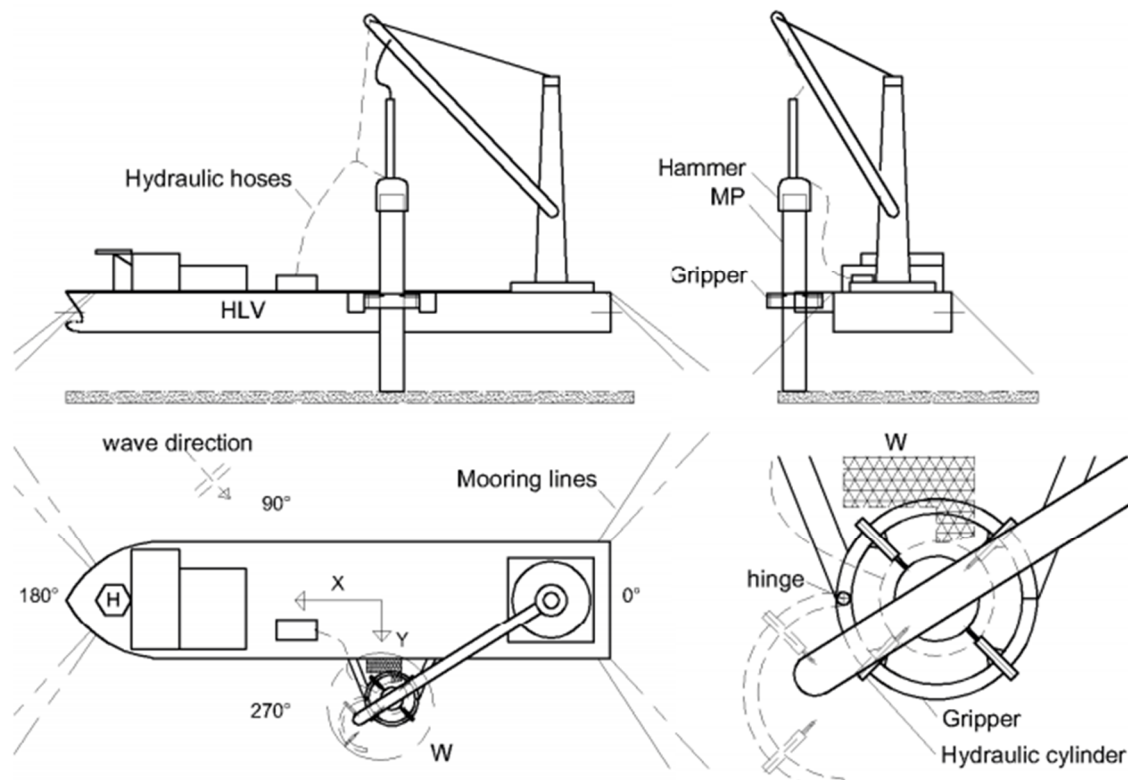


Figure 5: Set up for MP Hammering procedure (L.Li 2015)

Main particulars of the Global Model are presented in the following table:

Parameter	Notation	Value	Units
HLV			
<i>Displacement</i>	∇	5.12E4	Ton
<i>Length</i>	L	183	m
<i>Breadth</i>	B	47	m
<i>Draught</i>	T	10.2	m
<i>Metacentric height</i>	GM	5.24	m
<i>Vertical position of COG above keel</i>	VCG	17.45	m
Monopile			
<i>Mass</i>	M_{MP}	500	Ton
<i>Diameter</i>	D_{MP}	5.7	m
<i>Length</i>	L_{MP}	60	m
Hammer			
<i>Mass</i>	M_{Hammer}	300	Ton

Table 1: Main particulars of the MP hammering system[2]

According to method suggested by Lin Li [2] the general Monopile hammering procedure can be divided into following steps:

1. *Placing the hammer on top of the MP*: The weight of the hammer increases the MP's self-penetration depth and moment of inertia and also modifies the dynamic properties of the system.
2. *Measuring and correcting the mean inclination of the monopile*: Wave and current forces generally cause an initial mean inclination of the MP which could be increased further at deeper penetrations if the hammering process starts without any correction. The corrections of MP inclination can be done using hydraulic cylinders of the gripper by varying the pressure of the cylinders.
3. *Pre-compressing the hydraulic cylinders and hammering a few number of blows*: After the correction of the inclination, fluid supply valve is closed so the piston stroke length

becomes fixed. Additionally, pre-compression force is applied so that the cylinder rod always remains in contact with the MP to avoid gaps and subsequent impact load. The penetration rate of the MP depends on the soil conditions and decreases with the increasing depth.

4. *Measuring the Mono pile's inclination and correcting it with hydraulic cylinder:* After every hammering operation MP inclination is corrected to avoid cumulative inclination angles. During this period, only hydraulic cylinders can provide force to correct the MP's inclination until the soil resistance becomes too large.
5. *Repeating step 3 and 4 until the hydraulic cylinders are not able to correct the MP's inclination.*
6. *Correction of the inclination using thrusters and varying mooring line tension:* When the correction force is beyond the limit of the hydraulic cylinder to correct due to the soil resistance then HLV's thruster forces and mooring line can be used to correct the mean inclination.
7. *Retracting the hydraulic rods and drive MP to the final Penetration:* When the MP penetration is deep enough to stand by itself and the inclination cannot be corrected due to the soil resistance then the hydraulic rods are retracted.

For a successful operation requires the system to be intact and the final inclination to be within the acceptable limit. So, we have to perform the global analysis to find the responses of the different body and local analysis of the gripper system to identify the failure modes.

2.3 Critical events and possible failure modes

Failure of the Gripper hydraulic system: During the hammering, hydraulic system might fail due to the extreme force. These forces might arise from mainly three sources:

1. Coupled HLV-MP dynamic motion
2. Correction forces to rectify the mean inclination angle
3. Local discontinuities like welding seam of the MP, speed of the MP, the stroke length of the cylinder and gap between the MP to the gripper. Local failure modes are discussed elaborately at the monopile contact problem section.

So if the force exceeds the allowable limit then the hydraulic system might fail and that will cause not only interruption of the operation but also may pollute the environment if leakage

of hydraulic fluid occurs. So from the global and local analysis, we have to identify the maximum allowable forces on the hydraulic system.

Insufficient thruster forces and mooring line forces available: As we have discussed in the previous section that when mean inclination is beyond the capacity of the hydraulic system then HLV thruster system and mooring lines can be used to correct the inclination. But this HLV and mooring line also have a specific limit which are also limiting criteria. So we have to identify the maximum force that can be applied due to the thruster and mooring line.

Unacceptable MP inclination: If the inclination of the MP exceeds allowable limit then the installation process will be unsuccessful. Normally, the maximum allowable limit is below 1 degree [2]. Though during the installation, at every stage inclination will be measured and corrected but we have to keep an eye at the final stage because HLV-MP coupled motion may cause inclination just before retracting of the rods.

Critical events and limiting parameters can be different for different equipment and procedure. In our study, we will focus on the first event 'failure of the gripper hydraulic system'. [2]

2.4 Finding Allowable sea state

As our future goal is to establish the allowable sea states and limiting parameters of each critical events so here we have discussed the procedure to establish the allowable sea states. DNV-GL recommends [3] that for operation, first the allowable environmental conditions to defined then the weather criteria for starting and interrupting operation have to be identified. First, from the installation procedure and numerical model, critical limiting parameters have to be identified. Then from the global dynamic time domain analysis and local analysis of the gripper system, we can quantify the characteristic response and local stress concentration. By comparing those global and local limiting parameters we can define the allowable sea states for the different environmental condition then we can establish the allowable sea states. [2]

2.5 Theory and methodology for numerical modelling and analysis

The numerical model for our problem was established using MARINTEK SIMO program [4]. The model comprises coupled two-body HLV-MP system with mooring line positioning arrangement on the HLV and soil interactions forces on the MP at variable penetration depths. Overview of the global model and time domain simulations process are discussed briefly in the following section.

2.5.1 Overview of the Global model

The coupled dynamic equation was established based on the Lin li's paper and an overview of the model is presented here because establishing the global model is not our main focus in this study. For more details, readers are encouraged to read the paper written by Lin Li, 2015 [2]. Where the HLV-MP coupled dynamic system has 12 degrees of freedom(DOFs) and for each body, the following six equations of motion are solved in the time domain:

$$(M + A(\infty))\ddot{x} + D_1\dot{x} + D_2\int_0^t (\dot{x}) + Kx + \int_0^t h(t-\tau)\dot{x}(\tau)d\tau = F_{ext}(t) \quad (1)$$

$$F_{ext}(t) = q_{WA}^{(1)} + q_{WA}^{(2)} + F_{moor} + F_{cpl} + F_{soil} \quad (2)$$

- The Wind and current load were not included as they do not affect the dynamic response of the coupled analysis. [2]
- The second-order wave excitation forces were obtained based on the Newman's approximation [24].
- The eight catenary mooring lines for HLV were also modelled.
- Two-panel models were built and hydrodynamic interaction problems were solved using the panel method program WAMIT [23] in the frequency domain. [2]

2.5.2 Time domain simulation

- Step-by-step integration methods are applied to calculate the responses of the coupled HLV-MP system.
- The equations of motions were solved using Newmark-beta numerical integration with $\alpha=0.5$, $\beta=0.1667$ and a time step 0.01s.

- The first order and second order wave forces are pre-generated using the Fast Fourier Transformation(FFT) at the mean position of the HLV and the MP. [2]
- Mooring, gripper coupling and soil-MP interactions forces are calculated in the time-domain. [2]
- Short-crested waves with index $n=3$ for the spreading function \cos^n is applied for all the sea states. [2]

2.5.3 Modelling of gripper device

In the numerical model, the gripper device is simplified by four fender modules with chosen stiffness and damping coefficients. In the present study, the parameters for the gripper are chosen based on specifications of typical hydraulic cylinders which are applied in practice for MP installation [14]. The valves of the hydraulic cylinders are normally closed during the hammering process. For of the elasticity of the hydraulic fluid, the hydraulic cylinder acts like a mechanical spring. The stiffness of the spring was calculated according to Ref. [5] and depends mainly on the fluid elasticity (which is more closely investigated in the later part of this thesis), the area of the piston and the total compression volume for the fluid. Damping is caused by friction in the actuator and the pipe system. By using technical data of hydraulic cylinders, the stiffness of the cylinder with closed valves was found to be about 10^7 N/m to 10^8 N/m. So, we have chosen spring constant 3×10^7 N/m for our current model. The damping in the numerical model is taken to be 20% of critical damping which is a rational value for hydraulic cylinders. During hammering, to ensure zero gap between MP and gripper normally a pre-compression force is applied. [2,5]

2.6 Soil-MP interaction

Modelling of the soil-pile system is important for the global dynamic analysis of the structure embedded in the soil. Normally soil pile interaction model are based on the winker's hypothesis and API p-y curve recommendation. API is based on the results obtained from the field test of large slender piles with very high length to diameter ratio which is not the ideal case for the wind turbine Mono Pile. A new design method has been developed by adding additional terms to the existing p-y curve. Four separate components of soil reaction forces

were added to the proposed design those are the traditional distributed p-y curve, the distributed moment curve due to the vertical shear friction, the base shear curve and base moment curve (Bryne, 2015). It has been found from the study that for the pile with larger length (embedded length) to diameter ratio, only traditional p-y curve response dominates the total response of the system while for shorter length to diameter ratio which is the case for initial shallow penetration both traditional p-y curve and distributed moment should be account for. In this study, we will discuss briefly different methods for developing p-y curves, especially API recommendation procedure which is followed in during the modelling of our soil-MP system.

There are several analysis methods available for the analysis of laterally loaded pile which can be classified into mainly three approaches:

- Beam on Winker foundation approaches
- Elastic continuum approach
- Finite element approach

In Winker Foundation approach, the beam represents the foundation and the foundation represents the soil mass. Winker proposed that the vertical resistance of a ground against external forces can be assumed to be proportional to the ground deflection. On the basis of this idea, the researchers represented the ground with a series of elastic spring so that the compression or extension of the spring is proportional to the applied load. The spring constant represents the stiffness of the supporting ground against the applied load. This concept was extended by placing a Euler-Bernoulli beam on top of the elastic foundation and applying loads on the top of the beam

Elastic Continuum method is based on Midlin's closed form solution for the application of point loads to a semi-infinite mass. The accuracy of this solution is directly related to the evaluation of the young's modulus and the other elastic parameters of soil.

Finite element method is the most powerful method for conducting soil pile interaction analysis though developing a proper soil pile interaction model is the main challenge for this method.

In the following section, we will discuss different methods for calculating p-y curves based on the Winker's theory. The governing equation for calculating the soil reaction force and deflection for a laterally loaded soil-pile system based on winker's theory is discussed in appendix 01.

2.6.1 Static p-y generation

First, we will discuss the conventional methods of determining p-y curves then later we will calculate those curves based on the API recommendation.

In the analysis of piles supporting offshore structure, the key element in predicting the response to lateral loads is the determination of the appropriate lateral load deformation relationships (p-y curves) for the soil. The present practice of constructing the p-y curves are based on the result of lateral load tests on instrumented piles and strength-deformation characteristics of the soil. The pile analysis method commonly used in practice is the p-y approach (Reese et al. 1974) and p-y approach (Matlock, 1970), where the p-y curves represent the relationships between the lateral load (p) and the displacement (y) at a point in the pile.

Some studies have been done for developing the p-y curve for the pile at different times and some have been ongoing continuously to improve the existing methods. A number of different methods have been proposed for the development of the p-y curves. The p-y curve which is originated from the subgrade reaction method represents the lateral load per unit length, p, which is an integral of the shear and normal pressure acting on a pile segment when the pile is translated laterally into the soil by a displacement of y (Matlock, 1970). Because of the complexity of the manner in which unit soil resistance is mobilized, its characteristics have generally been determined empirically from the results of full scale and model pile load tests. Empirical determination of the p-y behaviour from load test result is valid and reasonable in most cases but it is important to recognize the limitation of such empirical approach. The accuracy of such empirical methods depends on upon the data from which it was developed. The reliability of the approach is based on the number of tests (Kramer, 1988). The most commonly used p-y curve criteria (Matlock, 1970) is based on a very limited number of tests.

The magnitude of ultimate soil resistance i.e. the soil resistance under fully plastic behaviour P_u is related to the undrained shear strength and varies with the depth and will depend on upon the governing type of failure mechanism of soil surrounding the pile. For laterally loaded piles, two types of failure mechanism are considered.

- The first type of failure mechanism usually occurs at relatively shallow depths involves the failure of a wedge of soil in front of the pile with a gap forming behind the pile.
- The second type of failure mechanism occurs at greater depth and represented by the plastic flow of the soil around the pile as it deflects laterally (Randolph & Susan, 2011).

The depth at which these two failure mechanisms predict the same ultimate soil resistance is known as critical depth (Z_{cr}). The ultimate soil resistance up to critical depth varies with depth but below critical depth, it was taken constant.

There are different approaches have been used for the development of p-y curves for clays. All the approaches are based on the result of full-scale lateral load test for static and cyclic loading conditions. In the following section, some important and popular approached are mentioned:

- Soft clay criteria(Matlock,1970)
- Above Water Table(AWT) stiff clay criteria (Reese & Welch,1975)
- Below Water Table (BWT) Stiff Clay Criteria (Reese et el, 1975)
- Design Codes recommendation for p-y curve(API,1993)
- Unified clay criteria (Sullivan, Reese & Fenske,1980)
- Integrated clay criteria (O'Neill & Gazioglu,1984)
- Representation of p-y curve using Beizer Equations (Kdikar, Haque & Lee,2010)

Among those methods described above, we are going to discuss two methods, first Soft clay method then API method. Later we will compare different methods and finally discuss the limitation of the static p-y curve in this section. [6,7]

Soft clay Criteria (Matlock, 1970)

Matlock (1970) proposed a procedure for the development of p-y curves for piles in soft, saturated clays. The strain hardening criteria are based on the results of four lateral load test performed on a fully instrumented 12.75-inch diameter pile driven into soft to medium silty clays at two different sites (Stevens & Audibert, 1979). The parameters used for calculation are:

P = lateral soil resistance

p_u = ultimate lateral soil resistance

y = lateral pile deflection

y_c = The reference displacement which occurs at 50% of the ultimate soil resistance.

ε_{50} = Strain at one-half the maximum deviator stress in the undrained test.

$$y_c = 2.5 * \varepsilon_{50} * d \quad (3)$$

Where d is the pile diameter

The ultimate soil resistance p_u is calculated from the following equation,

$$p_u = N_p * S_u * d \quad (4)$$

S_u = undrained shear strength of soil.

N_p = ultimate lateral soil resistance coefficient

Matlock suggested that $N_p = 9$ for the greater depths where sufficient confinement exists that corresponds to the horizontal flow of the soil around the cylindrical pile. But near the surface, the soil in front of pile is not well confined and as the pile deflects the soil is pushed up and away from the pile $N_p = 3$ at the surface and increases with depth with the following relationship:

$$N_p = 3 + \sigma'_z / S_u + J * Z / d \quad (5)$$

σ'_z = Effective overburden stress at depth z

S_u = undrained soil shear strength at depth z

J = an empirical constant with an approximate value of 0.5 for the soft offshore clays and a value of 0.25 for somewhat stiffer clays.

Design Code recommendation for p-y curve (API, 1933)

As per API, three types of curves are recommended to properly model the soil pile reaction forces. Those are:

1. Axial Load Transfer(T-z) curves:
2. Tip load transfer curve(Q-Z)
3. Lateral soil Resistance-Deflection(p-y) curves

Axial Load Transfer(T-z) Curves:

API Clay and API Sand Models (Refer to G.4.2, G.4.3, and G.7.2 API RP2A LRFD)

The unit skin friction and the T-z curves for clay and sandy soils can be determined as per Section G.4.2 and Section G.4.3 API RP2A LRFD respectively. Figure 5 shows the T-z curves for non-carbonate soils, recommended by API RP2A LRFD.

For pipe piles in cohesive soils, the skin friction can be calculated by the equation.

$$f = \alpha c \quad (6)$$

Where,

c = undrained shear strength of the soil in stress units

α = a dimensionless factor, which is defined as

$$\alpha = 0.5\psi^{-0.5} \leq 1.0 \quad \text{for } \psi \leq 1.0$$

$$\alpha = 0.5\psi^{-0.25} \leq 1.0 \quad \text{for } \psi > 1.0$$

$$\psi = \frac{c}{p'_o}$$

p'_o = effective overburden pressure in stress units.

For our Soil-MP model, T-z curves are generated using piecewise linear function based on the data given in the following table:

$\frac{z}{D}$	$\frac{t}{t_{\max}}$
0.0016	0.30
0.0031	0.50
0.0057	0.75
0.0080	0.90
0.0100	1.00
0.0200	0.90
∞	0.90

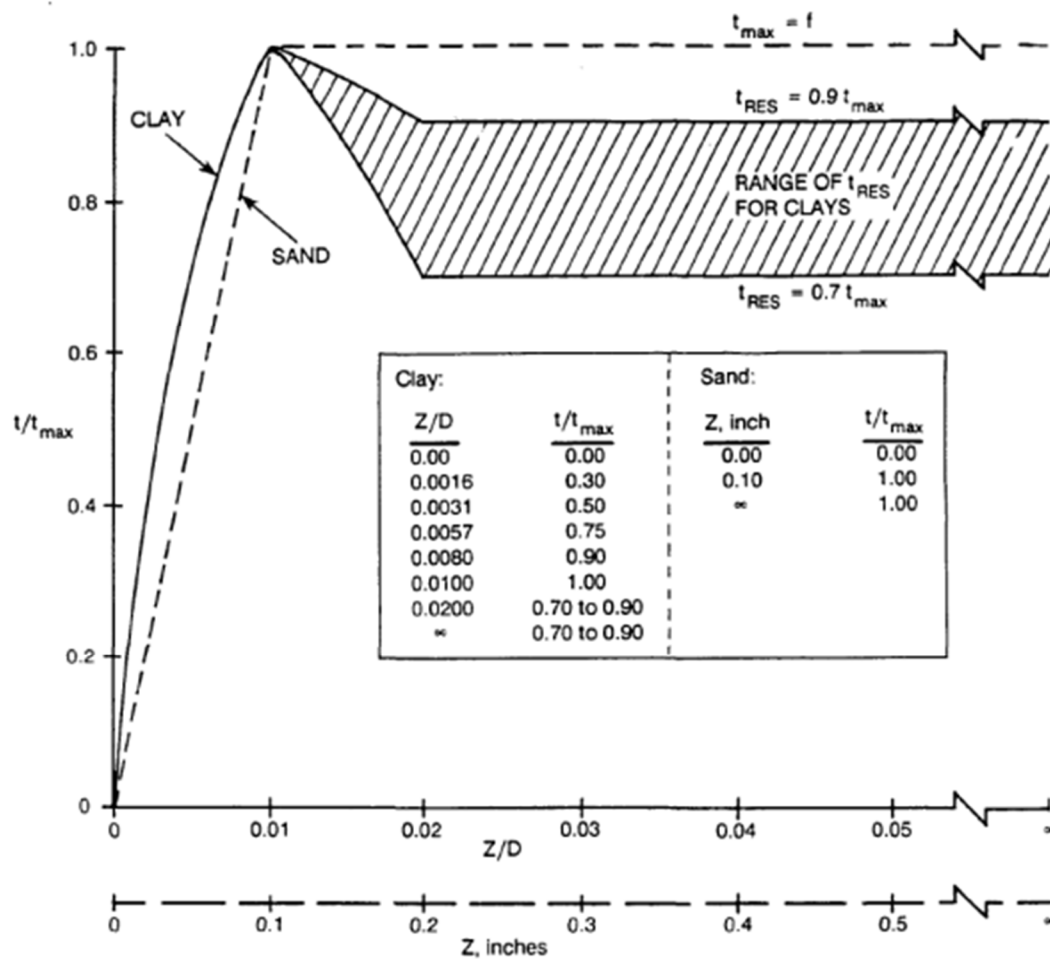


Figure 6: Axial Pile Load Transfer-Displacement (T-z) curves (API)

Where,

Z = Local pile deflection

D = Pile diameter

t = mobilized soil pile adhesion in stress units

t_{\max} = maximum soil pile adhesion or unit skin friction capacity computed

For pipe piles in cohesionless soils, the unit skin friction is calculated as

$$f = Kp'_o \tan(\delta)$$

Where,

K = dimensionless coefficient of lateral earth pressure (ratio of horizontal to vertical normal effective stress, for unplugged $K=0.8$ and for plugged $K=1.0$)

p'_o = effective overburden pressure in stress units

δ = friction angle between the soil and pile wall, which is defined as

$$\delta = \phi - 5^\circ$$

ϕ = internal friction angle

Tip Load-Displacement (Q-z) Curves:

API Clay and API Sand Models (Refer to G.4.2, G.4.3, and G.7.3 API RP2A LRFD)

The unit end bearing capacity and Q-z curves for clay and sandy soils can be determined as per Section G.4.2 and Section G.4.3 API RP2A LRFD respectively. A relatively large pile tip movement which is required to fully mobilize the end bearing resistance may be achieved by a pile tip displacement up to 10% of the pile diameter. Figure 6 shows the Q-z curves of both sand and clay soils as recommended in API RP2A LRFD.

The unit end bearing of Monopile founded in cohesive soil is given by:

$$q = 9c \tag{7}$$

c = undrained shear strength of the soil, in stress units, at the pile tip

The unit end bearing of MP founded in cohesionless soil is given by:

$$q = p'_o N_q \tag{8}$$

Where,

p'_o = effective overburden pressure, in stress units, at the pile tip

N_q = dimensionless bearing capacity factor, which is defined as

$$N_q = e^{x \tan(\phi')} \tan^2\left(45^\circ + \frac{\phi'}{2}\right)$$

ϕ' = effective internal friction angle at the pile tip.

The ultimate end-bearing capacity is then calculated,

$$Q_p = qA$$

Where,

A = sectional area at the tip of pile, which is based on the pile end condition;

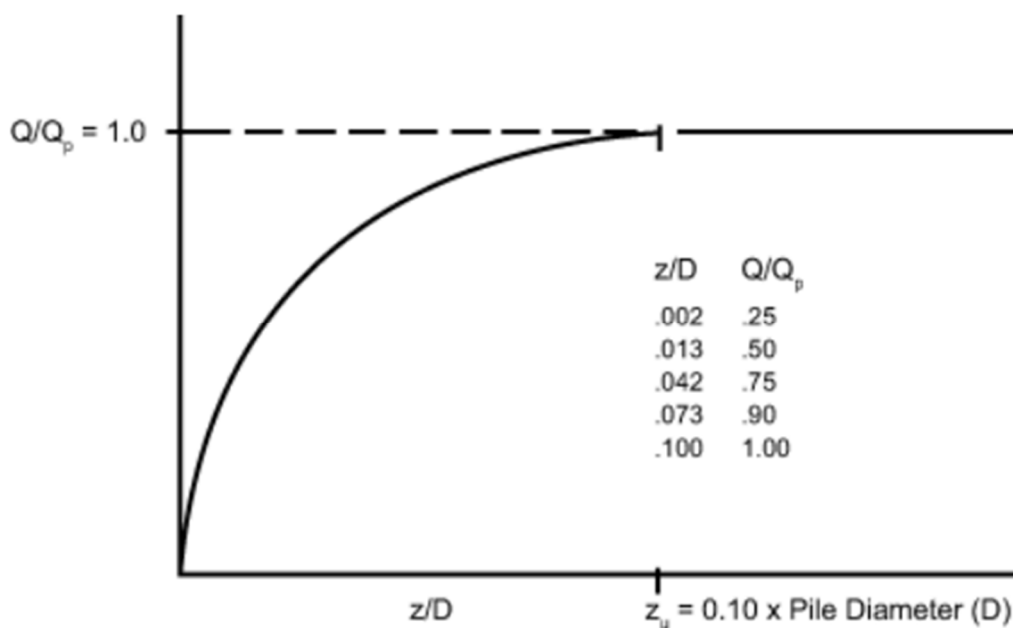


Figure 7: MP Tip-Load Displacement(Q-z) Curve(API)

Where,

Z = Axial pile deflection

D = pile diameter

Q = mobilized end bearing capacity in force units

Q_p = total end bearing computed

It is recommended that the ultimate (limiting) values of unit end bearing for cohesionless soils, q_{ult} , be considered, which are given in Table G.4.3-1 API RP2A LRFD.

For our, soil-MP modelling, Q-z curves of API sand are defined as a piecewise linear function based on the data given in the following table:

$\frac{z}{D}$	$\frac{Q}{Q_p}$
0.002	0.25
0.013	0.50
0.042	0.75
0.073	0.90
0.100	1.00
∞	1.00

Lateral Soil-Pile Resistance-Deflection (p-y) Curves:

API Clay and API Sand Models (Refer to G.8.2 to G.8.7 API RP2A LFRD)

The ultimate lateral soil resistance and P-y curves may be calculated using section G.8.2 to G.8.7 API RP2A LFRD. The soil resistance equations are not applicable if the strength variation along the depth of the soil is inconsistent.

The ultimate unit lateral resistance, p_u , of soft clay under static loading conditions can vary between $8c$ to $12c$ except at the shallow depths. In the absence of more definitive criteria, we can use the empirical equation given by API RP2A LFRD:

$$p_u = 3c + p'_o + J \frac{cz}{D} \quad \text{for } z < X_R \quad (9)$$

$$p_u = 9c \quad \text{for } z \geq X_R \quad (10)$$

Where,

c = undrained shear strength of undisturbed clay soil samples in stress units

p'_o = effective overburden pressure in stress units

z = depth below ground surface

$D =$ diameter of the pile

$J =$ dimensionless empirical constant

$X_R =$ depth from the ground surface to the bottom of reduced resistance zone, which is defined as:

$$X_R = \frac{6D}{\frac{\gamma D}{c} + J}$$

Lateral soil resistance-deflection relation for piles in soft clay are generally nonlinear. The p-y curves for the short-term static load case may be generated from the following table:

p / p_u	y / y_c
0	0
0.5	1.0
0.72	3.0
1.00	8.0
1.00	∞

Where,

$p =$ actual lateral resistance, in stress units

$y =$ actual lateral deflection

$y_c = 2.5 \varepsilon_c D$

$\varepsilon_c =$ The strain which occurs at one-half the maximum stress on laboratory undrained compression test of undistributed soil samples.

For the case where equilibrium has been reached under cyclic loading, the p-y curves may be generated from the following table:

Static loading		Cyclic loading			
p/p_u	y/y_c	$z > X_R$		$z < X_R$	
		p/p_u	y/y_c	p/p_u	y/y_c
0.00	0.0	0.00	0.0	0.00	0.0
0.50	1.0	0.50	1.0	0.50	1.0
0.72	3.0	0.72	3.0	0.72	3.0
1.00	8.0	0.72	∞	$0.72 z/X_R$	15.0
1.00	∞			$0.72 z/X_R$	∞

The ultimate lateral bearing capacity for sand at a given depth is used as the smaller value between p_{us} (ultimate lateral resistance at shallow depths) to p_{ud} (ultimate lateral resistance at greater depths), which are determined by the following equations:

$$p_{us} = (C_1 z + C_2 D) p_o' \quad (11)$$

$$p_{ud} = C_3 D p_o' \quad (12)$$

Where,

z = depth below ground surface

p_o' = effective overburden pressure in stress units

D = diameter of the pile

C_1, C_2, C_3 = coefficients determined from Figure 7, which is a function of φ'

φ' = effective internal friction angle

The variation of coefficients of C_1 , C_2 , and C_3 with φ' is given in the graph below:

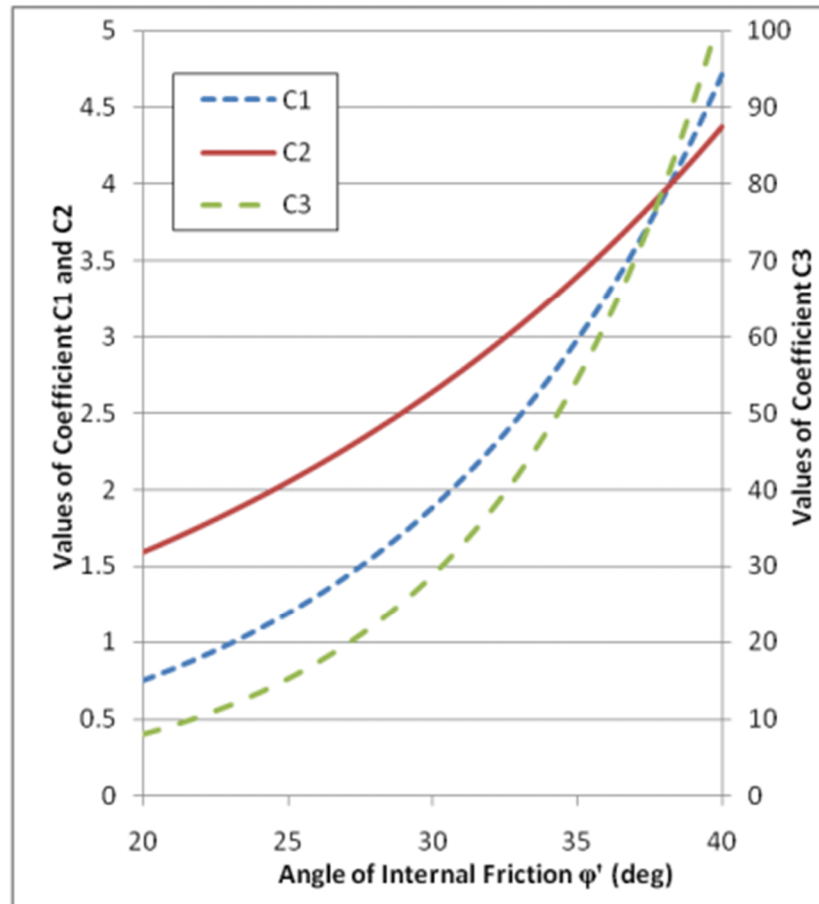


Figure 8 Variation of coefficient C1, C2 and C3 with ϕ' (API)

Using the ultimate lateral resistance, the lateral soil resistance – deflection (P-y) relationship for sand is approximated as:

$$P = Ap_u \tanh\left(\frac{kz}{Ap_u} y\right) \quad (13)$$

Where,

p_u = ultimate bearing capacity, which is defined as smaller value of p_{us} and p_u

k = subgrade modulus, force per volume units, is determined from Figure G.8-2(API), which is a function of ϕ'

ϕ' = effective internal friction angle

z = depth below ground surface

$y =$ lateral deflection

$A =$ factor to account for cyclic or static loading conditions, which is defined as

For cyclic loading, $A = 0.9$

For static loading, $3.0 - 0.8\left(\frac{z}{D}\right) \geq 0.9$

Limitation:

The penetration of the MP during the initial hammering process ranges from around 2m (self-penetration) to around 6 to 8 m [2]. Here in our study, we will model up to 6 m. As the API code was developed for smaller diameter pile and the effect of pile diameter has not been considered. Moreover, those piles used in the API curve was much more flexible than that of offshore wind piles. For that reason, from different papers, it has been found that the soil resistance is much higher than the API curve predicts. Damping behaviour of soil and degradation of soil stiffness is not considered in this criteria also. So, initially our plan was to develop new dynamic p-y curve with Plaxis 3D software but due to the unavailability of the software, we have used the same Soil-Pile interaction curves recommended by API.

2.6.2 Soil-MP Model for Global Analysis

As we have already discussed that in the shallow penetration phases, the soil-MP interaction forces are three-dimensional, therefore the 2D Winkler model is extended to 3D by using non-linear springs distributed in both axial and circumferential directions along the MP. The distributed springs include the traditional lateral load-deflection p – y curve, the friction T – z curve which is significant for large diameter piles with shallow penetrations [8], the base shear curve and the tip load-displacement Q – z curve.

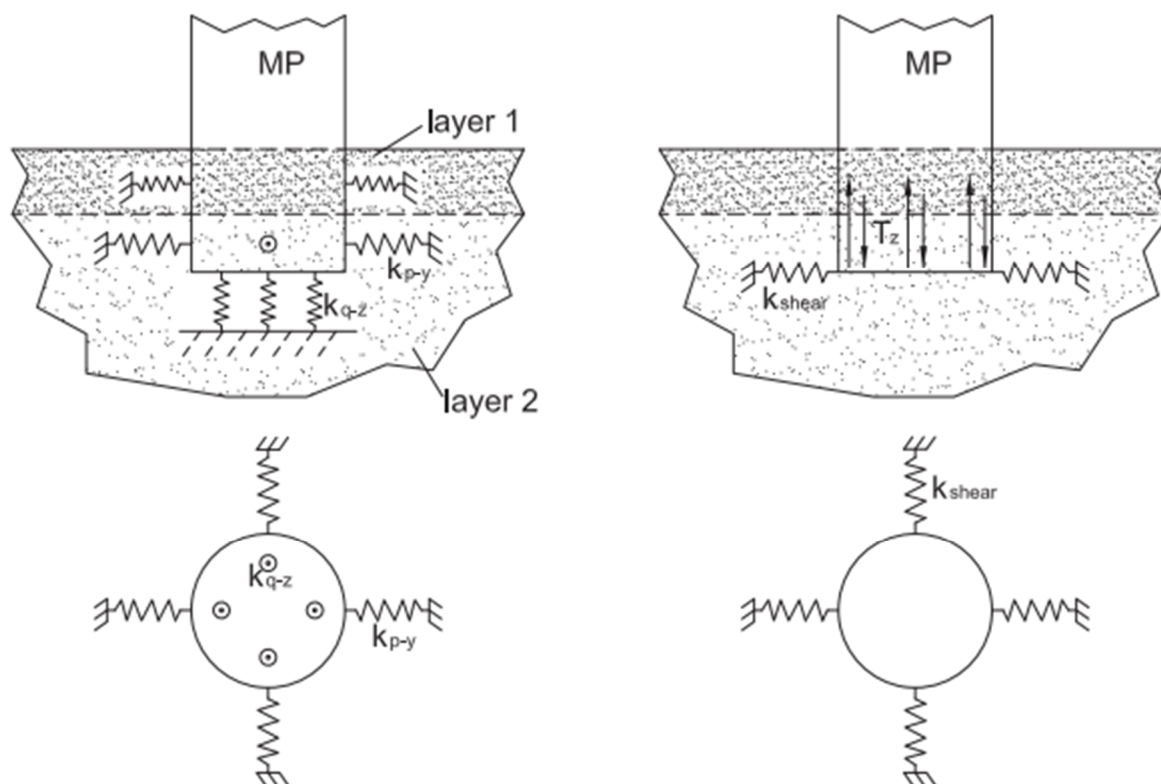


Figure 9: Soil-MO interaction model [Lin Li, 2015]

The configuration of springs as shown in figure 9, can be summarized as follows: For $p - y$ curves, the whole penetration is divided into three, 2m-layers, and 4 circumferential springs K_{p-y} are applied for each layer. On the bottom of the MP, 4 springs K_{shear} are used to model the shear resistance force. The number of the distributed spring is considered to be sufficient since the MP bottom tip will experience small displacement (less than 10 cm for typical sea states) [2]. Moreover, K_{q-z} represents 4 vertical springs which have been used to model Q-z curves at the bottom of the MP and 4 springs T_z were used on the side of the MP to model the $T - z$ curve for the friction force from both inside and outside wall of the MP. [2]

The curves were calculated from the following properties:

Mass of the MP and hammer: 800000 Kg

Weight: 7878 KN

Diameter of the MP: 5.7 m

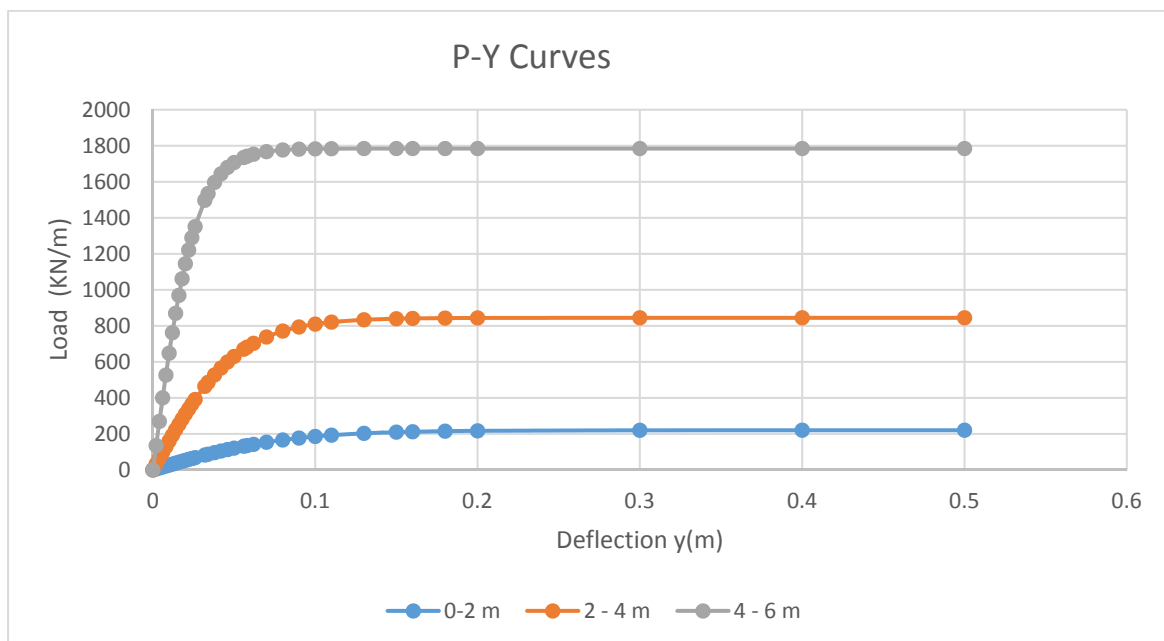
Thickness: 0.06 m

Soil type: sand

Soil properties (from project upwind):

Layer	Type	Unit weight	Internal Angle	Skin friction	Unit tip Resistance
		KN/m ³	deg	KPa	KPa
0m-2m	sand	10	36	20	1900
2m-4m	sand	10	36	24.8	2300
4m-6m	sand	10	37	39.1	3400

Table 2: Soil properties [9]



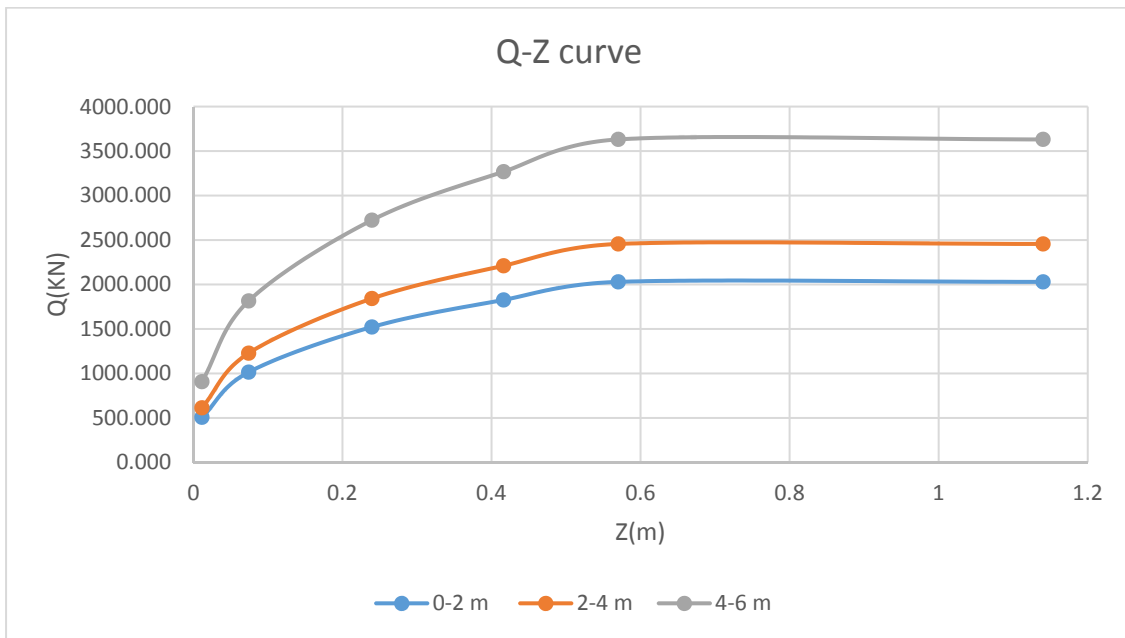
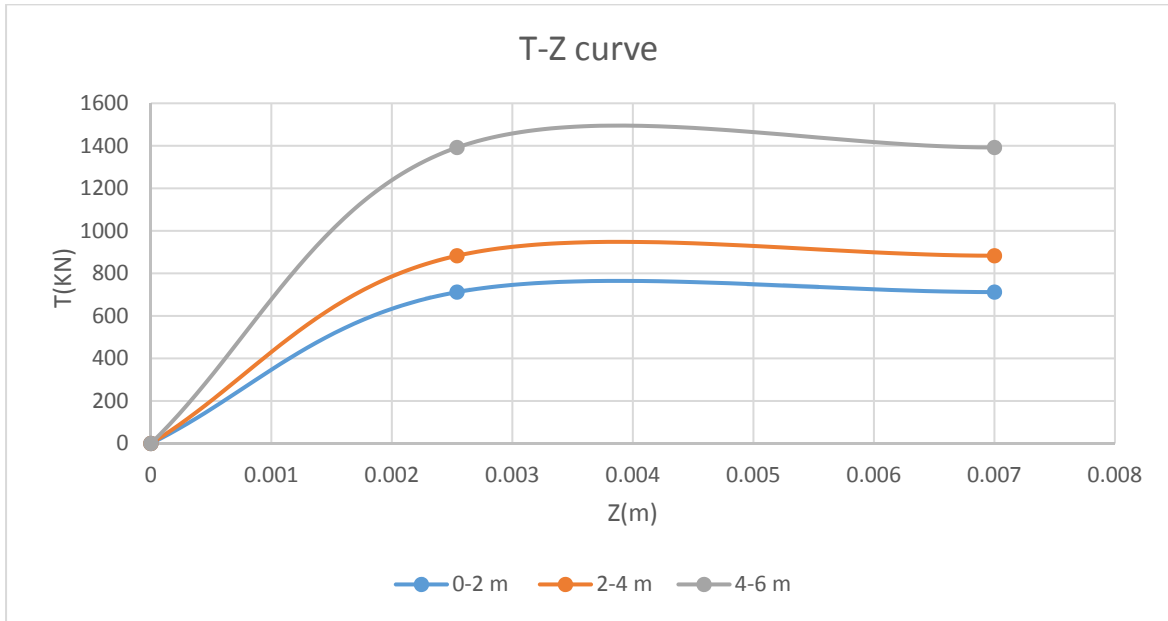
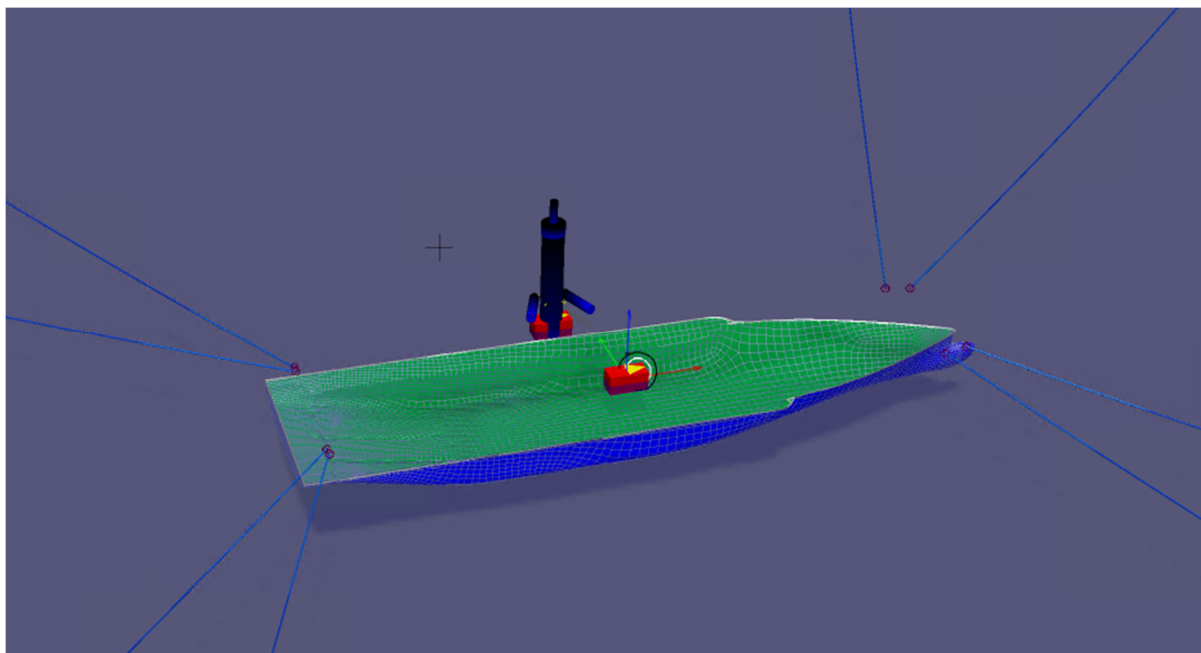
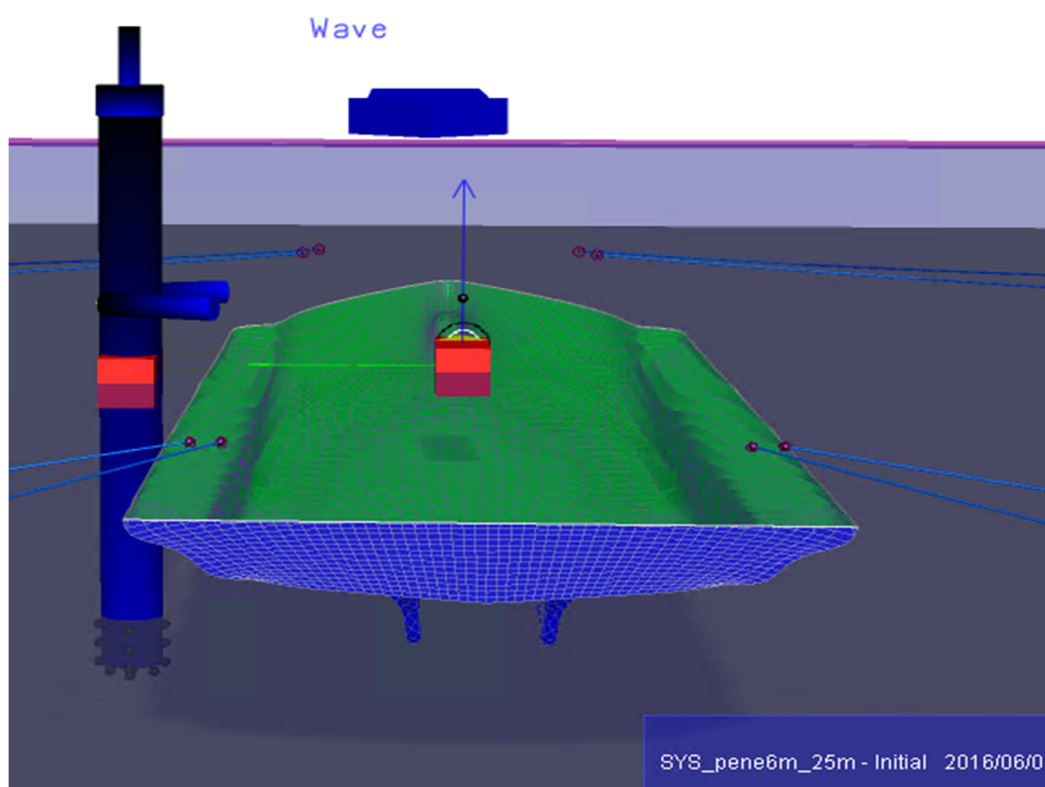


Figure 10: Figure shows P-y, T-z and Q-z curve

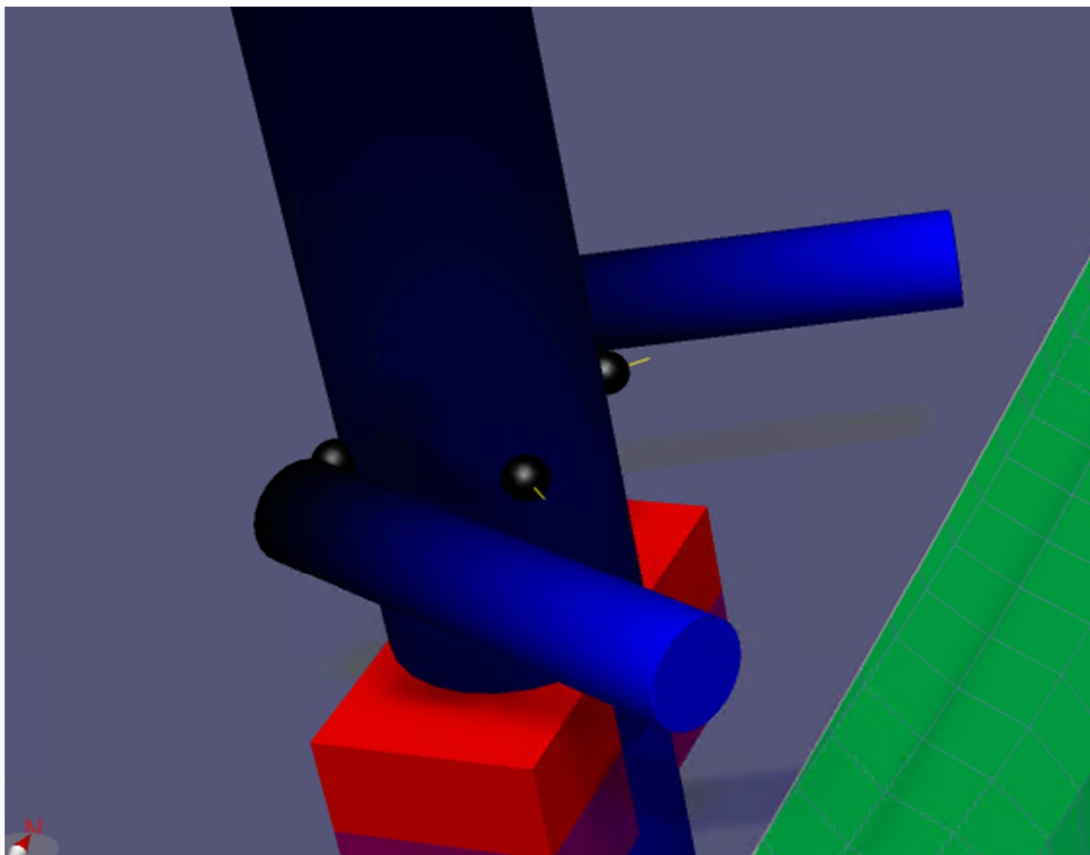
2.7 Dynamic response of HLV-MP System at Different Penetration



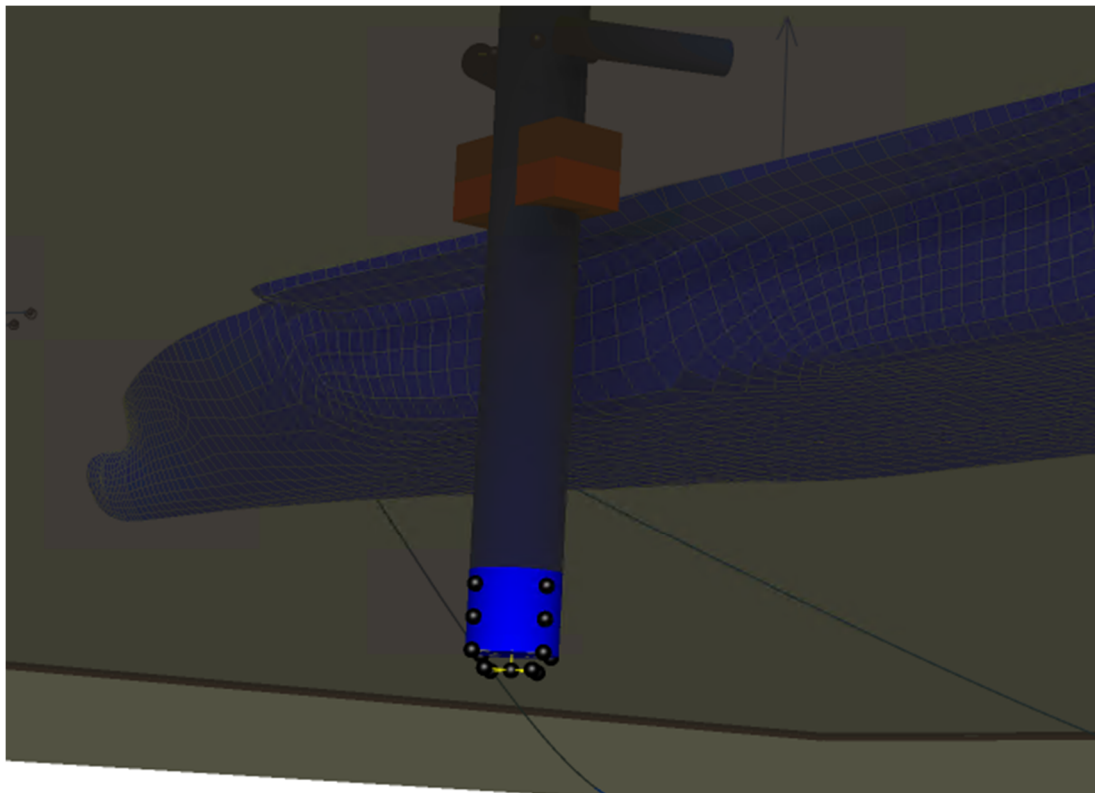
Global model with HLV, MP, Hammer on top of MP, Gripper system and Mooring line



View from Aft of FLV with wave direction zero degree



MP-gripper connection, circular sphere represents the cylinder arm



Soil-pile Modelling with spring under the sea surface

Figure 11: Global model for HLV-MP-Soil responses

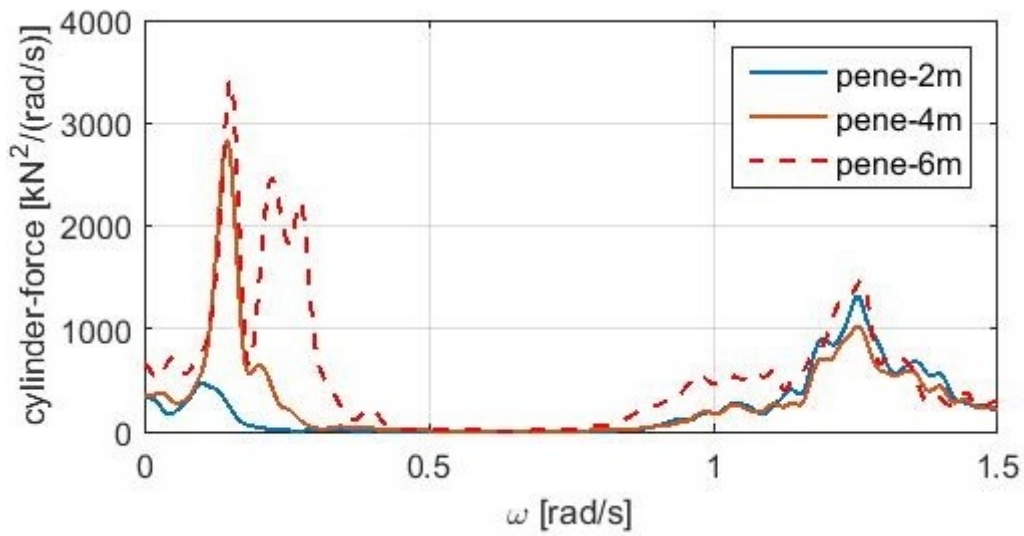
The figure [11] shows the HLV-MP coupling model with gripper, mooring line and soil-pile spring model. Cylinder response forces are calculated at every cylinder separately, modelled in the picture above. Though, results of the responses are presented with varying wave conditions for only one cylinder which represents the maximum value.

The results of the time domain simulations are presented here to identify the response spectra of the hydraulic cylinder. The numerical model was established using MARINTEK SIMO program [4] and based on the model developed by Lin Li [2]. Cylinder response spectra are presented for three different MP penetrations, i.e. 2m, 4m and 6m.

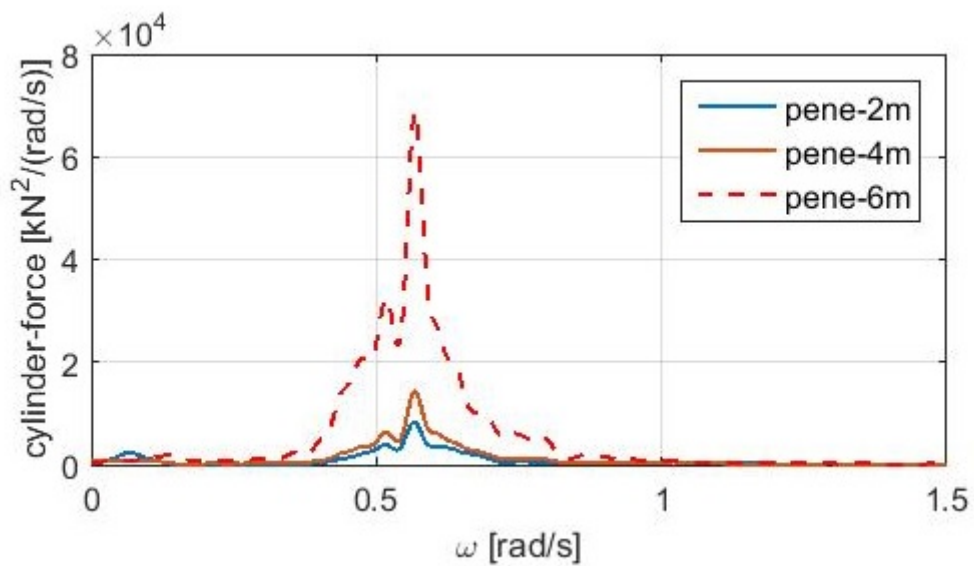
From the figure 12, we can see that the response spectra of the cylinder increase with the increase of the MP penetration and peak period. From the figure 13, it is also evident that with the increase of the significant wave height the response spectra increase. Cylinder contact force will increase with the increase of the response spectra and penetration [Table 3]. So, cylinder contact force is a limiting parameter as it is directly related to the environmental condition and MP penetration. Though from this analysis it not possible to identify that whether the hydraulic cylinder can withstand that force locally or not. So, it is important to conduct a local analysis of the hydraulic gripper system to identify the effects and limiting parameters.

Wave conditions	Penetration [m]	Cylinder-Force[KN]
$H_s=1.5\text{m, Dir}=150\text{ degree,}$ $T_p=5\text{ sec}$	2	25.1
	4	27.7
	6	38.9
$H_s=1.5\text{m, Dir}=150\text{ degree,}$ $T_p=7\text{ sec}$	2	25.2
	4	27.6
	6	50.4
$H_s=1.5\text{m, Dir}=150\text{ degree,}$ $T_p=10\text{ sec}$	2	48.1
	4	56.3
	6	97.5

Table 3: Standard deviation of the contact forces on one hydraulic cylinder at different penetration and wave conditions from 3-hour time-domain simulation

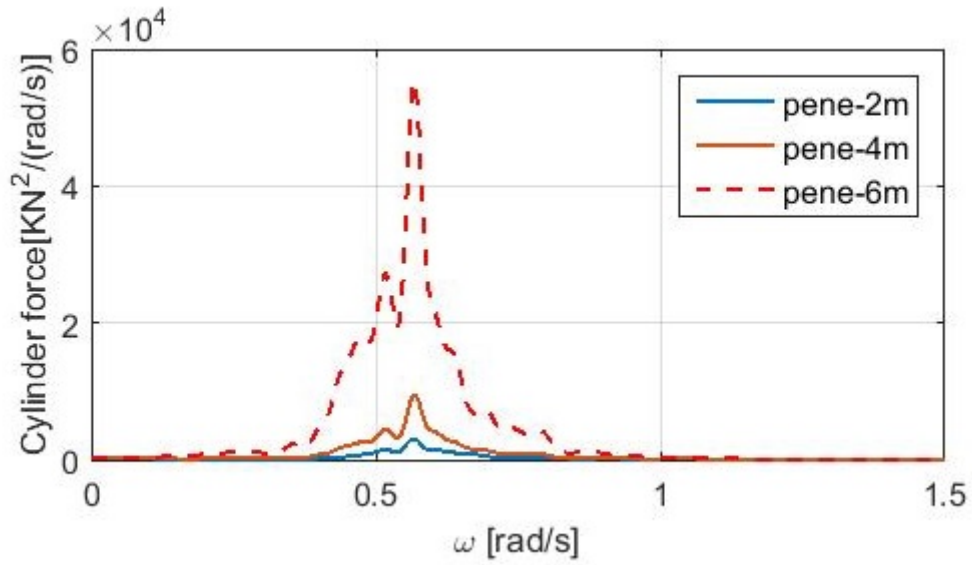


$T_p=5\text{ s}$, $Dir=150\text{ degree}$, $H_s=1.5\text{ m}$

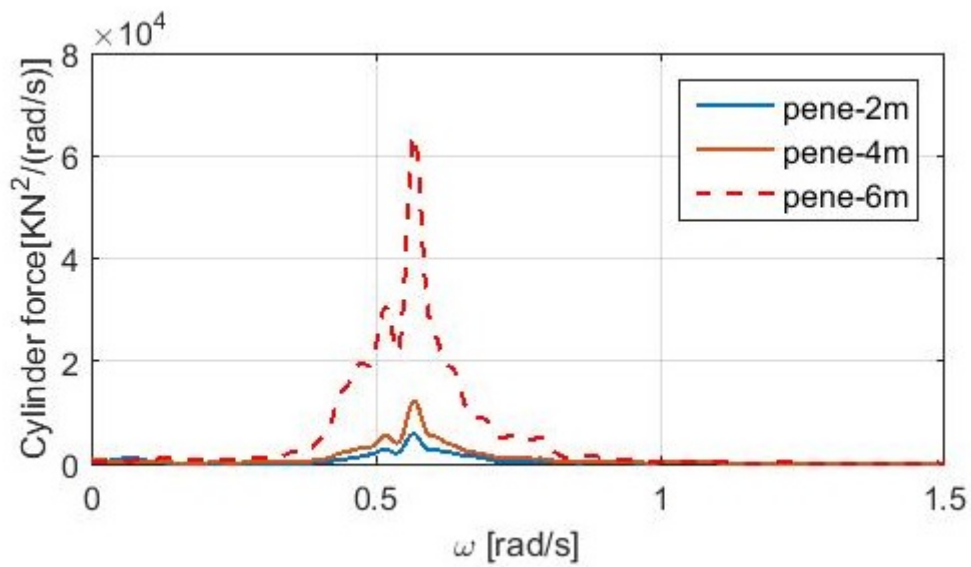


$T_p=10\text{ s}$, $Dir=150\text{ degree}$, $H_s=1.5\text{ m}$,

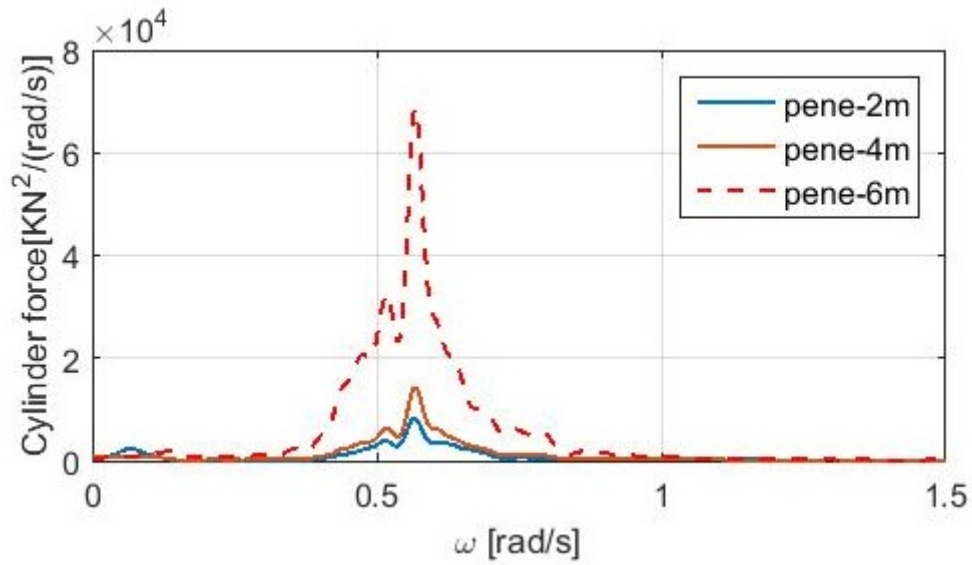
Figure 12: Response spectra of the hydraulic cylinder force for two different wave peak period conditions at different MP penetration depth (pene)



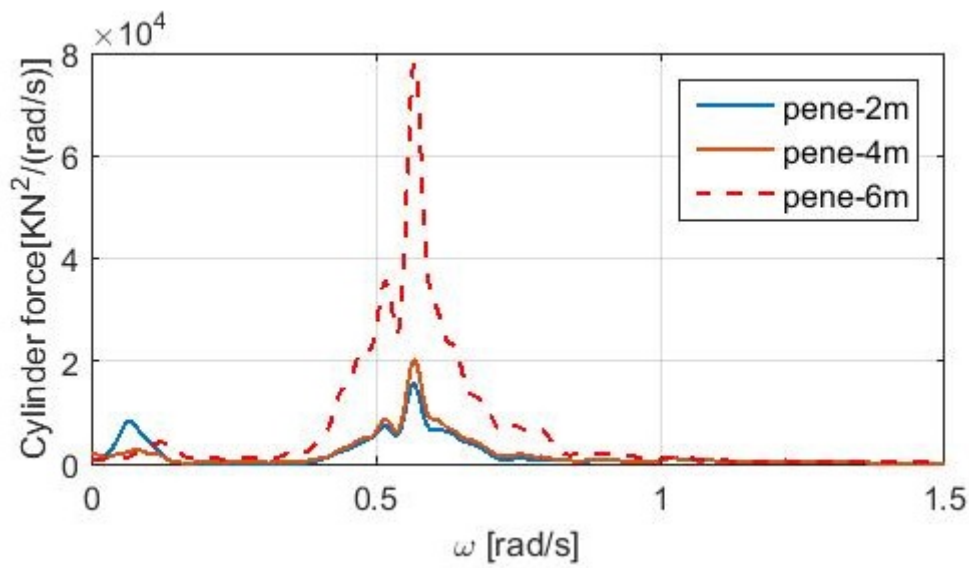
$H_s = 1.0$ m, $T_p = 10$ s, Dir = 150 degree,



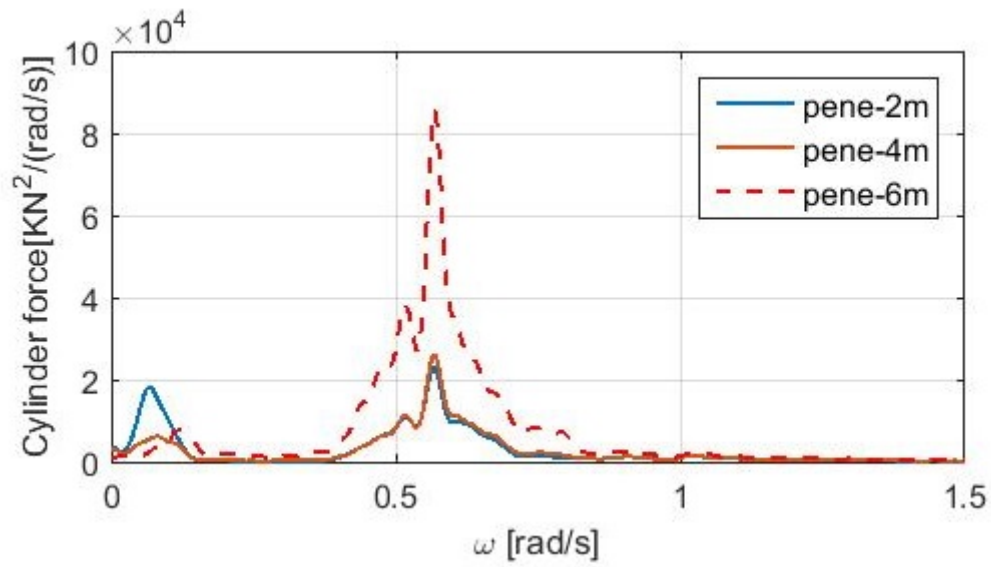
$H_s = 1.3$ m, $T_p = 10$ s, Dir = 150 degree,



$H_s = 1.5$ m, $T_p = 10$ s, Dir=150 degree,



$H_s = 2.0$ m, $T_p = 10$ s, Dir=150 degree,



$H_s = 2.5$ m, $T_p = 10$ s, Dir = 150 degree,

Figure 13: Response spectra of the hydraulic cylinder force for different significant Wave height at different MP penetration depth (pene)

3. Gripper- Monopile Contact Problem

In this section, properties of the hydraulic gripper system and the local analysis of the gripper system are discussed. Generally, gripper device is consisting of three or four hydraulic cylinders those are connected to the cylinder wall to absorb the excitation force caused by the wave or the floating vessel. As we have already discussed earlier in our report that failure of those cylinder devices is major limiting criteria for monopile initial hammering process so here we will discuss the effect of the correction force and welding seam on the gripper device. We have also conducted the sensitivity analysis of the cylinder and monopile properties.

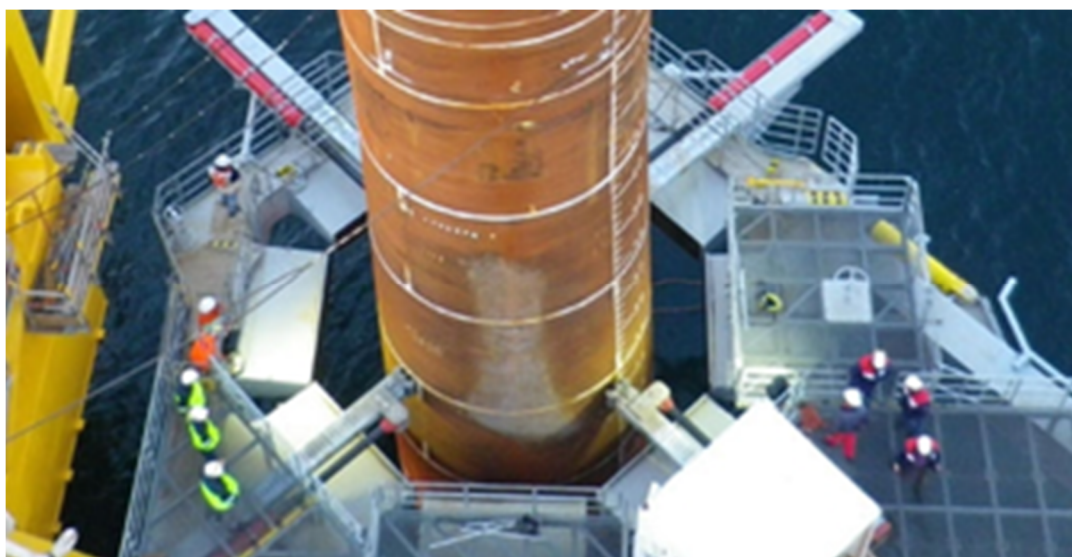


Figure 14: Typical Gripper device configuration

3.1 Problem Statement

During global analysis, we have shown that the global responses of the hydraulic cylinder for different sea states and penetration. If we add axial compression force induced on the gripper device due to the correction of inclination, then those forces can be considered as a quasi-static force. On the other hand, due to the downward movement of the MP, the impact between welding seam of the monopile and the roller will formulate a dynamic problem that will also introduce additional axial and non-axial load which is important for the failure analysis of the cylinder and this phenomenon cannot be captured during the global analysis. So, in this section first we will apply that quasi-static axial load on the hydraulic system then

we will simulate the hammering operation to find out the stress concentration and displacement at different parts of the system. From there we can identify the local limiting criterion like the maximum speed of the MP, size of the roller, type of hydraulic fluid and type of seal, etc. As identifying the limiting parameter of the operation is our future goal so here we will only discuss the result of the analysis.

The hydraulic cylinder might fail due to the,

- Bending of the cylinder Piston,
- Buckling of the cylinder piston,
- leakage of the hydraulic fluid due to the non-axial load caused by the welding seam,
- Plastic deformation
- Excessive reaction force.
- Failure of the rollers system

So first we have discussed Gripper - monopile set up then we have generalised the system to transform an Abaqus model and finally simulate the static and dynamic problem.

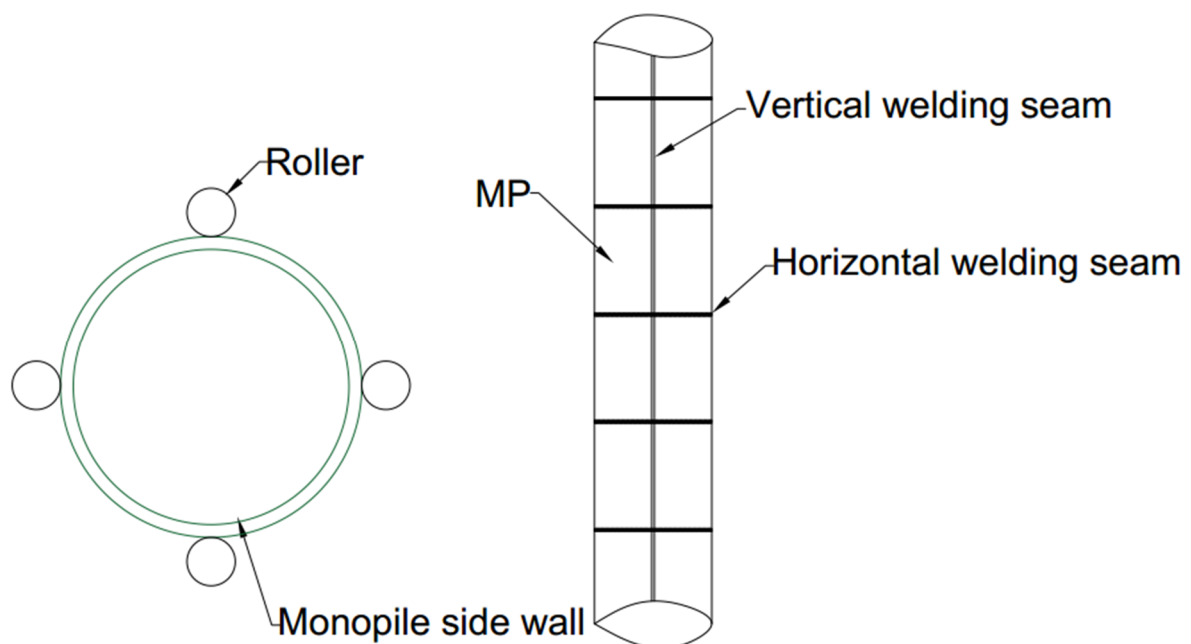


Figure 15: Top view of Gripper (roller) monopile system and side view of monopile with welding seam.

Generally, a monopile is a hollow pipe (Figure 15) which is constructed with a separate ring-shaped smaller segment. Those segments are constructed by bending and welding flat plate. Later those rings are welded by full penetration welding from the both side. So the surface of the monopile is not smooth rather it contains welding seam which has curvature like shape (figure 16).

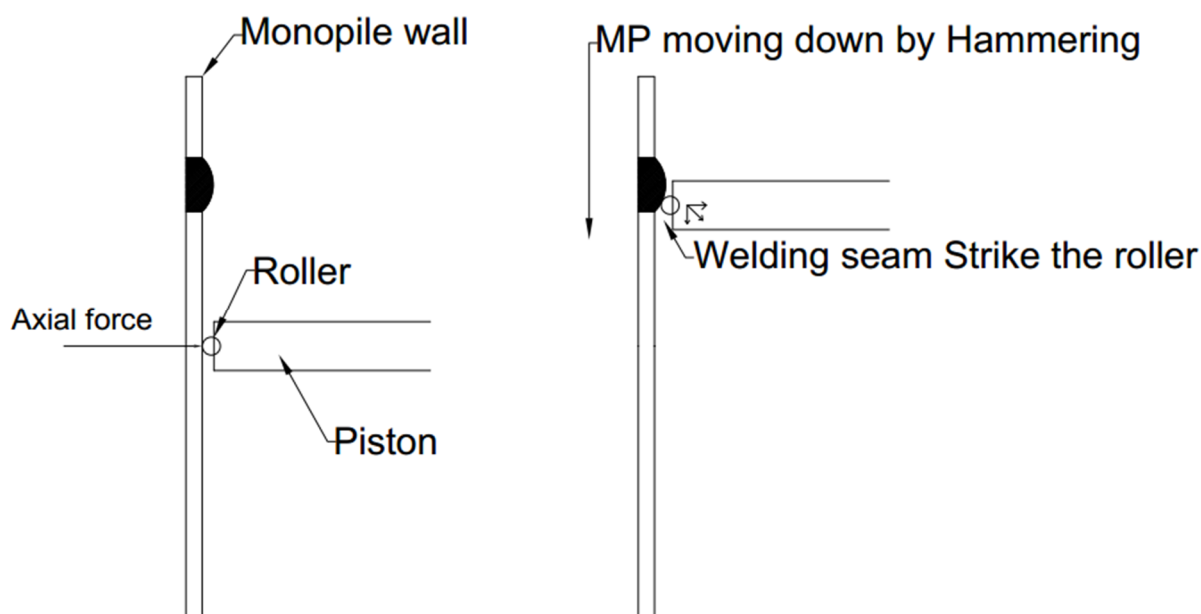


Figure 16: Monopile wall and roller contact and when roller hit the welding seam

During the installation phase, a compressive force applied on the monopile wall by the gripper [2.5.3]. Moreover, due to the wave and soil reaction, an external force is applied to the roller. Additionally, during the correction of the inclination of the MP, an external force is applied by thruster or mooring device. Though, all of these forces acts perpendicular to the Monopile wall.

During the hammering process, the monopile moves into the soil while gripper hold in upright position and mitigate all the external disturbance (motion). But from the figure 16, we can see that when roller hit the welding seam then the forces do not act perpendicular to the cylinder. The external forces and initial compressive force will be divided into both perpendicular and horizontal direction and the moving velocity of the monopile will also increase the force that might affect the cylinder mounting, seal, roller and Piston. So the problem can be divided into two different problems. Those are:

- The static problem, when hammering process is stopped but environmental force, initial compressive force and external force (correction force) will be active.
- The Dynamic problem, when there is no external force but monopile is moving, environmental and compressive force is active.

3.1.1 Basic Layout of the Gripper Monopile System

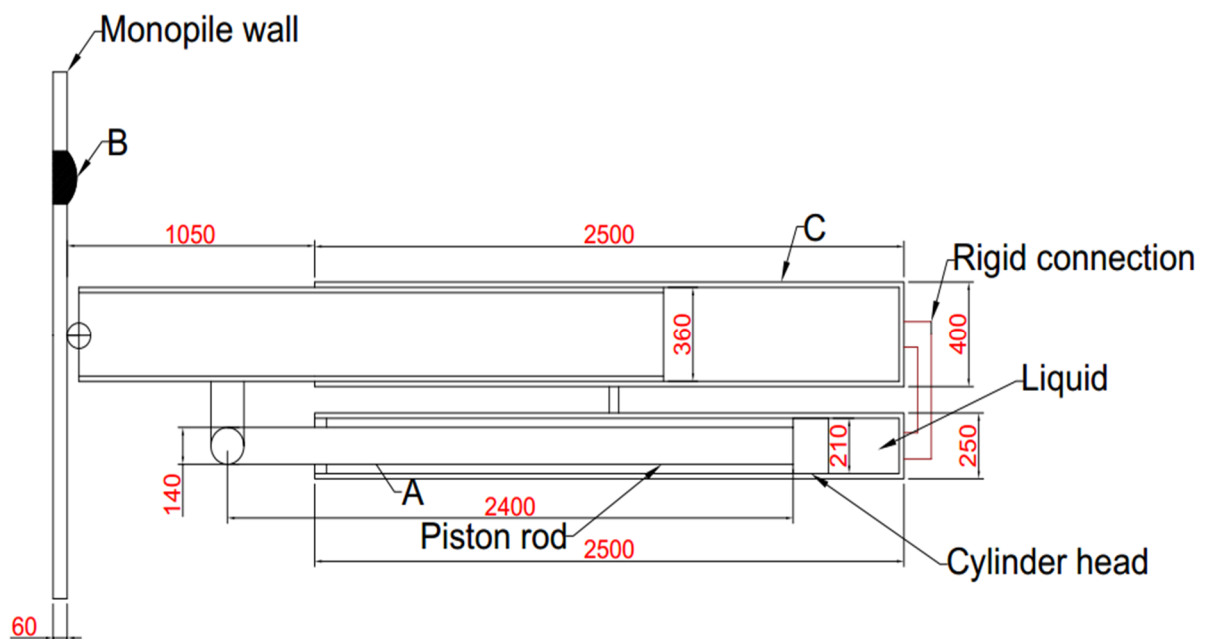


Figure 17: Basic layout of the gripper system during initial hammering.

Figure 17, shows the typical layout of the gripper system. Where, a cylinder is connected with an extendable, hollow square sliding arm by pin joint while the arm is connected with the monopile wall by a roller. So the arm takes the load from the monopile and then transmits it to the cylinder. Both cylinder and arm are rigidly connected together at the back and in the middle.

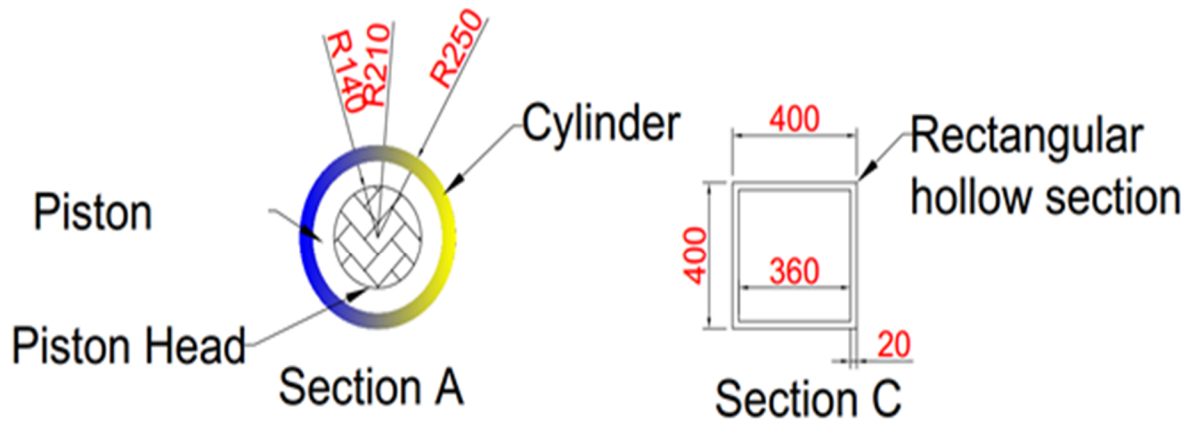


Figure 18: Details of Section A and C

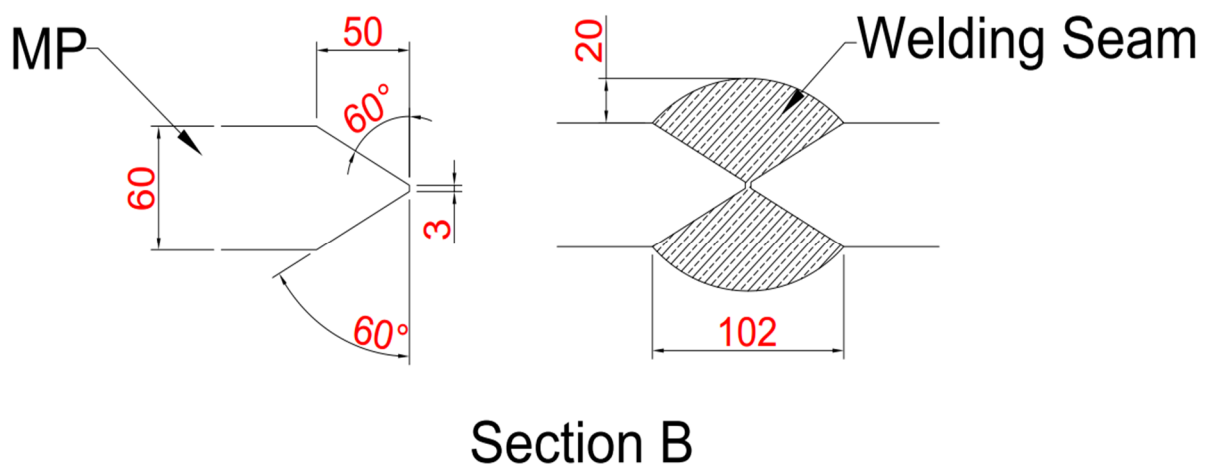


Figure 19: Welding details, section B

Figure 17, shows the welding details of the welding seam which is designed as per AWS and IACS 47 standard. It is a full penetration welding with bevelling 60 degrees on both sides and MIG welding procedure was followed. After welding the capping of the welding seam considered is 20 mm which is the maximum allowed (one-third of the plate thickness, DNV GL rule book). Later during the sensitivity analysis 10 mm and 5 mm capping was also considered to see the stress development on the cylinder.

3.1.2 Simplified Model

The initial detail model is simplified to the figure 20 model, where the square arm is replaced by the spring K_1 that is calculated by considering the arm as a cantilever beam and applied the load at the end of the beam (Appendix 02). The liquid in the hydraulic cylinder is modelled as a spring with stiffness K_2 [5]. Two pin support joint is applied, one at the forward portion and another one at the back of the cylinder to represent the connection between the arm and the cylinder body. The seal is modelled as a different material.

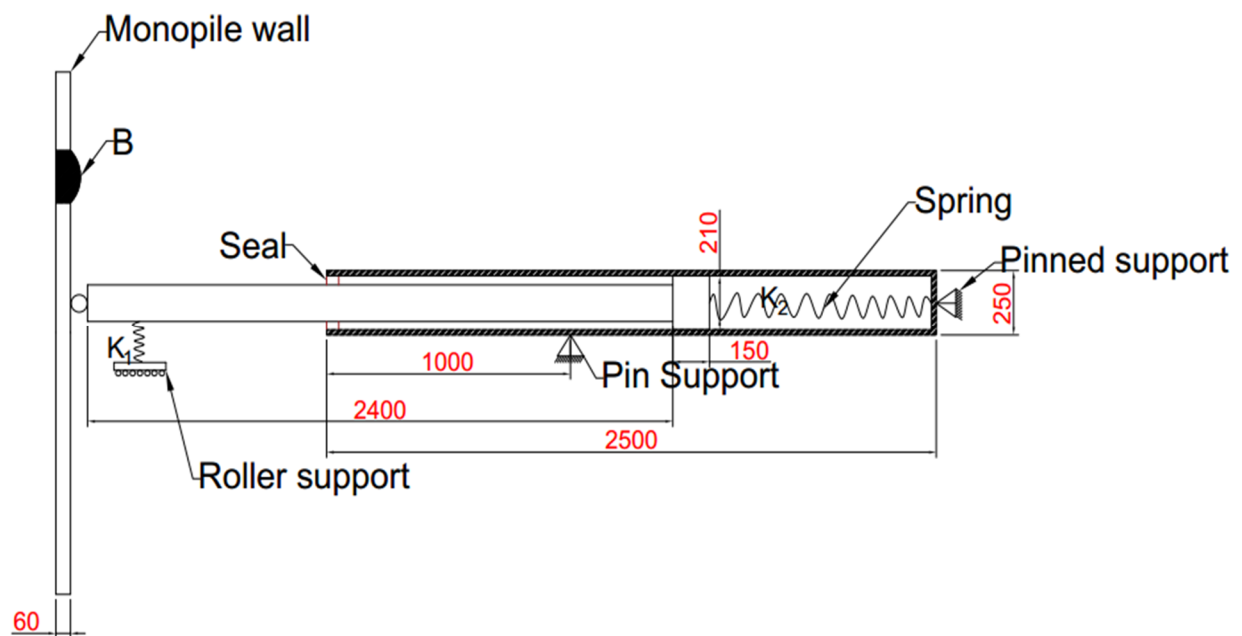


Figure 20: A Simplified model for Abaqus.

3.2 Fundamental Theory

The general procedures for solving non-linear analysis and the principle of virtual work is applicable to contact-impact problems and can be found in Finite Element (FE) textbooks like [10], [11]. The additional terms when formulating the FE problem for contact and impact problems has to do with the contact area, forces and assumptions made to solve these unknowns. Because we need to solve a problem within unknown parameters which are varying in time, it is very nonlinear.

The principle of virtual work for contact-impact problems could be formulated as follows.

The following formulation is valid is general and valid for elastic material and classical Coulumb friction law.

$$\delta W_S - \delta W_R - \delta W_C - \delta W_I = 0 \quad (14)$$

$$\int_{\Omega} {}^t \sigma \delta \varepsilon d\Omega - \int_{\Omega} {}^t b \cdot \delta u d\Omega - \int_{\Gamma_F} \bar{q} \cdot \delta u dS - \int_{\Gamma_c^2} {}^t q_i \cdot (\delta u^2 - \delta u^1) \cdot {}^t N_i^2 dS + \int_{\Omega} {}^0 \rho^t a \cdot \delta u d\Omega = 0 \quad (15)$$

Together with equations (14) and (15) the following conditions have to be satisfied [12], [13]:

1. Constitutive equation

$$\sigma = C\varepsilon$$
2. The initial conditions for velocities and displacements
3. Linear momentum balance
4. The boundary conditions for the forces and displacements on their respective boundaries
5. The contact conditions are summarized as follows:
 - The normal contact force in positive
 - The penetration between the hitting node and a target point at any time instant is zero
 - The tangential contact force is equal to the contribution of the tangential components and is less or equal than the normal force times the friction coefficient
 - The contact force is zero in other regions outside the contact area

- Sliding or stick condition depending on the friction coefficient and tangential contact force
- The gap is less than or equal to zero

Contact detection (searching):

Different types of algorithm are used to find the contact nodes, example:

- Master-slave algorithms
- Hierarchy-territory contact searching algorithm (HITA)
- The linear positioning c
- Ode algorithm
- The space filling curve algorithm
- The local gap function algorithm
- The local pinball algorithm

In our problem, we have used Master-Slave algorithms.

Master-slave algorithms:

The searching procedure is summarized as follows.

- Find a slave node in the expanded master territory (not in contact)
- In case a closer slave node is not matched with a segment and approaches a master node, then a match between both nodes is chosen.
- For a slave node with several master segments, the one with the closest distance is selected.
- If a slave contacting node slides away from the segment territory it will be checked against another segment territory.

3.3 Numerical Modelling

3.3.1 Properties of the Cylinder and Arm

For our study, we have chosen a hydraulic cylinder from Company 'IHC Vremac Cylinders' with type '210 bars'. The details of the hydraulic cylinder and the square arm are given the table below:

Cylinder Properties : Type: IHC Vremac Cylinder, 210 bars [14]			
	Dimension	Material	Mass
Bore/cylinder diameter	250 mm	Steel	
Piston rod diameter	140 mm	Steel	
Piston head area	49090 mm ²	Steel	40 Kg
Piston rod area	15390 mm ²		290 Kg
Pushing force	491 KN		
Pulling force	337 KN		
Length of the cylinder	2000 mm		
Length of the piston head	150 mm		
Length of the piston	2550mm		
Dimension of the square arm	400 x 400 mm*mm	Steel	
Thickness of the cylinder wall	20 mm		
Thickness hollow square arm	20 mm		
Stroke length of the cylinder (max)	2400 mm		
Horizontal environmental and correction compression force	400 KN(from Lin Li paper)		
Spring constant K1	4.89x10 ⁷ N/m		
Spring constant K2	3x 10 ⁷ N/m		
Damping C	3 x 10 ⁶ N/m		
Velocity of the Monopile	0.2, 0.4,0.6,0.8 m/s		
Monopile wall thickness	60 mm		

Table 4: Properties of the gripper system

3.4 Abaqus Modelling

SIMULIA Abaqus 6.14, NTNU student version is used to simulate the gripper problem. Abaqus analysis is divided into two problems. First, one is static, where axial correction and environmental force is applied directly on the cylinder and interaction with the monopile was ignored. Second, the problem is dynamic explicit, where interaction with the MP was observed. Note that, in this phase external correction force was ignored because this force can only be applied when MP is stable and the inclination angle can be measured. Moreover, Environmental force is not considered which is very low compared to an external force, to simplify the problem.

3.4.1 Modelling

The Unit used in the Abaqus for length, Force and stress are Metre(m), Newton(N) and Newton/Metre(N/m).

Cylinder:

This part is created from '**Part**' module by solid revolution, which is a 3D object and deformable. Only half of the model was created due to the symmetry of the object. Four planes were created at the XZ plane with different distance from the origin (at the back of the cylinder) to divide the whole object for the requirement of the meshing and constraint module.

Datum Plane-1: 50 mm

Datum Plane-2: 2470 mm

Datum Plane-3: 1800 mm

Datum Plane-4: 1950 mm

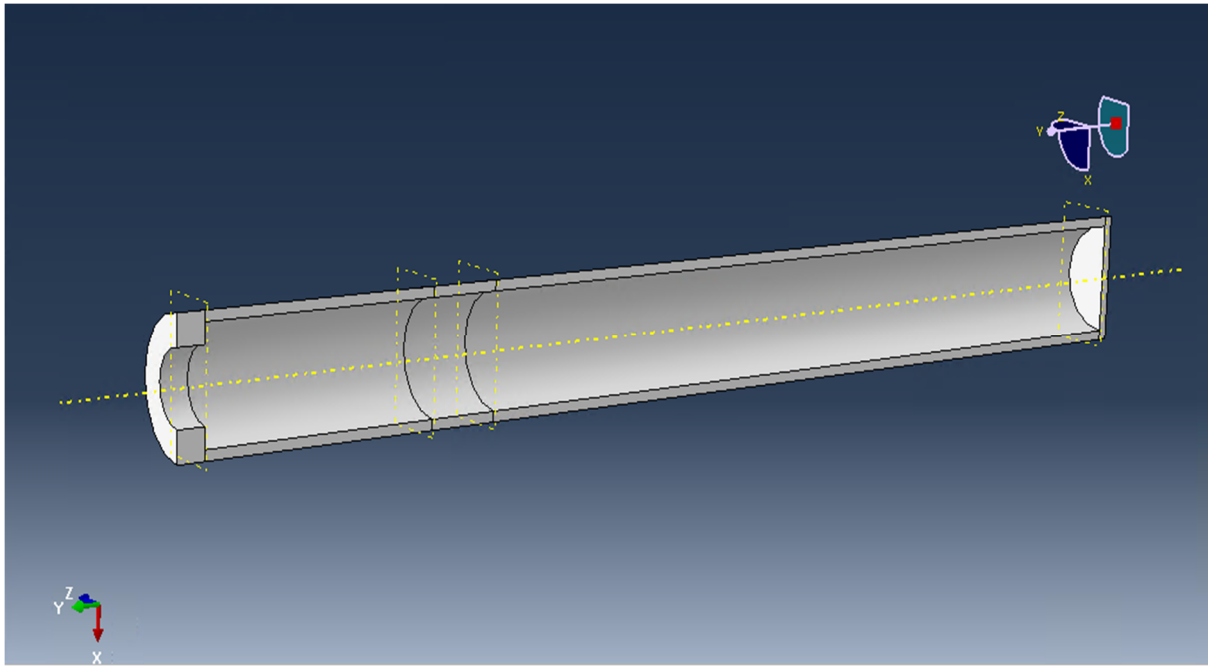


Figure 21: Cylinder model

Piston:

The piston has been created similarly from the '**Part**' module by solid revolution. Three Datum plane was created this and the whole object was divided into four parts for the ease of meshing later.

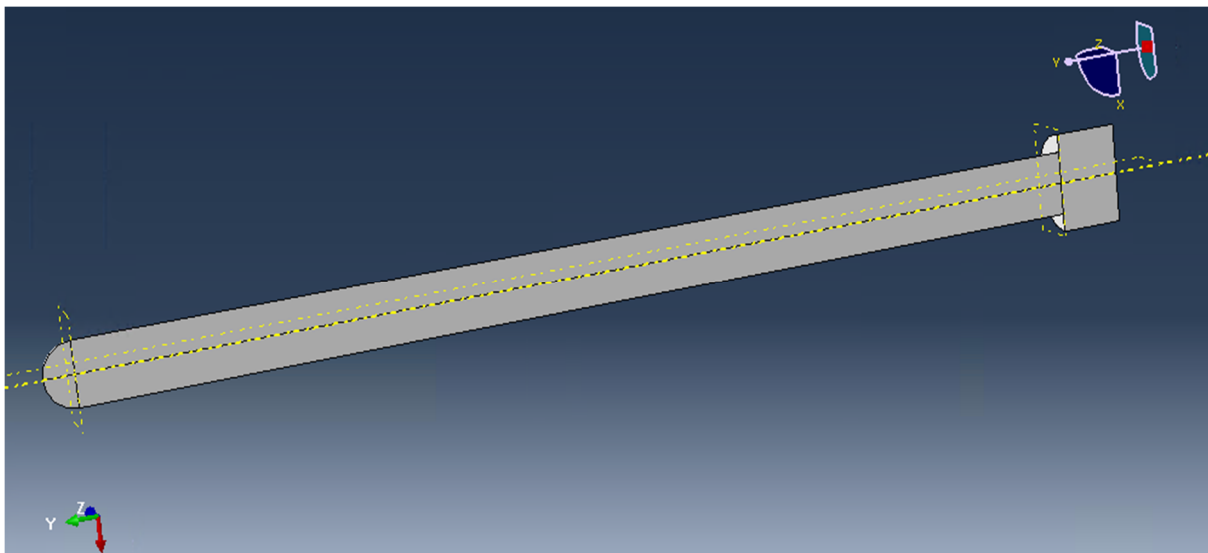


Figure 22: Piston model

Monopile:

Only a portion with dimension (500 mmX500 mm) of the MP wall was created by solid extrusion. This part is deformable.

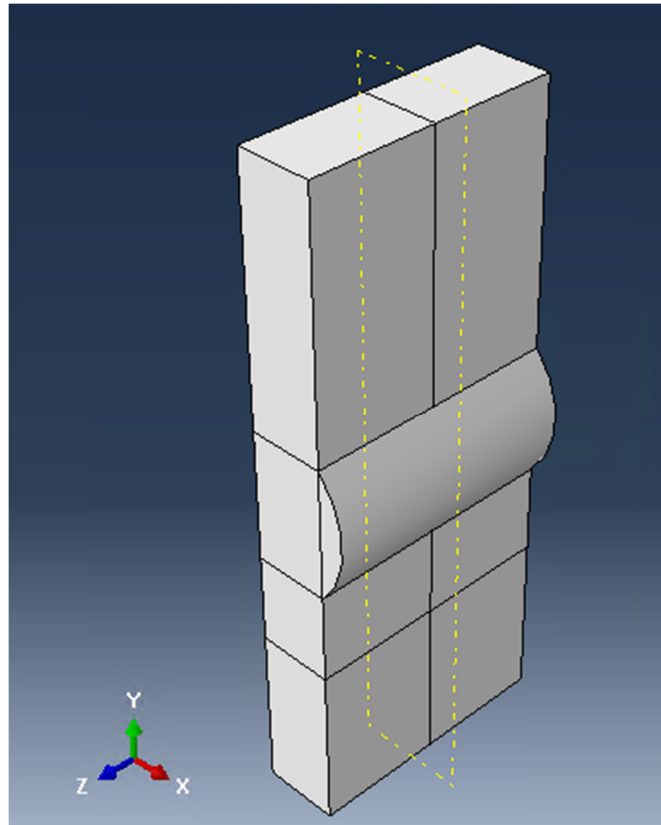


Figure 23:MP wall Model

3.4.2 Material Assignment

Two different Materials were created; those are:

- Steel
- Gasket

Steel:

Elastic properties:

density = 7850 Kg/m^3 ,

Young's Modulus: $2 \cdot 10^{11}$

Poisson's Ratio: 0.3

Plastic properties:

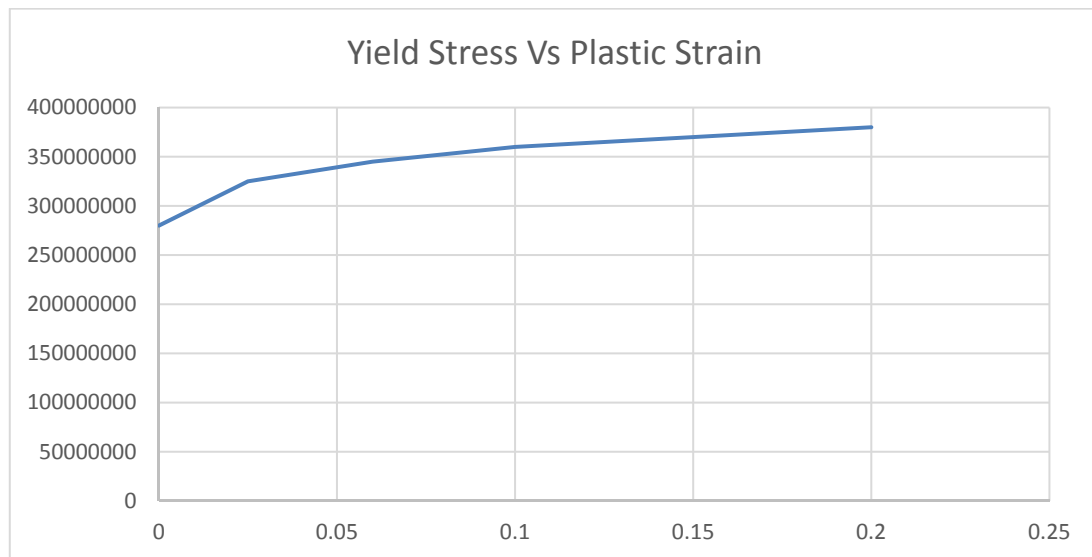


Figure 24: Plastic properties of steel from the elastic limit

Gasket:

Density: 2000 Kg/m³

Young's Modulus: 100*10⁰⁸

Poisson's Ratio: 0.45

During the static analysis gasket material was applied between piston cylinder neck connection but to simplify the problem, for dynamic analysis all the objects were modelled as a steel material. [15]

3.4.3 Assembly

All the three parts MP, cylinder and piston were assembled by **Parallel Face** and **coincide points** Constraints. Piston head was placed between Datum plane 3 and 4 of the cylinder.

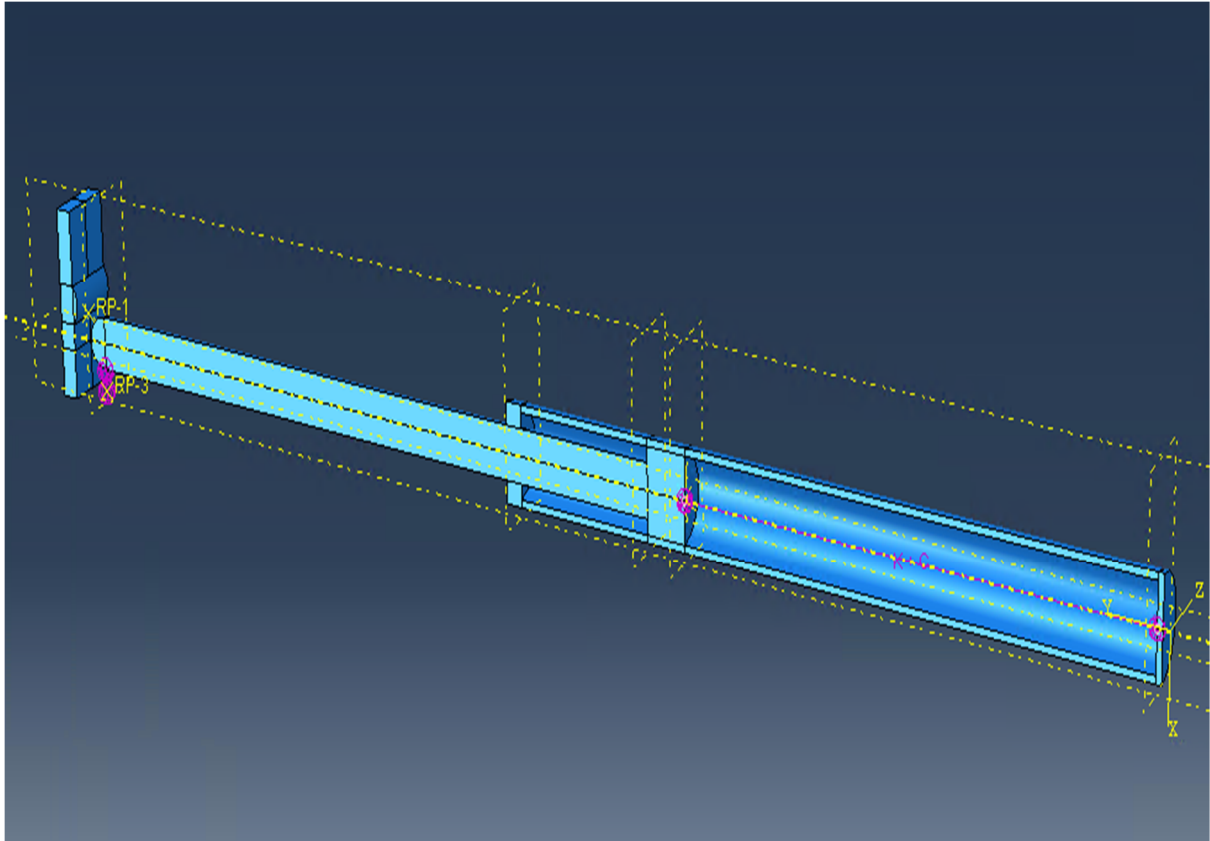


Figure 25: Assembly

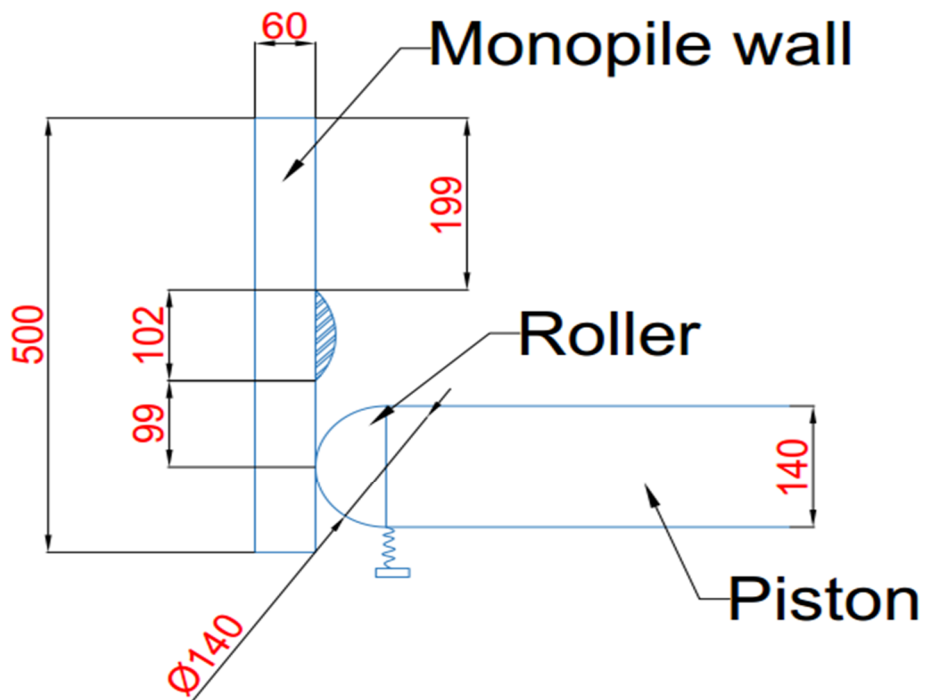


Figure 26: Details of the MP-Roller assembly

3.4.4 Interaction

Six surfaces were created during the modelling phase. Those are:

Cylinder:

1. ***Cylinder plus piston head***
2. ***Cylinder Neck plus piston rod***

Piston:

3. ***Piston head***
4. ***Piston Rod***
5. ***Piston_fore***

MP:

6. ***Monopile***

Interaction Property: Two interaction property were defined those are:

1. ***Monopile_cylinder:***

Tangential Behaviour: Frictionless

Normal Behaviour: Hard contact

2. ***Cylinder_piston:***

Tangential Behaviour: Penalty type (Friction coefficient: 0.3)

Normal Behaviour: Hard contact

<i>First Surface</i>	<i>Second Surface</i>	<i>First Surface type</i>
<i>Piston_fore</i>	<i>Monopile</i>	<i>Slave</i>
<i>Piston Rod</i>	<i>Cylinder Neck plus piston rod</i>	<i>Master</i>
<i>Piston head</i>	<i>Cylinder plus piston head</i>	<i>Master</i>

Table 5: Interaction formulation

Two datum points were created, first one, on the on the surface of the Piston and another one at the back of the cylinder. Then these two points were transferred to two new datum plane. **Coupling** constrained were applied between point and relevant surface. For static analysis, **Structural distribution** coupling and for Dynamic explicit analysis **Kinematic** coupling type were used (Appendix 05). From Special interaction module, a spring(k_2) with damper(C) was assigned between this two points. As the spring element can only be applied between two points where stress concentration will be much higher and incorrect so to avoid this problem, above coupling between point and surface was created.

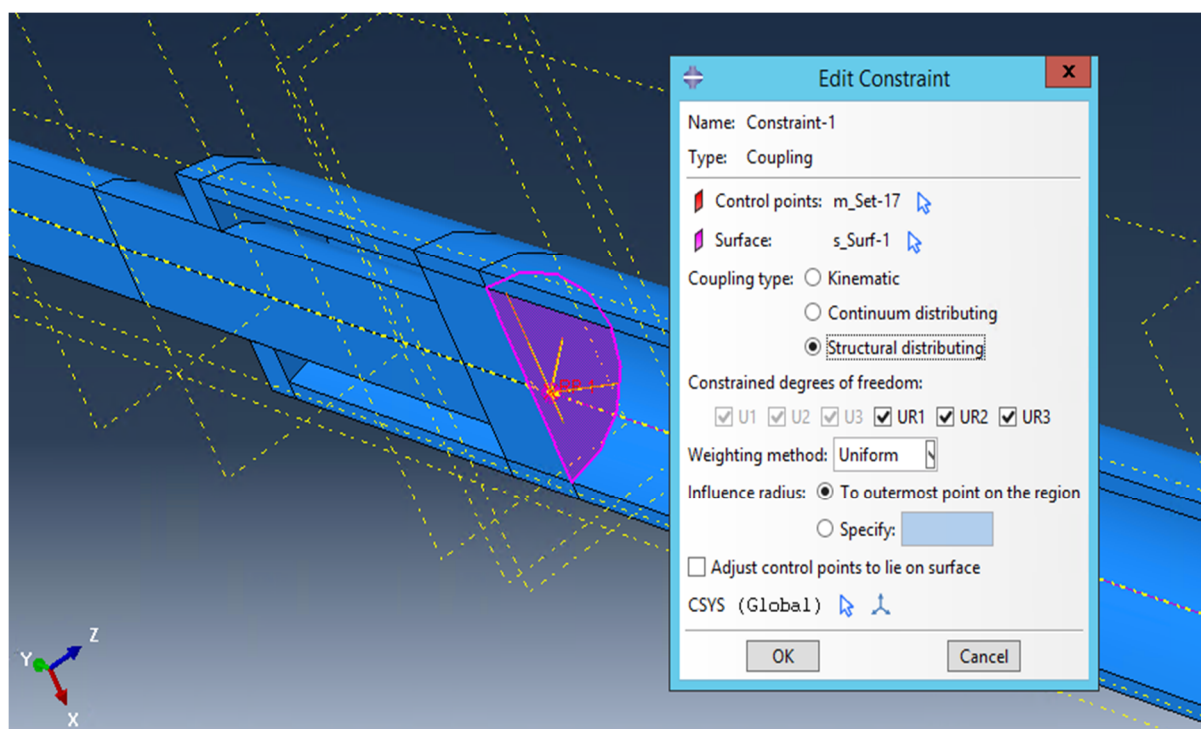


Figure 27: Example of the structural coupling on piston back surface

Another reference point was created below the fore part of the piston head and another spring with stiffness k_1 was attached between this reference point and the end point of the piston. No coupling was applied here as we are not going to measure any stress at this connection point.

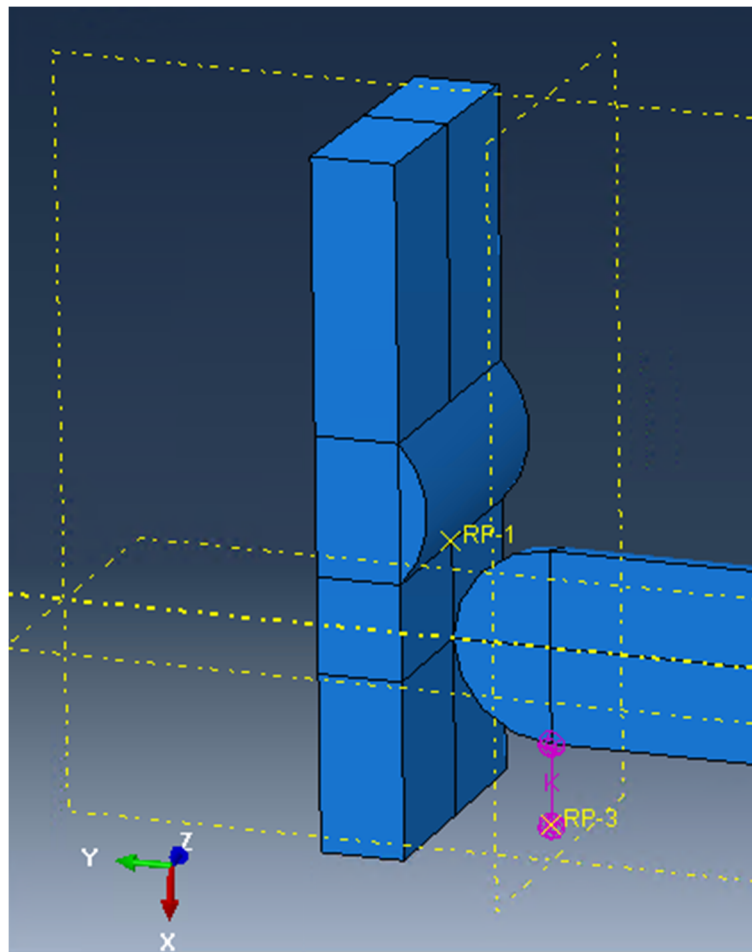


Figure 28: Spring, represents the arm

3.4.5 Step

After the **initial step**, for static analysis **Static, General** step was created with Nlgeom (non-linear effect) on and for MP movement problem, **Dynamic, Explicit** step was created. During **dynamic, explicit** analysis automatic time increment was selected but max time increment was limited to 0.001 seconds to avoid the unstable stress concentration. From the calculation at appendix 04, it was found that max time step for stability is 0.00221 seconds. **The time period** of the analysis was set according to the speed of the MP. **Field Output Request** was asked for **every x unit of time**, where x was set according to the **Time period**. The natural frequency of the piston was found 48.22 Hz.

3.4.6 Boundary Condition

Name of the BC	Position	Properties of the BC
Cylinder	Back of the Cylinder	$U1=U2=U3=0$
Cylinder_mid	On the surface of the cylinder between Datum plane-3 & 4 created in <i>Modelling</i> module	$U1=U2=U3=0$
Symmetry_Cylinder	The surface of the cylinder, from where it creates a mirror image.	$U3=0, UR1=UR2=0, ZSYMM$
Symmetry_Piston	Same as cylinder, but for Piston surface.	$U3=0, UR1=UR2=0, ZSYMM$
Monopile	Four outer corner points of the MP.	$U2=U3=0, UR1=UR2=UR3=0$
Velocity(only in dynamic analysis)	Whole MP	$V1= 0.2,0.4,0.6,0.8 \text{ m/s}$
Spring	End point of the forward spring K_1	$U1=U3=0, UR1=UR2=UR3=0$
Pressure (only static analysis)	On the piston face	XZ plane

Table 6: Boundary conditions and load description

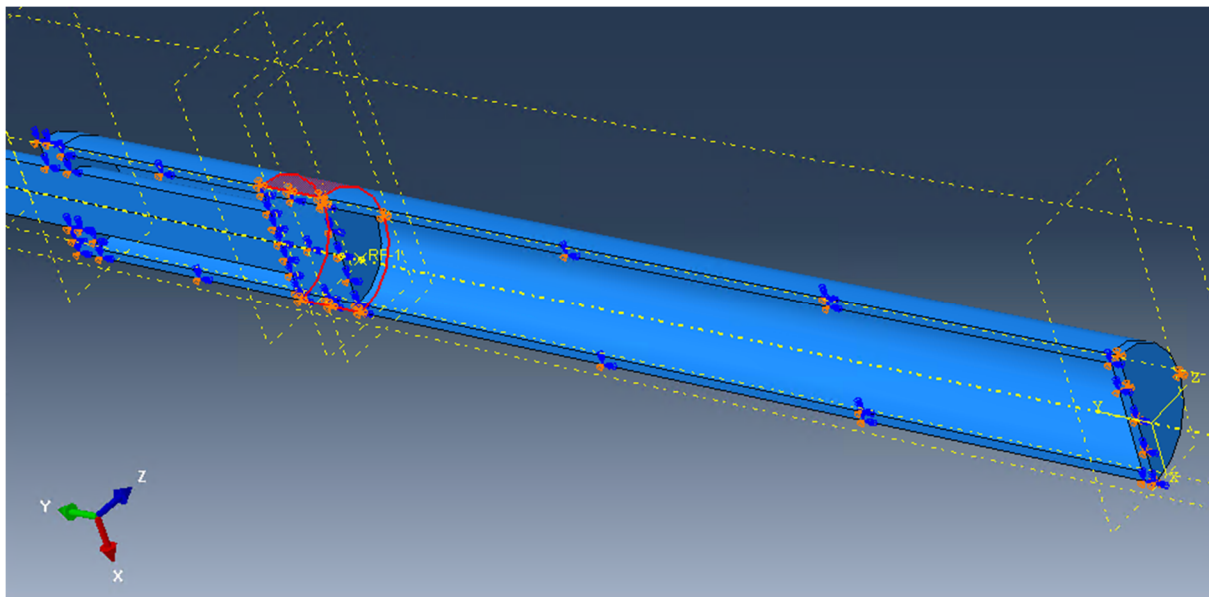


Figure 29: BC, Cylinder_mid indicated by red colour and Symmetric BC of Piston and Cylinder

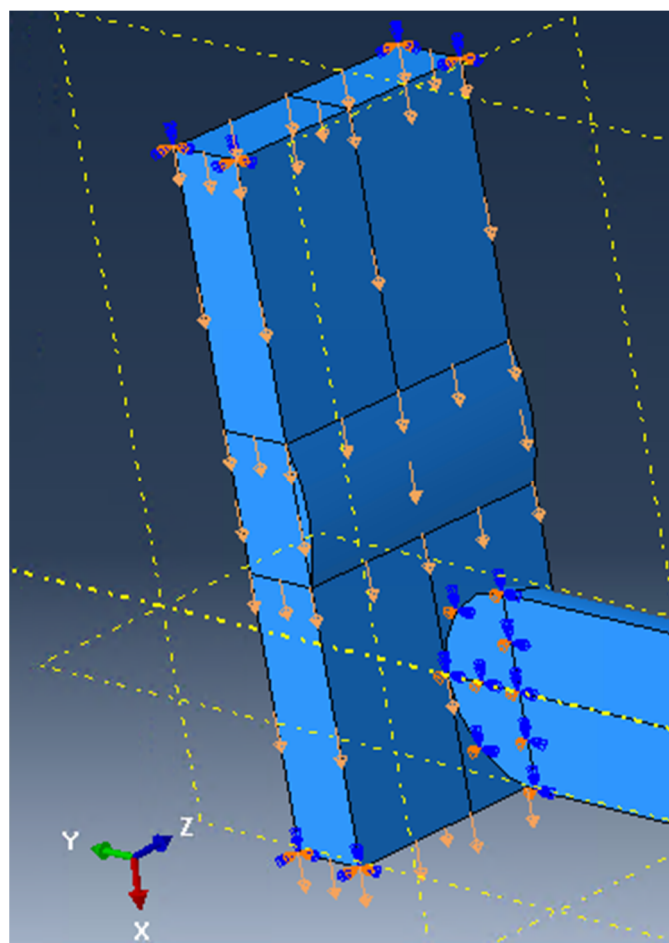


Figure 30: Boundary condition of MP and Piston

3.4.7 Meshing

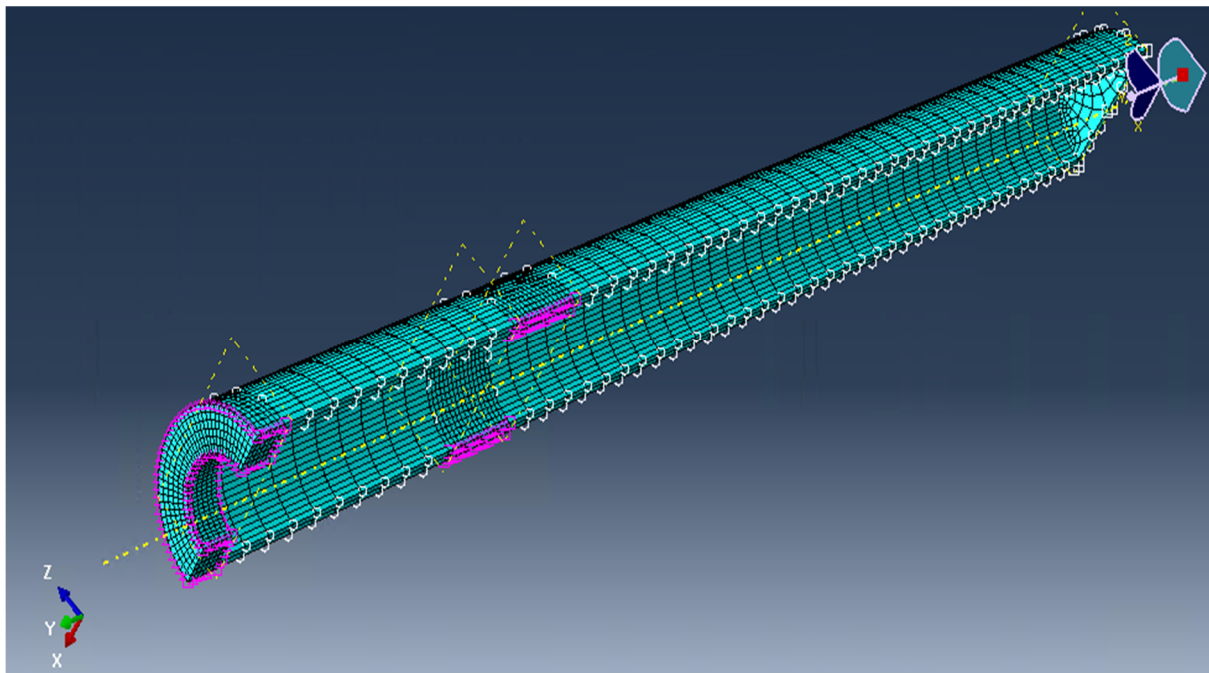
Element type:

- C3DR: An 8-node linear brick element (3D stress)
- Hex dominated
- Reduced integration
- Kinematic split: average
- Hourglass control

For cylinder and Piston:

Global element size: 50 mm

Local element size: 10 mm at interaction area and the critical area indicated in the picture below.



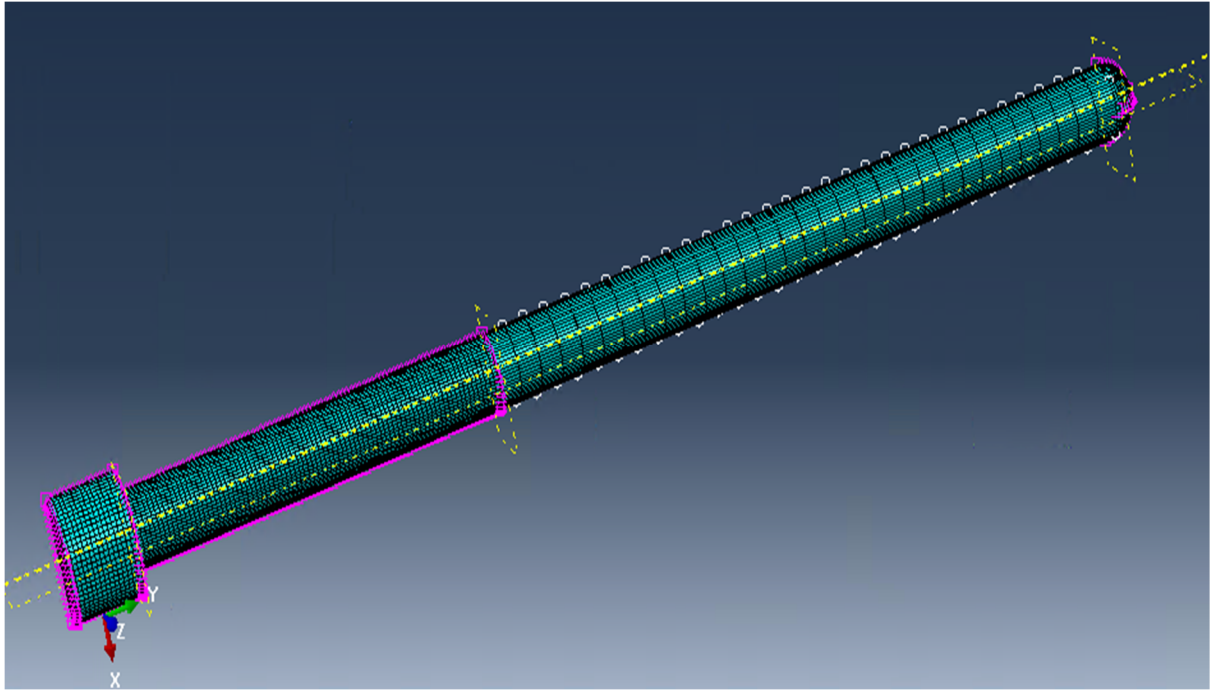


Figure 31: Local and global Mesh at cylinder and Piston.

For MP:

Global element size was 30 mm.

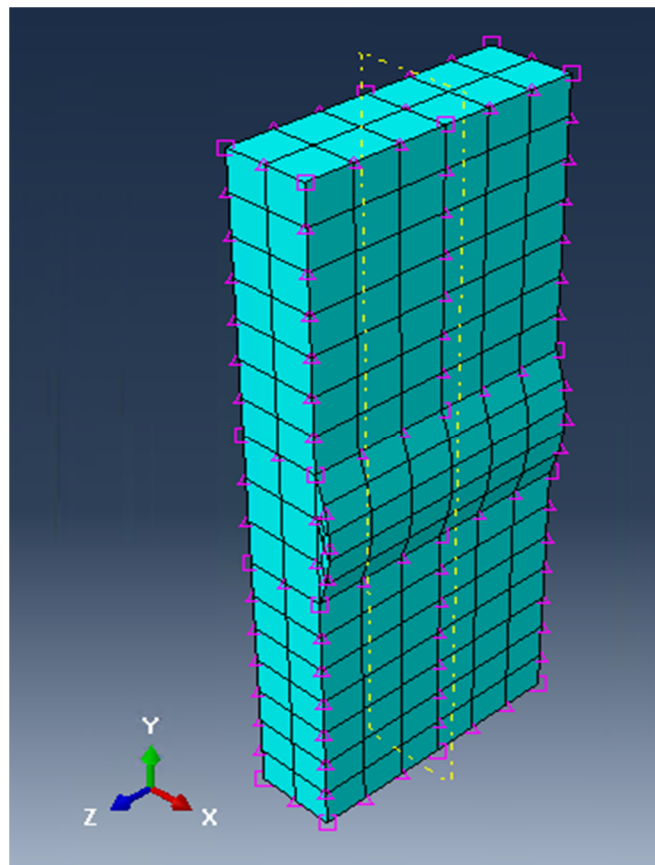


Figure 32: Mesh at MP

Mesh Sensitivity Analysis

During the static analysis which is discussed elaborately in the later part, five element size of 10mm, 20 mm, 30 mm, 40 mm and 50 were applied as global element size and load was applied at the end of the cylinder. The results were listed in the following table:

Element Size (mm)	Max Stress (MPa)
10	25.98
20	25.95
30	25.71
40	25.77
50	25.81

Table 7: Element size Vs Max Stress

From the above table, we can see that changing mesh size from 10 mm to 50 mm will change the maximum stress less than 1 %. So During our Static analysis we have taken the global mesh size 10 mm but during the dynamic explicit analysis, the global mesh was defined 50 mm but in our interest areas, we have chosen a mesh size between 10 to 30 mm to reduce computation time and data volume.

4. Analysis and Result

4.1 Static Analysis

From Lin Li's paper, it was found that for this type of cylinder maximum allowable force induced on each cylinder due to the correctional and environmental force was 400 KN. We have converted this force into pressure by dividing the sectional area of the piston.

Pressure,

$$P = \left(\frac{F}{A} \right)$$

$$F = 400$$

$$A = \pi r^2 = 0.15394m^2$$
(16)

Where,

r = radius of the piston rod.

From 16 we get,

Pressure $P = 2.598 \times 10^7$ (Pa)

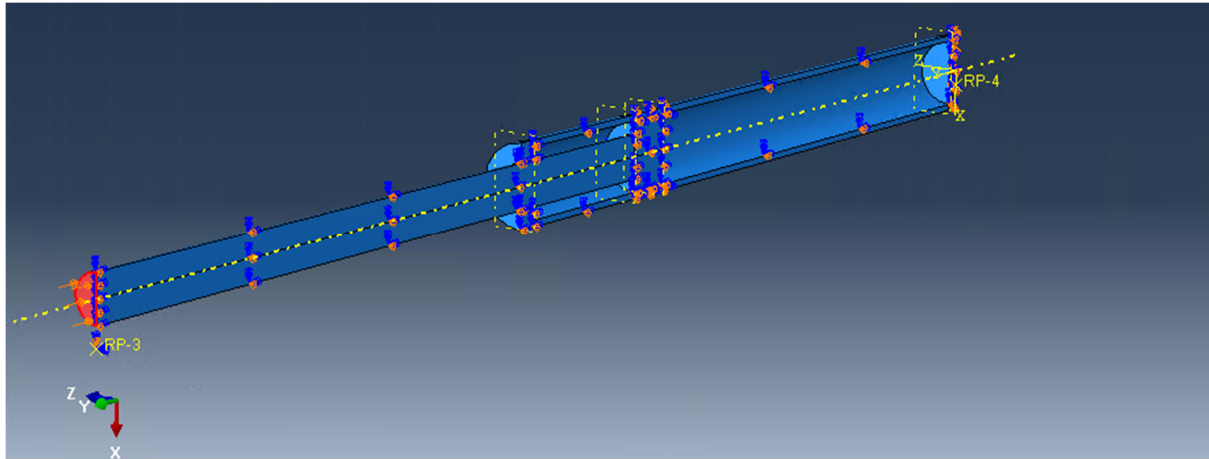


Figure 33: Pressure applied on the piston face.

4.1.1 Result

Maximum Von Mises stress found at the piston which is logical and equal as the applied stress (figure 36). We can see that the stress concentration at the back of the cylinder is quite high though in real life scenario instead of the spring there will be a fluid which will distribute the pressure not only back of the cylinder but also on the side wall. Some stress was found near the neck of the cylinder and cylinder wall on the interaction surface although the stress was very low.

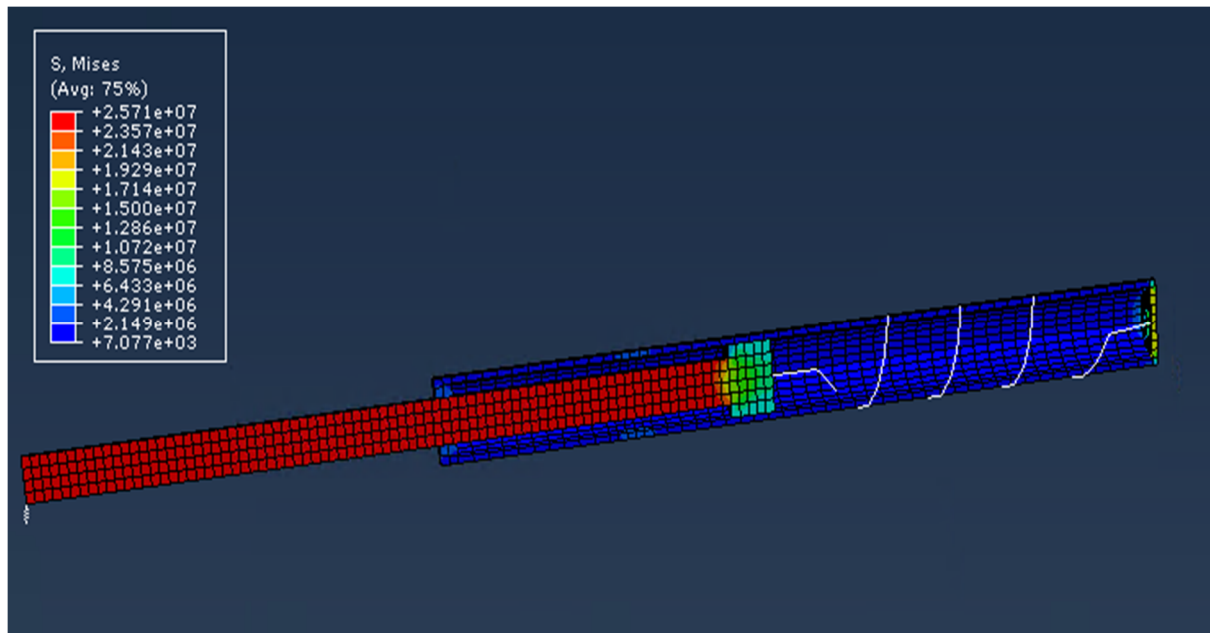


Figure 34: Static analysis

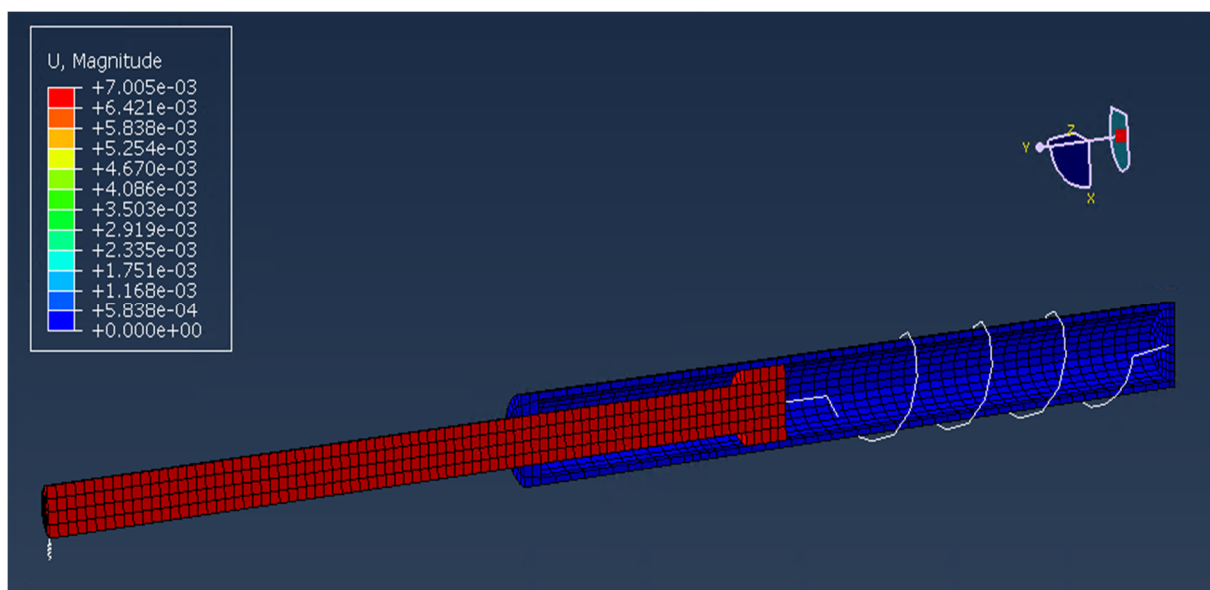


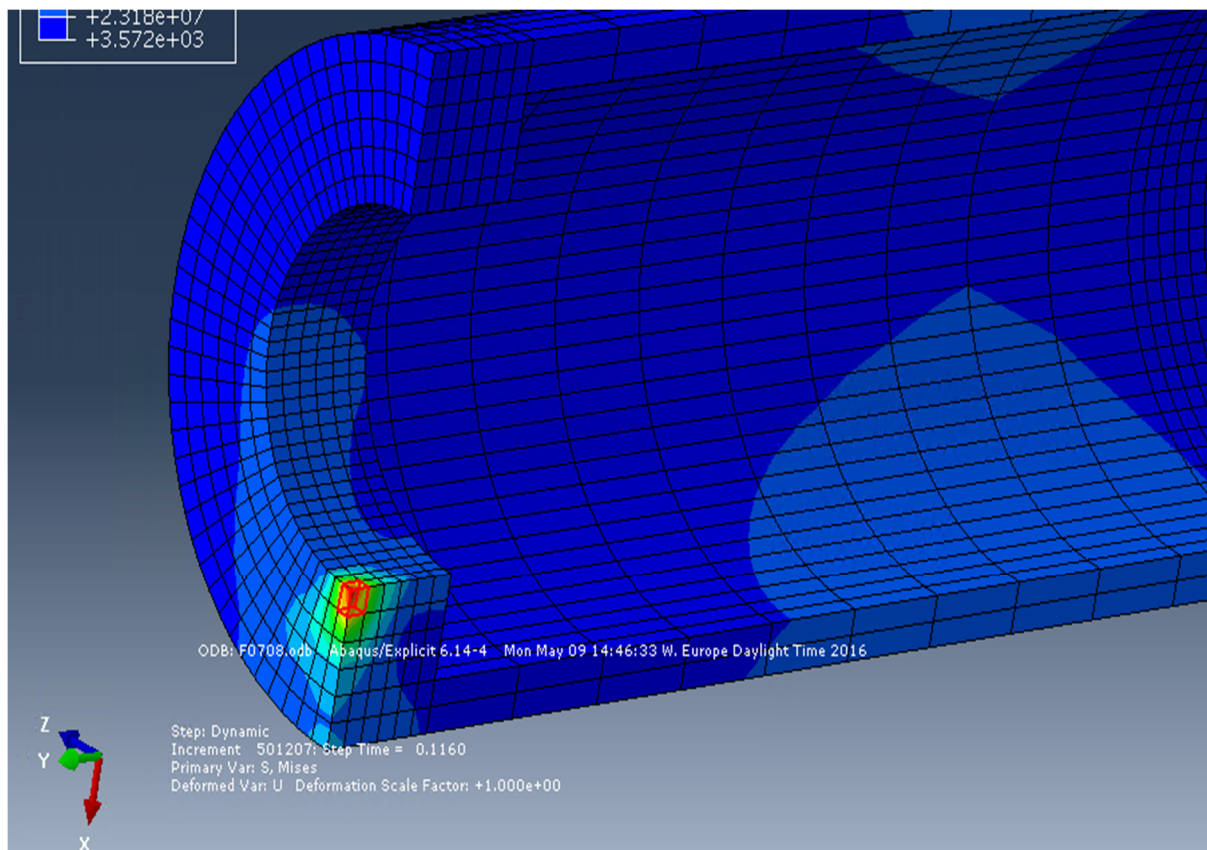
Figure 35: Displacement (mm)

The Figure 37, shows that maximum displacement occurs on the piston which is 7 mm. So we can see that no plasticity or bending occur in the system and it is possible to apply additional force. In the next step, we will do the dynamic analysis.

4.2 Dynamic analysis

Dynamic, explicit step was applied to simulate this scenario. During this step, correction and environmental force were not applied. As boundary condition was applied to keep MP and roller always in contact so pre-compression force was not applied. All the spring stiffness were taken half due to the symmetry of the structure.

The result was extracted in Von Mises stress. One particular element was selected from the cylinder(seal), piston and roller where relatively maximum stress was developed. All the results are presented from extracting results at that specific element. Position of those elements at different parts are presented in the following picture:



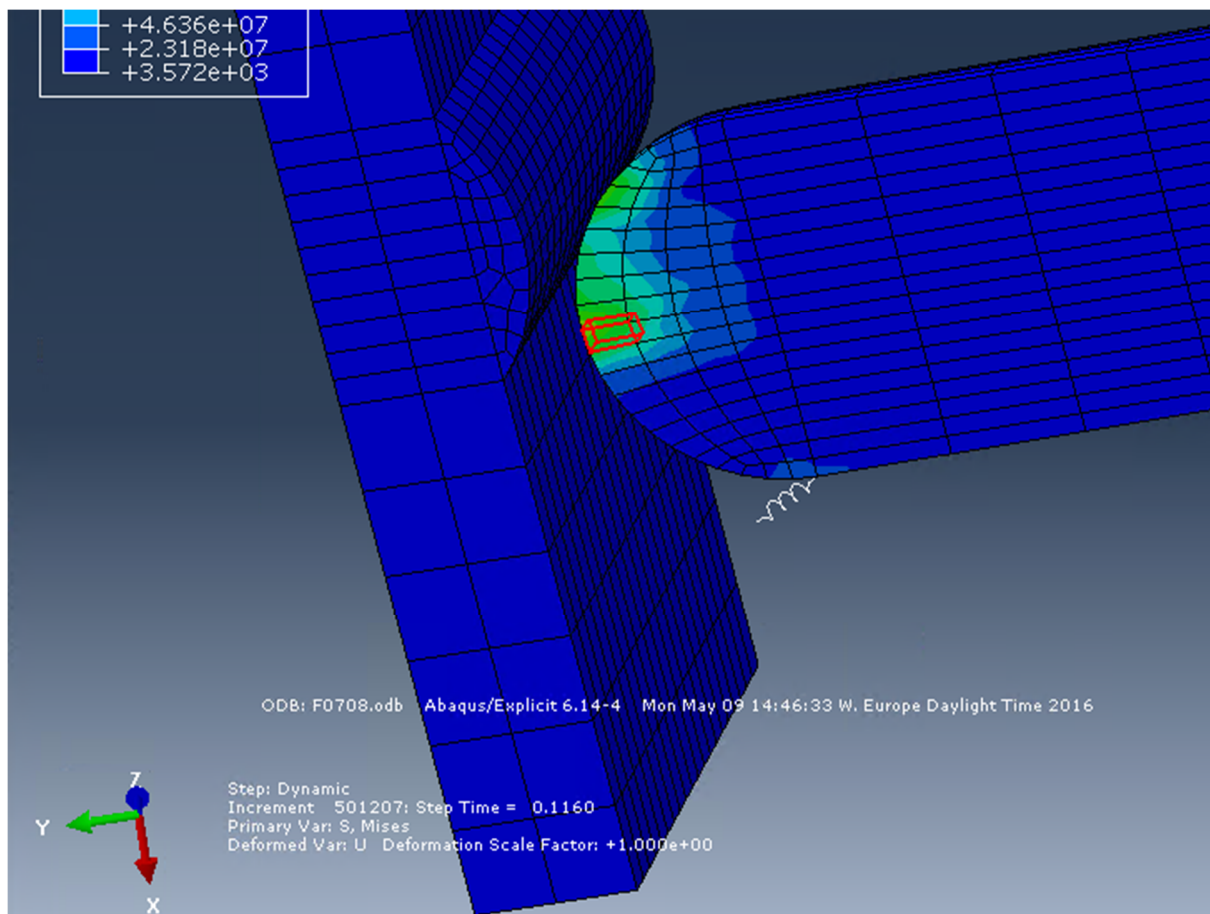
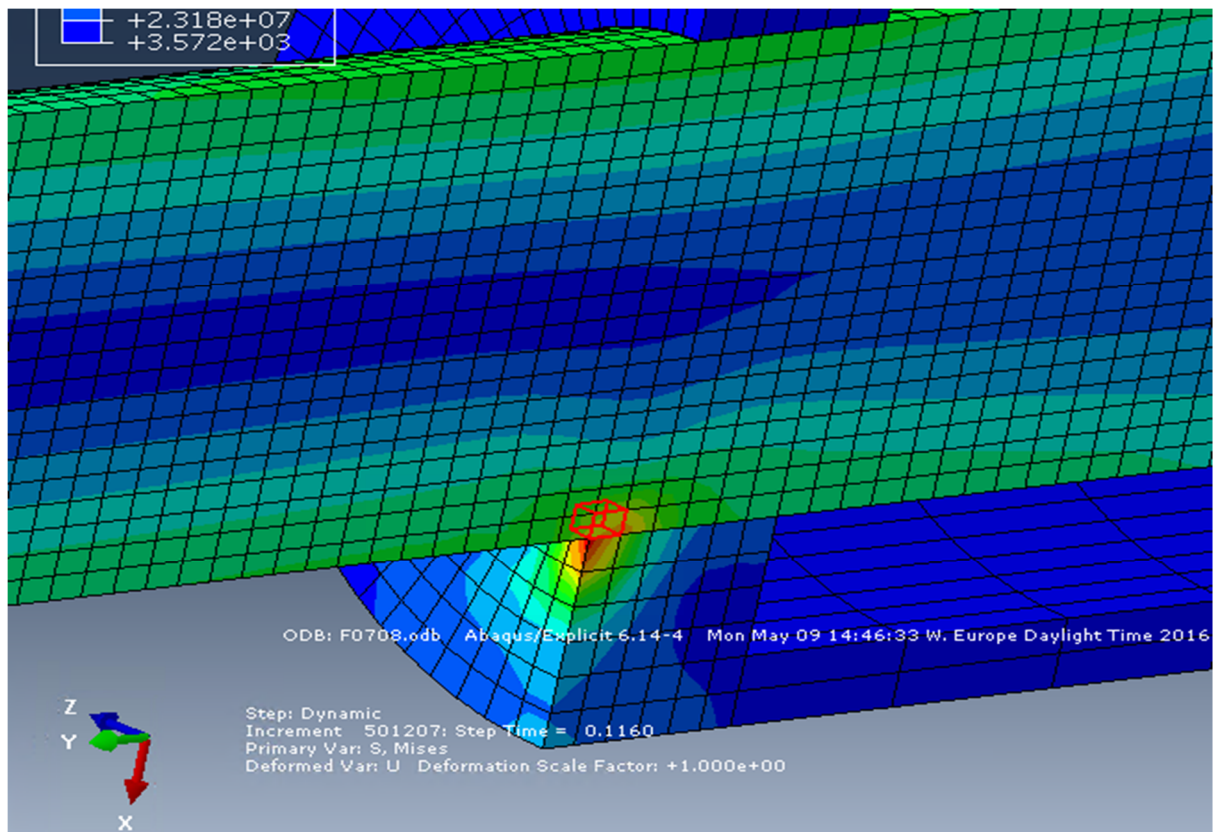


Figure 36: Reference elements for result extraction, Seal(cylinder), piston and roller

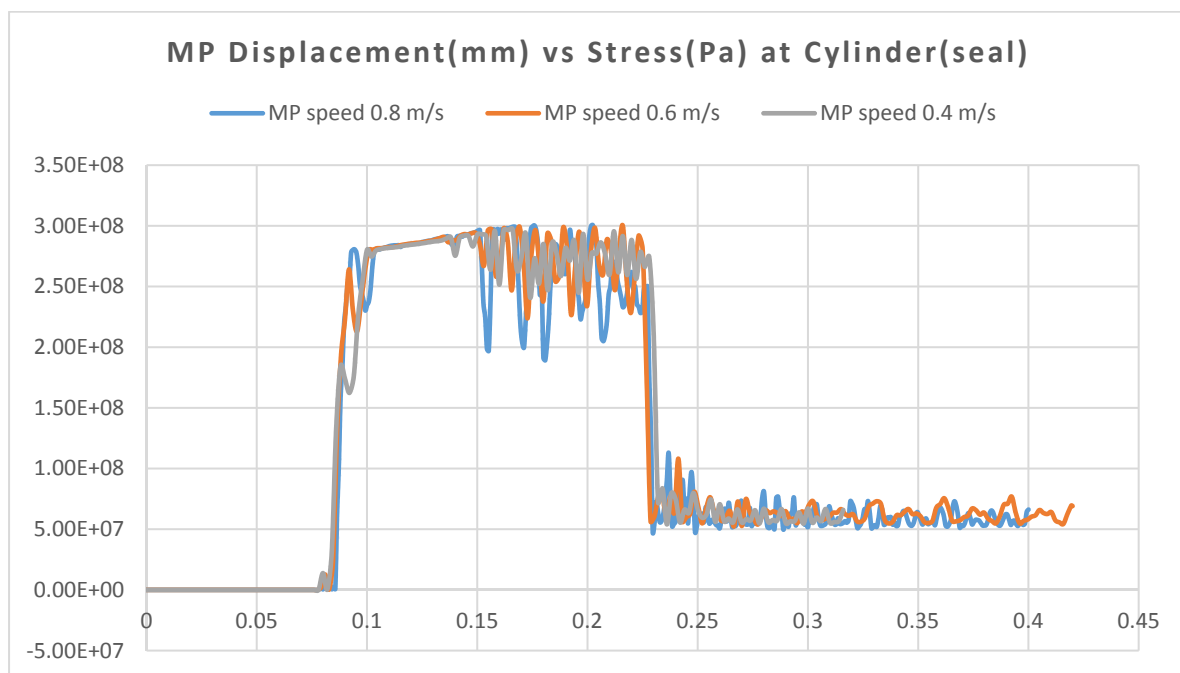
Case 1:

Capping of the MP welding seam: 20 mm

Roller size: $\varnothing 140$ mm

MP speed: 0.4, 0.6, 0.8 m/s

Other particulars same as described in the table 4.



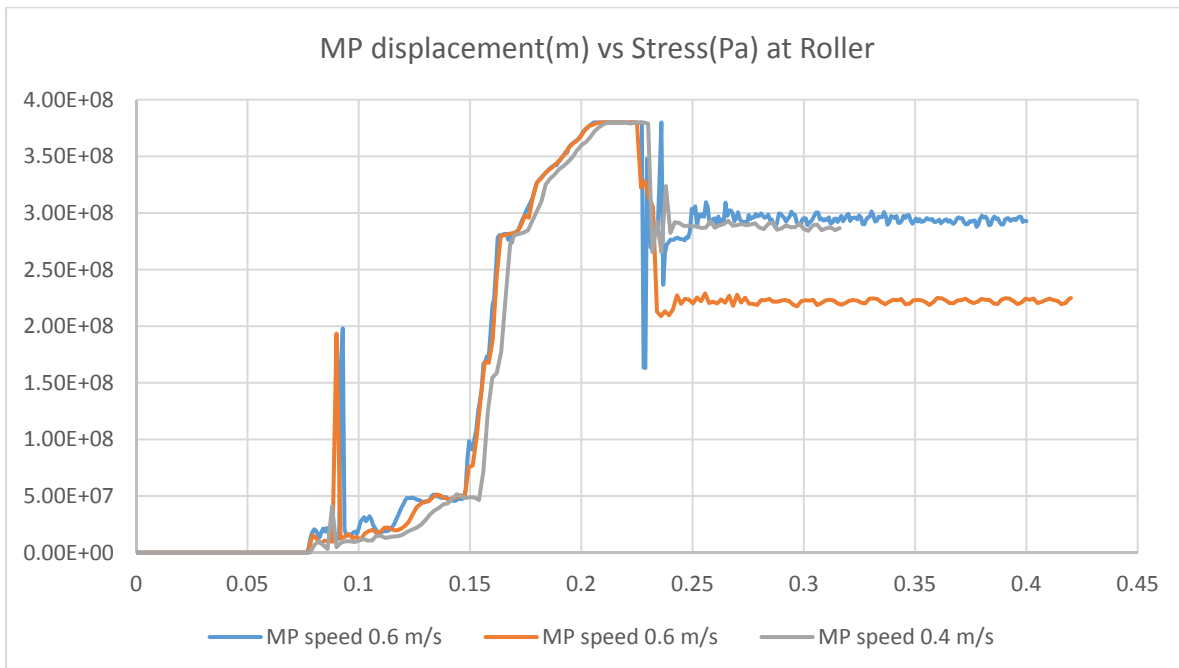
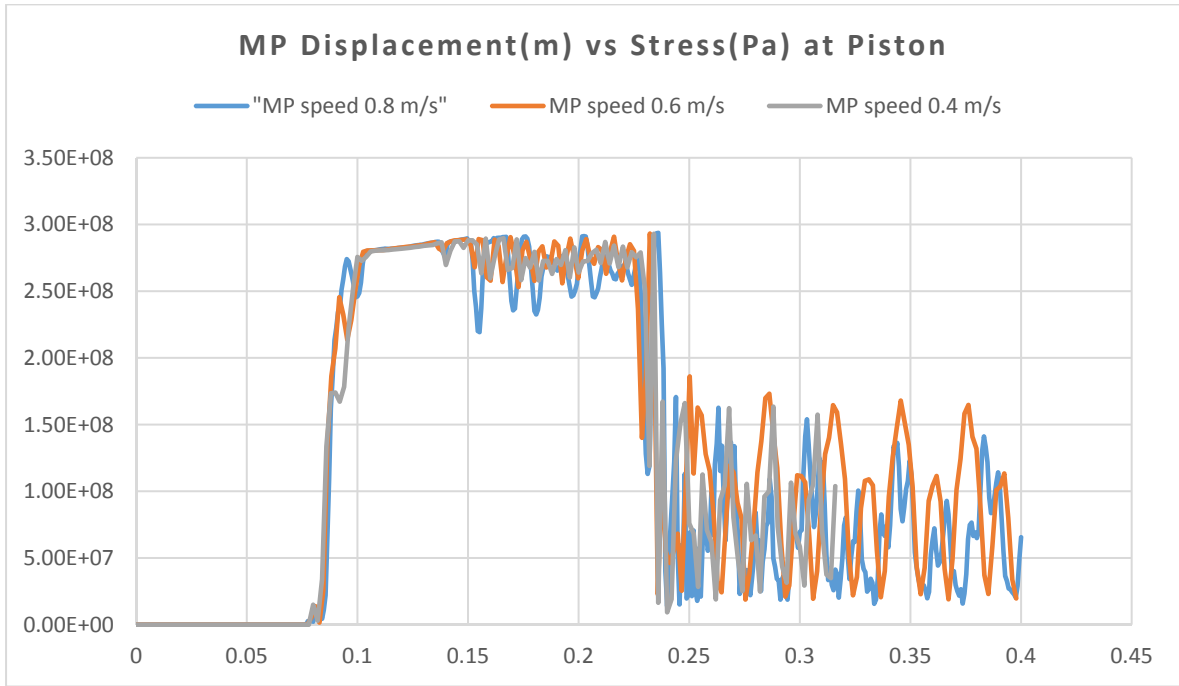


Figure 37: Displacement of MP(m) vs Mises(Pa) stress at seal, piston and roller

Interpretation of the results:

From the Above figure 39, it is clear that increasing or decreasing speed does not change the maximum stress significantly that is why we have not included the results from 0.2m/s MP speed. We can see from the figure 40 that When MP moves a distance around .082 to .085 m then the first stress spike occurs, which is the point where the first contact happens. After that, the stress starts to rise slowly due to MP movement from .090 to .15 m.

For seal maximum stress can be found when the face of the roller creates 45 degrees with the welding seam because at this point bending moment will be maximum. Here, the total force F can be divided into two component F_x and F_y . As soon as the roller leaves the mid-point of the welding seam the maximum stress starts to fluctuate and falls quickly as soon as the contact ends.

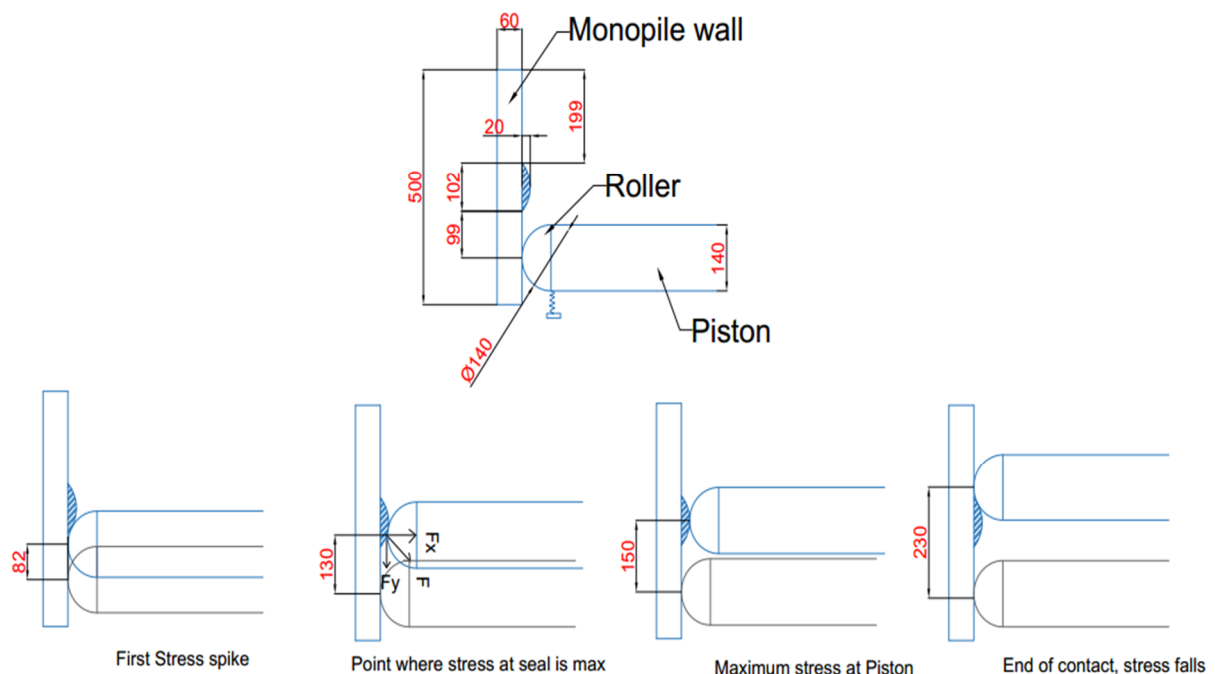


Figure 38: MP movement and roller position (units in mm)

For Piston, Maximum stress was found at the mid-point of the welding seam, 0.15m. Similar to seal, the stress starts to vary as soon as it leaves mid-point and finally falls when the contact ends.

For roller, due to the fixed choice of the element, the stress varies quite a lot as the contact shifts from one element to another. Though the maximum stress occurs near the 0.2 to 0.23 m where roller left welding curvature and strike the MP wall firmly due to the high stiffness of the spring.

Most important thing to note that is all the cases the maximum stress passes over the elastic range 280 MPa mark. So none of the curves goes back to zero due the plasticity of the structure. So we have to find a way to reduce the stress and keep it within the elastic limit. In the next step, we will reduce the capping size of the welding seam from 20 mm to 10 mm.

Before that, one analysis was conducted to see the result if we define all the structure as completely elastic. In that case following result was found at the piston which is compared with the elastic-plastic material definition.

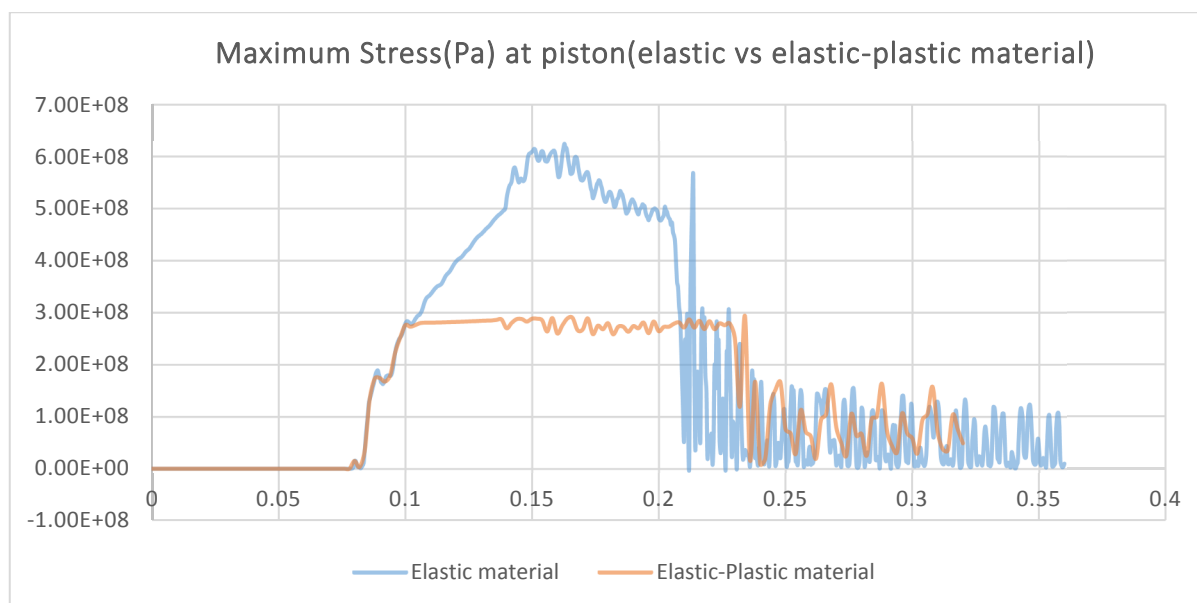


Figure 39: Max stress(Pa) at Piston for elastic vs elastic plastic material, MP speed 0.4 m/s

From the above figure 41, we can see that if we define all the materials completely elastic the maximum stress reach around 600 MPa, which completely impractical. Moreover, after

leaving the welding seam, stress does reach to zero mark as there was no plasticity developed. But due to the vibration, some spikes still remain which will die out with time.

Case 2:

MP welding seam capping: 10 mm

Others parameters are same as case 1.

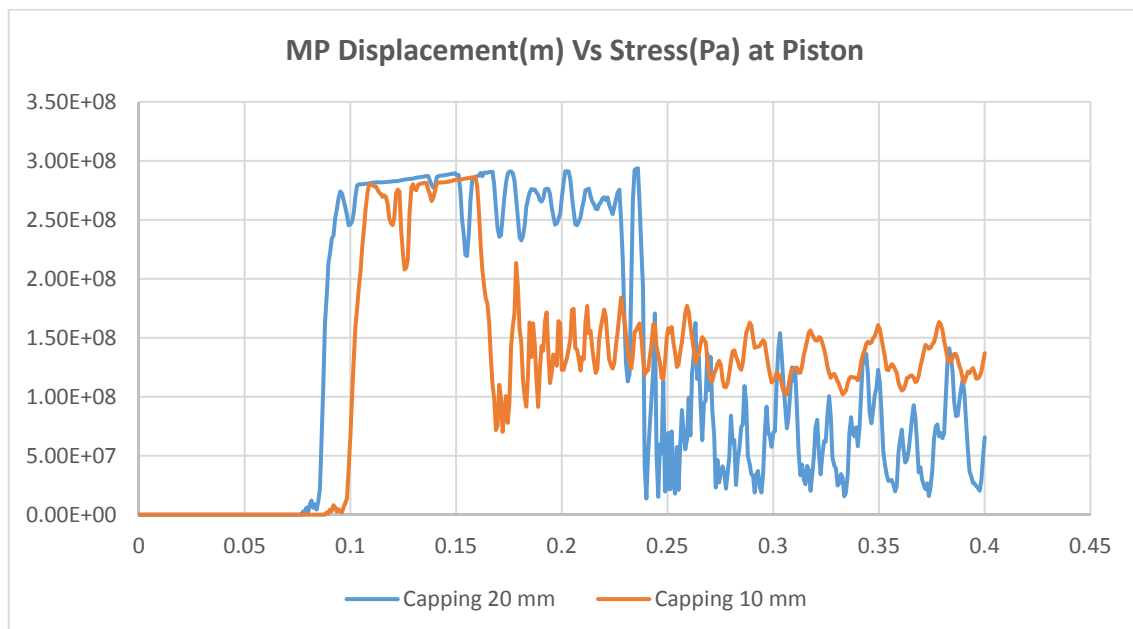
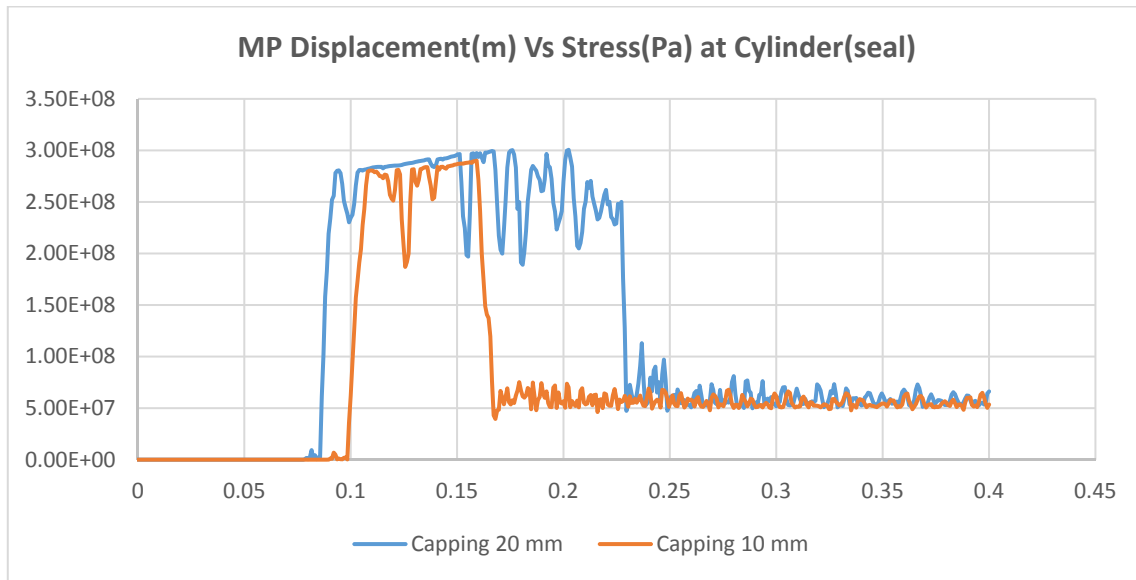


Figure 40: comparison of Mises stress for different welding capping at MP speed 0.8 m/s

From the figure, we can see that maximum stress does not change that much but pattern change a lot due to the geometry of the welding seam. So, the analysis is more geometry dependent than the speed of the MP.

Case 3:

We have changed the roller size to see the effect.

Roller size = $\varnothing 100$ mm

MP speed = 0.4 m/s

Capping of the welding seam = 20 mm

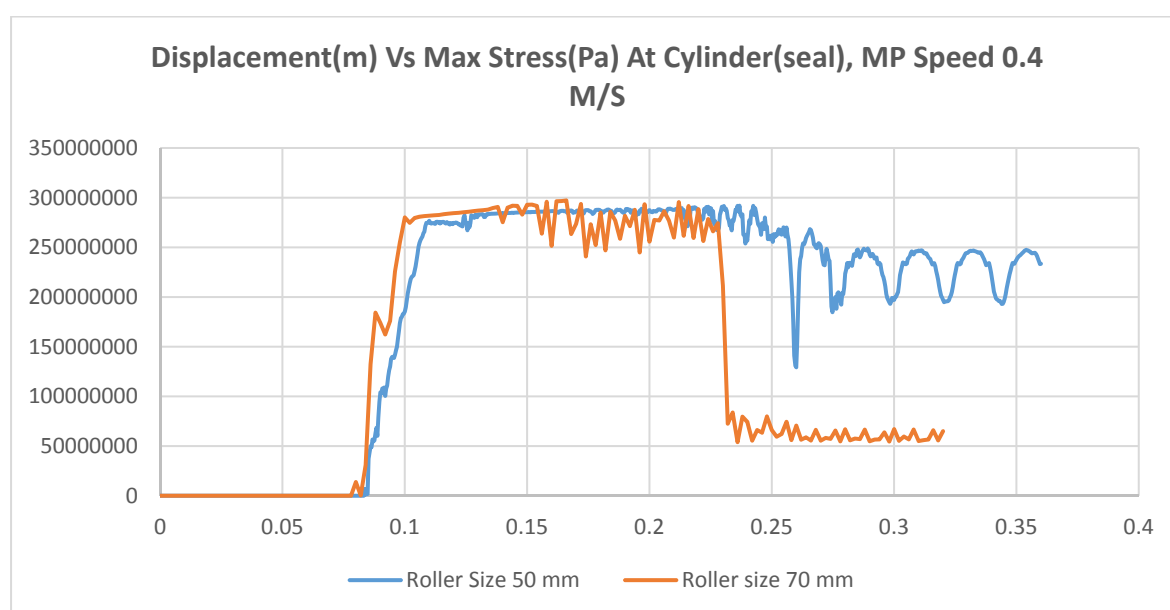


Figure 41: Comparison of stress at seal with different roller size

From the figure 43, it is obvious that Maximum stress declines if we reduce the roller size but not a significant amount. Moreover, during this analysis with 50 mm roller size, max stress at roller was found 385 MPa which was higher than the result of 70 mm roller. So decreasing roller size will increase the roller stress. Still, all the maximum values are well above the plasticity range.

From all the previous analysis and from simulation frame, it was discovered that the spring under Piston at the front which represent the square arm, did not take all the compressive load generated due to the geometry of the welding seam.

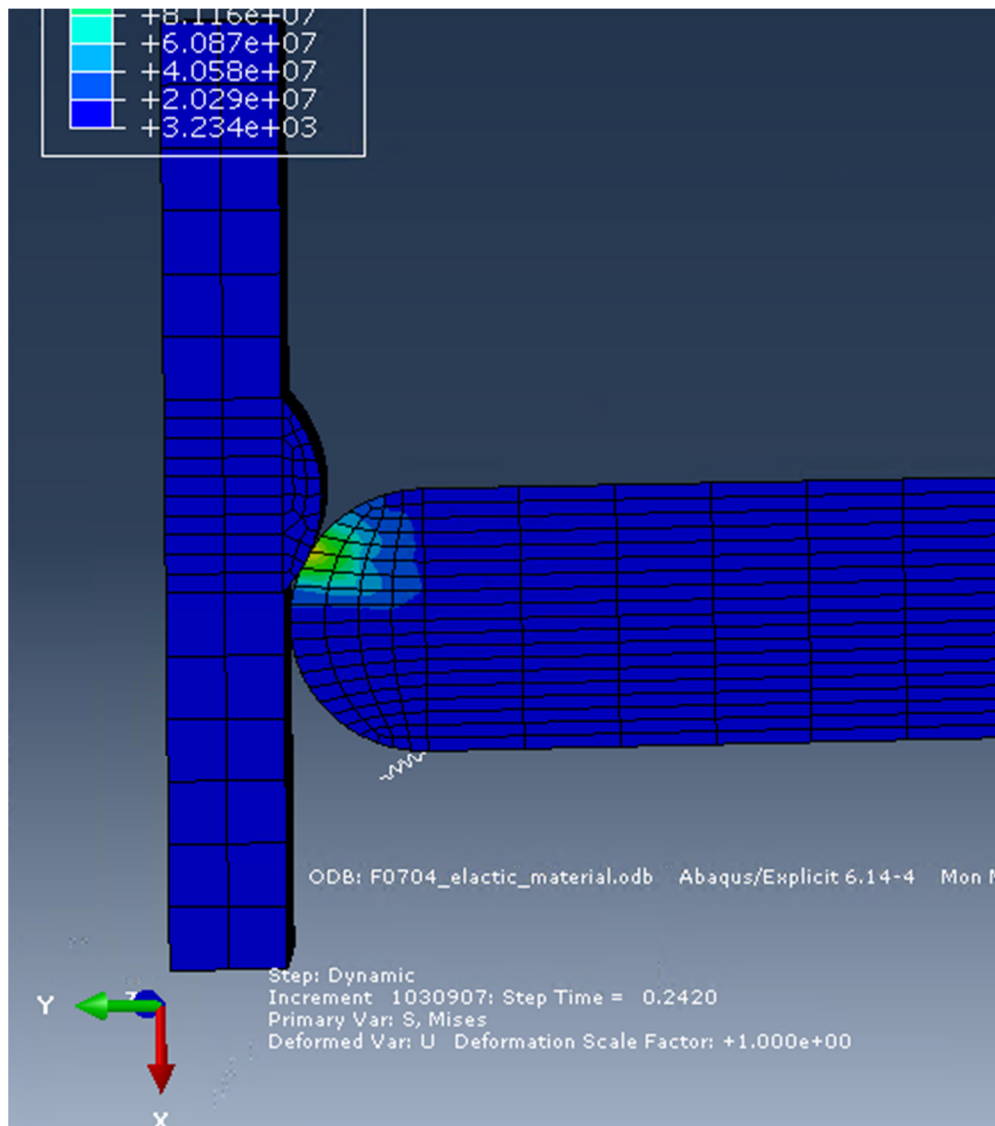


Figure 42: Sliding off the forward spring due to boundary condition

The boundary condition of the spring K_1 at the lower end was defined as it can only move along the y direction. So, virtually it should move along with the roller and always should be perpendicular to the piston. But, practically, when cylinder moves negative y direction due to the contact with the welding seam then the lower end of the spring moves positive y direction. As a result, spring does not take all the compressive load so the piston bends much higher than expected. As it is not possible to apply such boundary condition that a point will only move positive or negative y direction so what we can do is to fix the point. Though, in practical, this point is not fixed rather moves with the piston but for our analysis fixing the point will give more accurate result than the roller support.

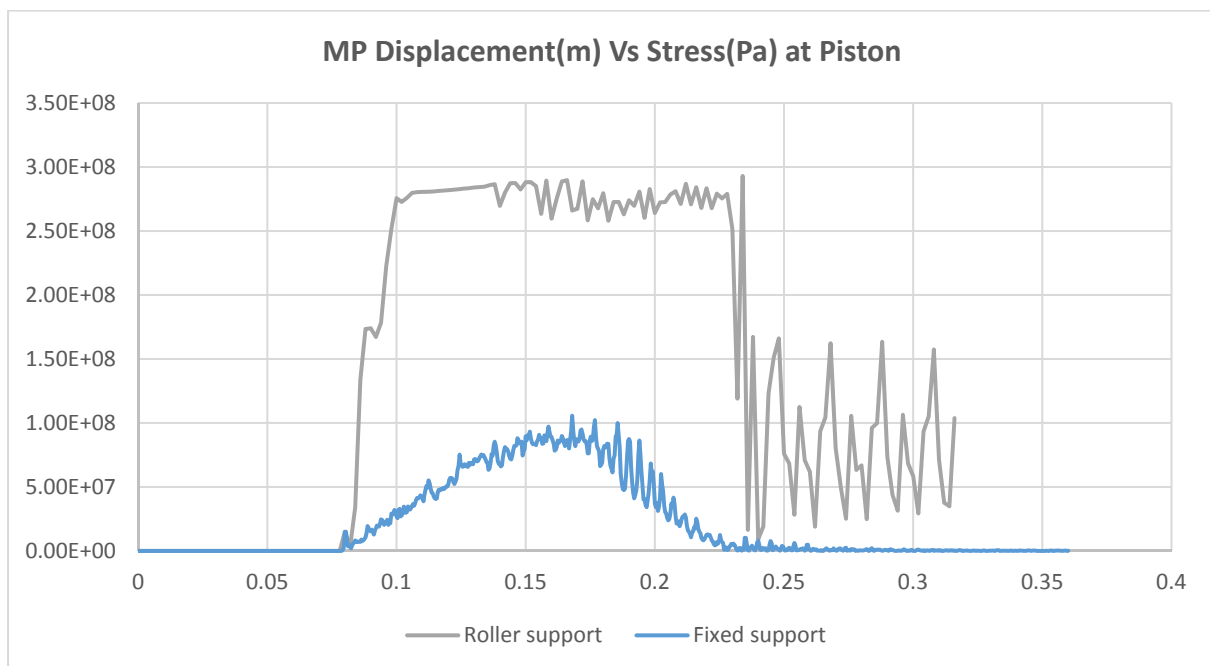
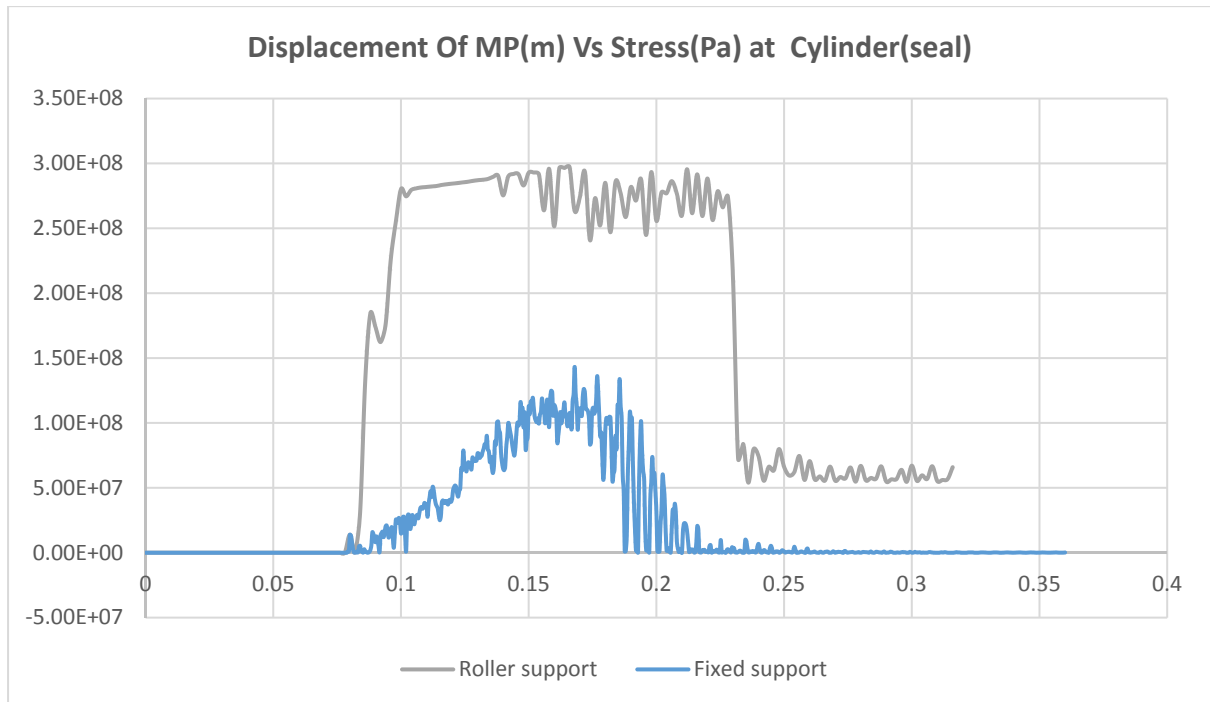
Case 4:

Roller size: $\varnothing 140$ mm

Capping: 20 mm

MP speed: 0.4 m/s

Fixed support for the forward spring K_1 . Other properties remain same as case 1.



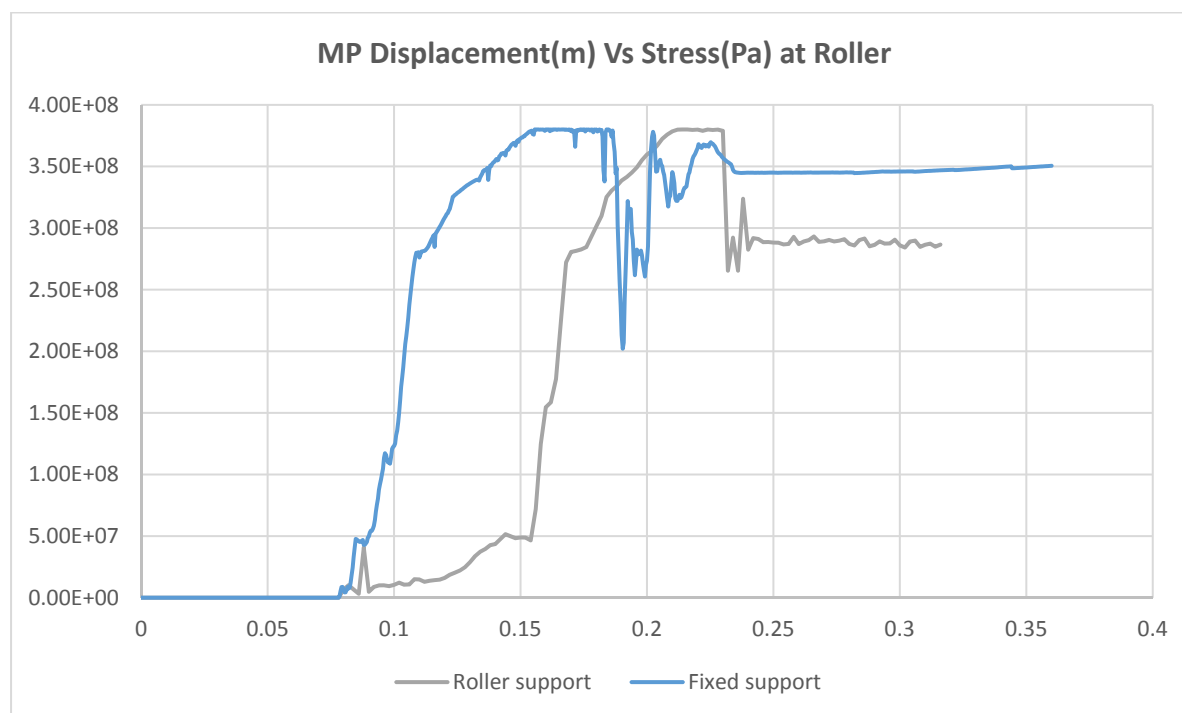


Figure 43: Displacement vs Stress, at Seal, Cylinder and Roller for Fixed BC at K1

As per prediction, the stress at the seal(cylinder) and piston reduces significantly and also there was no plasticity development. For roller, though maximum stress remains same which way over the plasticity limit but the stress curve due to fixed BC (boundary condition) rises earlier than stress curve for roller support.

Changing the boundary condition reduces the stress concentration both at cylinder and piston. But the stress at roller still remains above plasticity limit, may be due to the stiffness of the spring attached to the piston cylinder which represents the cylinder fluid. By varying the fluid property, it is possible to change the stiffness of the spring. In, the next step we will apply fixed boundary condition for spring K_1 with 10 mm welding capping size and compare with 20 mm result.

Force at the spring K1 and K2:

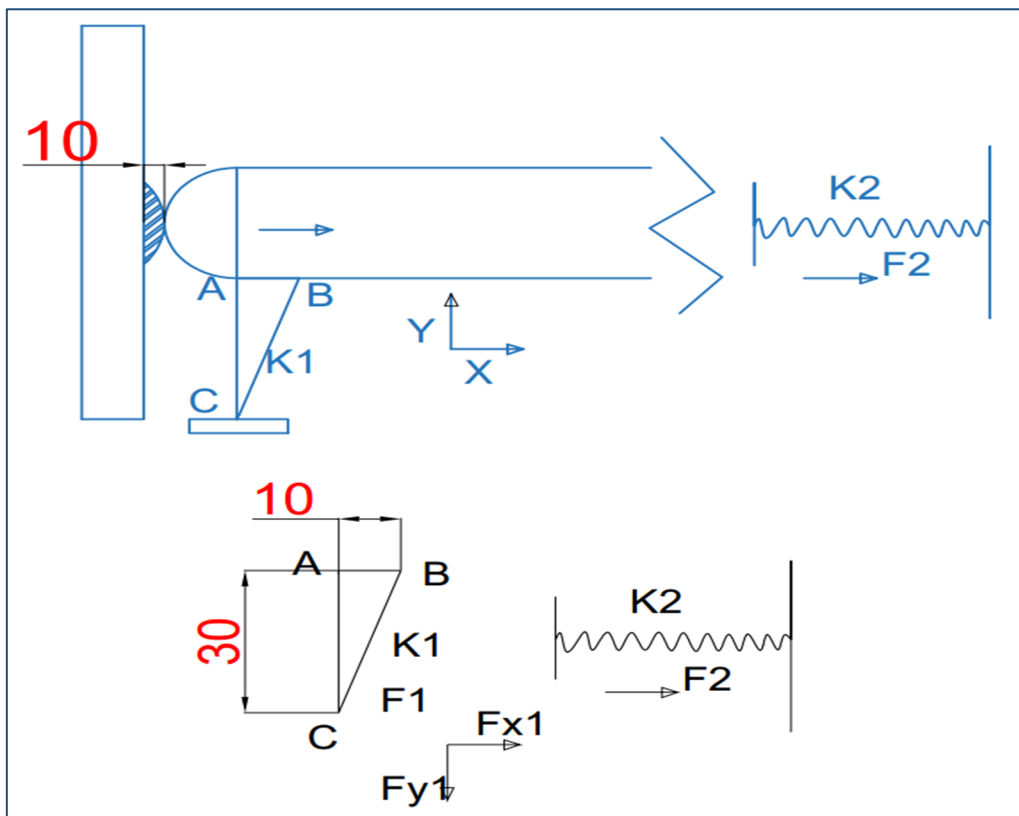


Figure 44: Calculation of forces on both of the spring

When we apply fixed boundary condition at the bottom of the spring K_1 , indicated by point C then some artificial force will arise due to the tension of the spring k_1 . If we consider that the force is F_1 then it will have two components F_{x1} and F_{y1} . F_{x1} will work directly opposite to the force F_2 (force due to the compression of the spring k_2) arise in spring k_2 . If $F_{x1} > F_2$ then the analysis might be wrong.

From the triangle ΔABC , we can calculate that,

$$BC = 31.63 \text{ mm}, AC = 30 \text{ mm}, AB = 10 \text{ mm} \text{ and } \angle ACB = 18.43^\circ$$

$$F_1 = k_1 * (BC - AC) = 3 * 10^7 * (31.62 - 30)$$

$$= (4.89 * 10^7 * 1.63) / (1000 * 1000) = 79.7 \text{ KN}$$

$$F_{x1} = 79.7 * \sin 18.43 = 25.19 \text{ KN}$$

$$F_2 = (3 * 10^7 * 10) / (1000 * 1000) = 300 \text{ KN}$$

If $AB = 20 \text{ mm}$, then $F_{x1} = 161.3 \text{ KN}$ and $F_2 = 600 \text{ KN}$

So, $F_2 > F_{x1}$, set up is valid.

Case 5:

Roller size: $\varnothing 140$ mm

Capping: 10 mm, 20 mm

MP speed: 0.4 m/s

Fixed boundary condition for spring k_1

Other properties remain same as case 1.

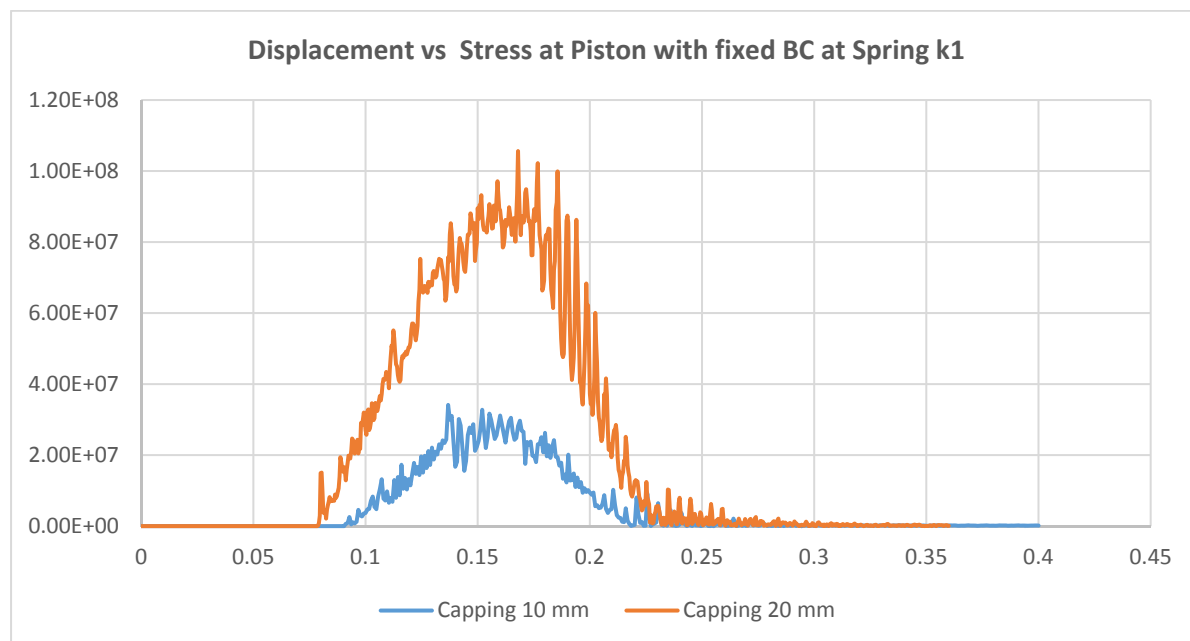
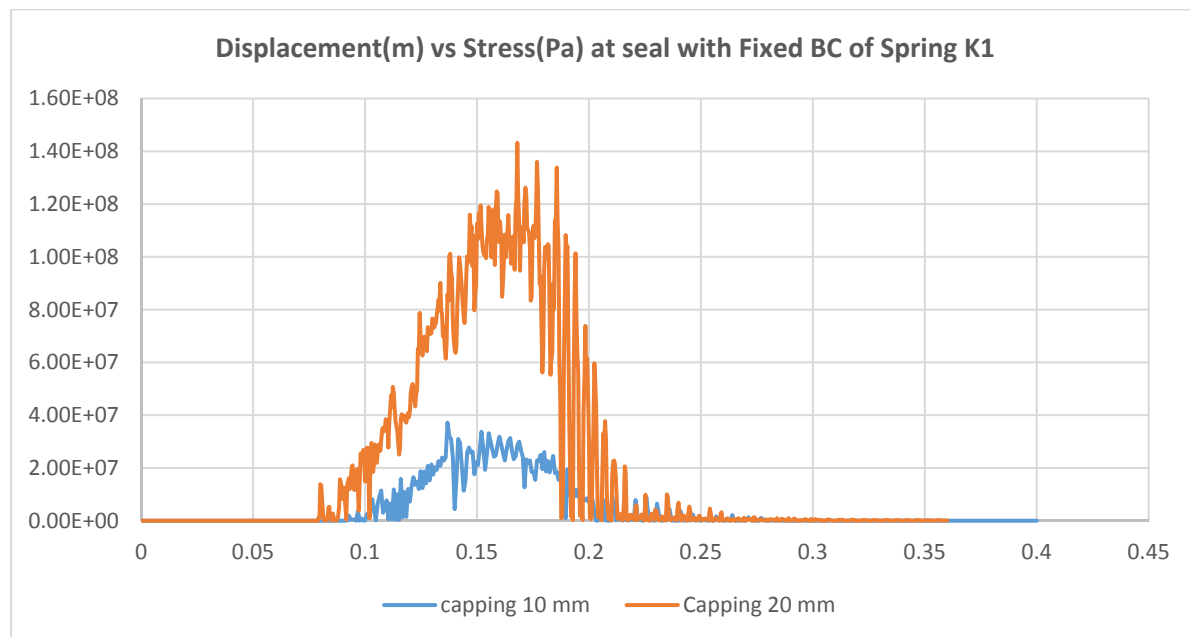


Figure 45: Displacement vs stress for 20 and 10 mm capping with fixed BC of K_1

We can see the above figure 47 that changing the boundary condition has changed the maximum stress both at seal and piston dramatically. Still stress at roller was recorded over the plasticity limit which justifies that stress concentration at roller depends mainly on the stiffness of the spring K_2 .

So we have run a couple of analysis keeping all the properties same as case 5 and only changing the stiffness of the spring K_2 . The results are presented in the following table:

Max stress at roller	
Capping size 10, roller size 70 mm, MP speed 0.6 m/s, Fixed BC at K_2	
Spring Stiffness K_2 (N/m)	Max Stress at Roller (MPa)
3×10^7 (initial)	355
1.5×10^7 (half of initial)	322
7.5×10^6 (One fifth of initial)	287
3.75×10^6 (One eighth of Initial)	259
3×10^6 (one tenth of initial)	245

Table 8:Max stress changes at roller with the change of spring stiffness K_2

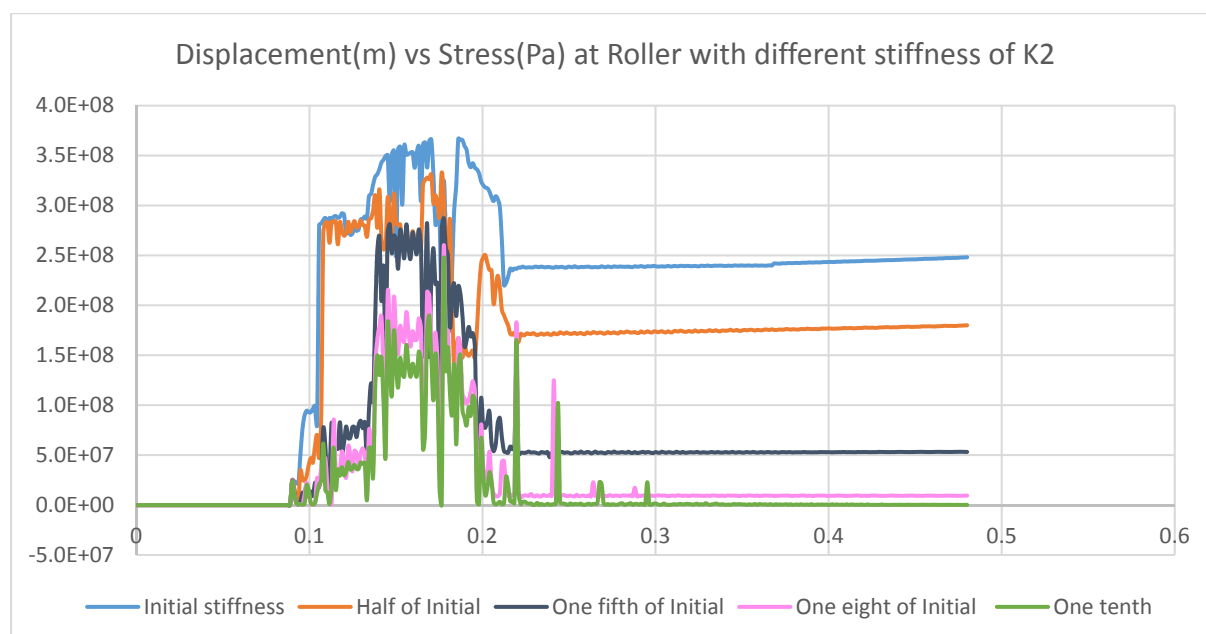


Figure 46:Change of roller stress with the change of spring stiffness K_2

Max Stress at Seal	
Capping size 10, roller size 70 mm, MP speed 0.6 m/s, Fixed BC at K_2	
Spring Stiffness K_2 (N/m)	Max Stress at Seal (MPa)
3×10^7 (initial)	97.9
1.5×10^7 (half of initial)	66.1
7.5×10^6 (One fifth of initial)	56.4
3.75×10^6 (One eighth of Initial)	62.1
3×10^6 (One tenth of initial)	63.1

Table 9:Change of seal stress with the change of spring stiffness K_2

Max stress at piston	
Capping size 10, roller size 70 mm, MP speed 0.6 m/s, Fixed BC at K_2	
Spring Stiffness K_2 (N/m)	Max Stress at Piston (MPa)
3×10^7 (initial)	98.1
1.5×10^7 (half of initial)	76.2
7.5×10^6 (One fifth of initial)	57.1
3.75×10^6 (One eighth of Initial)	60
3×10^6 (One tenth of initial)	59.3

Table 10:Change of piston stress with the change of spring stiffness K_2

Table 8, shows that decreasing the spring stiffness K_2 also decreases the maximum stress concentration at roller and the results show a linear pattern. By decreasing the stiffness of the spring also decreases the max stress concentration at the seal and piston (Table 9 and 10). Though max stress at the seal does not decrease after reducing the spring stiffness K_2 , one fifth of the initial.

We have run another analysis to see what happen if we reduce the stiffness of K_1 while keeping the other properties same as previous set up. We found that decreasing stiffness will increase stress both at cylinder and piston.

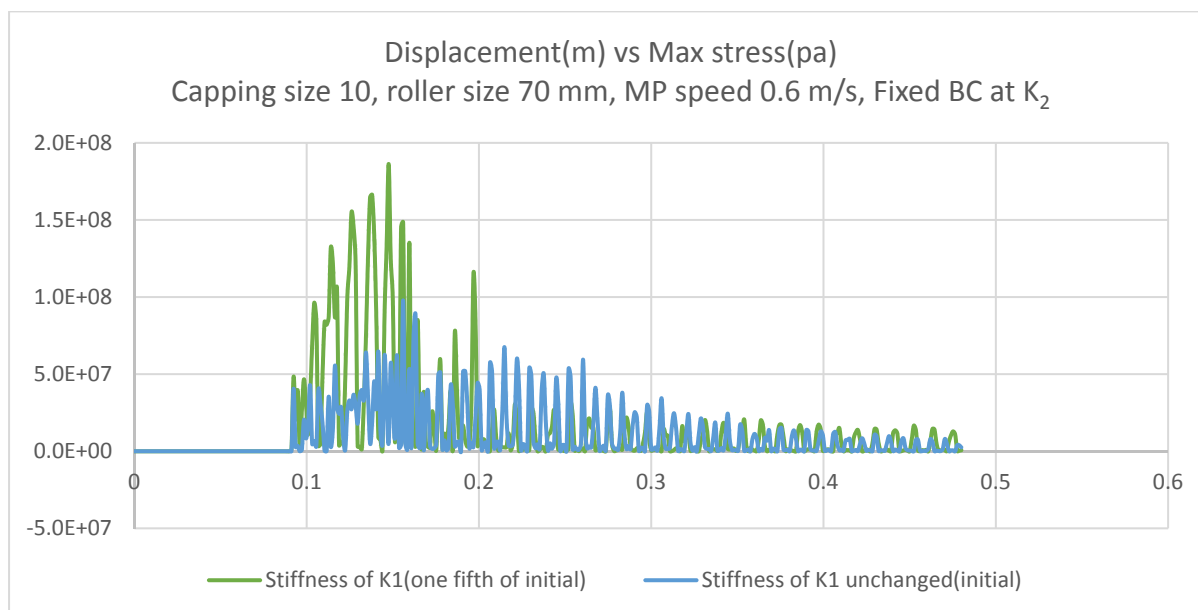


Figure 47: Change of stress at seal due to the change of Stiffness of the spring K_1

5. Conclusion and Recommendation

In this study, we have presented the MP installation procedure briefly and conducted global analysis with SIMO and local analysis of the hydraulic gripper system with Abaqus FEA. The main conclusions of this thesis and recommendations are presented below:

- From the time-domain simulation of the Coupled HLV-MP system shows that the penetration depths of the MP and wave conditions greatly influence the dynamic response of the gripper system.
- Hydraulic cylinder response/force increases significantly with the MP penetration depth for all wave condition.
- Stress concentration due to the welding seam is much higher than that of the applied correction force.
- The speed of the Monopile does not affect the result of the analysis that much.
- With roller Boundary condition at the end of the spring K_1 , changing welding seam height(capping) from 20 mm to 10 mm, decreases max stress both at piston and seal by around 4% while stress at roller remains same.
- Decreasing the roller size increases the stress concentration at the roller.

- Proper connection between the cylinder and square arm should be maintained so that stress generated due to the transition of the welding curvature can be abated effectively. Due to the limitation of the boundary condition definition in Abaqus, fixed Boundary condition was applied at the bottom of the spring k_1 . Though this is not the ideal case but for lower displacement of the piston, like 10 to 20 mm will mimic the actual scenario.
- With Fixed BC at k_1 , maximum stress both at seal and piston declines around 50% than that of roller BC of k_1 and remain within the elastic range. Stress at roller remains same and above elastic limit.
- With Fixed BC at k_1 , changing welding seam height from 20 to 10 has decreased the maximum stress at both cylinder and piston by around 70% but stress at roller remains same. Decreasing the welding seam height to 5 mm will decrease the stress concentration further.
- Stress at roller depends predominantly on the spring stiffness K_2 . Though reducing the spring stiffness too much will make the gripper, less firm so the MP will vibrate more which might cause an error in the inclination angle. So, it is recommended to use multiple rollers instead of one or change the material of the roller with higher elastic range.
- Stress at the seal depends both on the curvature of the welding seam and the stiffness of the spring K_1 .
- It is recommended to keep the welding seam height as minimum as possible.
- The stiffness of the square arm should be high enough to avoid stress concentration at seal and failure of the hydraulic system due to leakage.

6. Limitation and Future work

During our Global and local analysis, we have simplified our model and different parameters were assumed. The Wind and current forces were not applied. Moreover, soil-pile models were simplified to non-linear springs. Furthermore, hydraulic fluid inside the cylinder and the square arm was simplified into non-linear springs. Additionally, in practice, there are many uncertainties associated with the measurements, proposed methodology and numerical models.

In this thesis, only local analysis was done but the final goal is to establish the limiting parameters for offshore MP installation. Possible future works are listed below:

- Establishing limiting parameters.
- Developing dynamic p-y curve from Plaxis 3D to replace the API recommended curve.
- Abaqus modelling with hydraulic liquid and square arm instead of spring.
- Running the analysis for different type of hydraulic cylinder and different stroke length.

7. List of References

1. *Analysis of lifting operation of a monopile for an offshore wind turbine considering vessel shielding effects* by Lin Li, Zhen Gao, Torgeir Moan, Harald Ormberg.
2. *Assessment of allowable sea states during installation of OWT monopiles with shallow penetration in the sea bed* by Lin Li, Wilson Guachamin Acero, Zhen gao, Torgeir moan
3. DNV, 2011. *Offshore Standard DNV-OS-H101, Marine Operations, General, October*
4. MARINTEK, 2012. *SIMO - Theory Manual Version 4.0*
5. Albers, P., 2010. *Motion control in offshore and dredging*. Springer Science & Business Media.
6. *Development of P-Y Curves for Monopiles in Clay using Finite Element Model Plaxis Foundation* by Dhruva Lal Pradhan
7. American Petroleum Institute. 1991. *Recommended practice for planning, designing and constructing fixed offshore platforms. API Recommended Practice 2A (RP 2A)*.
8. "New design methods for large diameter piles under lateral loading for offshore wind applications". In *Proc 3rd International Symposium on Frontiers in Offshore Geotechnics (ISFOG 2015)* by Byrne, B., McAdam, R., Burd, H., Houlsby, G., Martin, C., Zdravkovi, L., Taborda, D., Potts, D., Jardine, R., and Sideri, M., 2015.
9. 'Integrated Wind Turbine Design' by Project Upwind
10. *Non-linear Finite Element Analysis of Solids and Structures* by Rene de Borst et al. Wiley Series, 2nd edition 2012.
11. *Finite Element Modelling and Analysis of Marine Structures* by Torgeir Moan. Compendium TMR 4190.
12. *Computational Contact and Impact Mechanics* by Tod A. Laursen. Springer Series, First Edition 2002.
13. *Finite Element Procedures for Contact Impact Problems* by Zhi Hua Zhong. Oxford University Press 1993.
14. IHC Vremac Cylinders catalogue 210/320 bar
(<http://www.ihcvremaccylinders.com/downloads/>) downloaded on 3rd April, 2016

15. *Definition of Poisson's ratio of Elastomers* by Vladimirs Gonca, Yurijs Shvabs
16. *EWEA, 2014. The European offshore wind industry - key trends and statistics 2013. Report, The European Wind Energy Association*
17. *Federal Highway Administration Research and technology* by Us Department of Transportation
18. *Analysis of single piles under lateral loading. Preliminary Review Copy, Research Report 244-1, Centre for Highway Research, The University of Texas at Austin, Austin, Tex., pp. 1–145. By Meyer, B.J., and Reese, L.C. 1979*
19. *Abaqus User Manual*
20. *Handbook of Offshore Engineering* by Subrata K. Chakrabatri
21. *Offshore Soil Mechanics* by Arnold Verruijtit
22. *Applied soil mechanics* by Sam Helway
23. *Lee, C,1995. WAMIT theory manual. Massachusetts Institute of Technology, Department of Ocean Engineering.*
24. *'Second-order, slowly-varying forces on vessels in irregular waves'* by Newman. J. N., 1974
25. *FB-Multiplier API soil Model Validation* by Jae chung, Anand Patil, Henry Bollmann

8. Appendices

8.1 Appendix 01: Governing Differential equation for laterally loaded pile problem

A laterally loaded single pile presents a soil-structure interaction problem in figure 50. The soil reaction depends on the pile movement, and the pile movement depends on the soil reaction. The solution must satisfy a nonlinear differential equation as well as equilibrium and compatibility conditions.

In the derivation of the differential equations the following assumptions have been used:

- The beam is straight and has a longitudinal plane of symmetry in which loads and reactions occurs.
- The beam material is homogeneous, isotropic and elastic. Furthermore, plastic hinges do not occur in the beam.
- Young's modulus of the beam is similar to tension and compression.
- Beam deflections are small
- Beam is not subjected to dynamic loading.

Elastic beam relationships that are used commonly in the analysis of laterally loaded piles are summarized in table 11. These quantities are obtained from differentiating deflection y with respect to the distance along the pile (x).

Variable	Formula	Units
Distance along the length of the pile(measure from the pile head)	x	[L]
Distance to neutral axis within pile cross section	z	[L]
Deflection	y	[L]
Slope or rotation of pile section	$\phi = \frac{dy}{dx}$	-
Curvature	$\kappa = \frac{d^2y}{dx^2}$	[Radians/L]

Elastic modulus of the pile	E_p	[F/L ²]
Moment of inertia of pile cross section	I_p	[M* L ²]
Bending moment	$M = E_p I_p \frac{d^2 y}{dx^2} = E_p I_p \kappa$	[F*L]
Shear Force	$V = E_p I_p \frac{d^3 y}{dx^3}$	[F]
Axial Load	Q	[F]
Soil Reaction	$p = E_p I_p \frac{d^4 y}{dx^4}$	[F/L]

Table 11: Elastic Beam Relationship

The following figure 50, shows a loaded pile and typical profiles of net soil reaction, deflection, slope and moment.

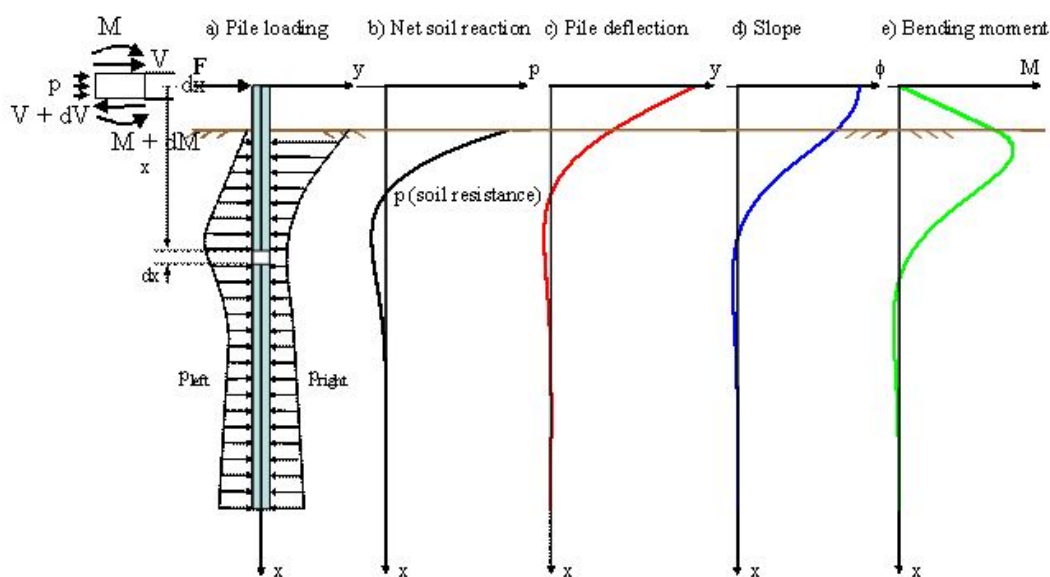


Figure 48: Laterally Loaded Soil-Pile system

The governing differential equation for the problem of a laterally loaded pile was derived by Hetenyi (1946). The differential equation can be obtained by considering moment equilibrium of the infinitesimal element of length (dx) as shown in above figure:

$$\sum (M + dM) - M - Vdx + Qdy - (pdx) \frac{dx}{2} = 0 \quad (17)$$

Neglecting quadratic terms, and differentiating twice with respect to x , we obtain

$$\frac{d^2M}{dx^2} + Q \frac{d^2y}{dx^2} - \frac{dV}{dx} = 0 \quad (18)$$

The magnitude of the bending moment acting on a given section of a pile can be calculated by integrating the normal stresses, $\sigma(z)$, acting within the cross section of area, A , as follows:

$$M = \int_A \sigma(z)z dA \quad (19)$$

If we assume that plane sections of the pile remain plane after loading, we can calculate the strains across the pile cross section if we know the rotation of the section, $\sigma = dy/dx$, and the position of the neutral axis. For a given rotation, σ we have the following:

$$\begin{aligned} u(x, y) &= \phi z = \frac{dy}{dx} z \\ \varepsilon(z) &= \frac{du}{dx} = \frac{d^2y}{dx^2} z = \kappa z \\ \sigma(z) &= E_p \varepsilon(z) = E_p \kappa z \end{aligned} \quad (20)$$

Where

$u(x, y)$ = is the displacement in the x-direction across the pile cross section

$\varepsilon(z)$ = strains in the x-direction across the pile cross section

z = distance to the neutral plane

Substituting the expression for $\sigma(z)$ from equation 20 into equation 19, we obtain,

$$M = \int_A (E_p \kappa z) z dA \quad (21)$$

If the pile material is linear elastic with a constant Young modulus, E_p , we would have:

$$M = E_p \kappa \int_A z^2 dA = E_p I_p \kappa = E_p I_p \frac{d^2y}{dx^2} \quad (22)$$

Substituting equation 22 into equation 18 we obtain:

$$E_p I_p \frac{d^4 y}{dx^4} + Q \frac{d^2 y}{dx^2} - \frac{dV}{dx} = 0 \quad (23)$$

From consideration of the horizontal force equilibrium of the infinitesimal element of the pile shown in figure 50, we obtain:

$$\sum F_H = p(x)dx - dV = 0 \quad (24)$$

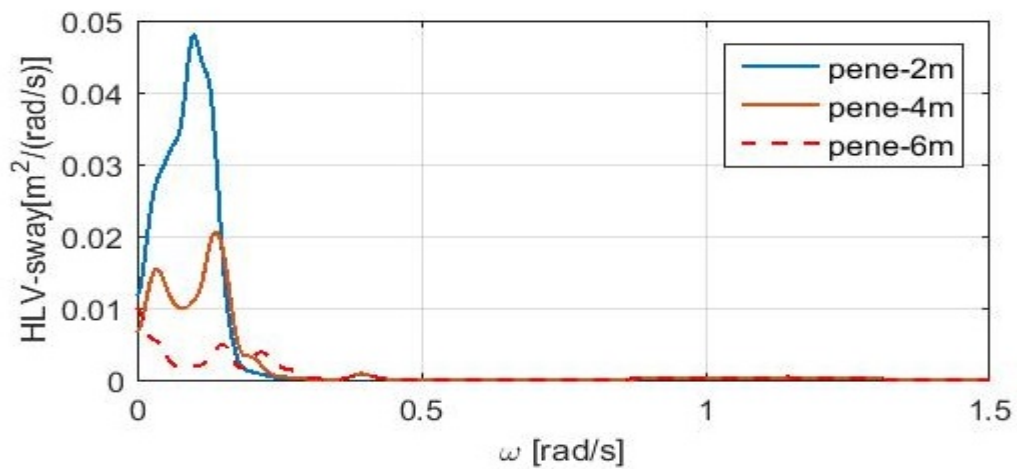
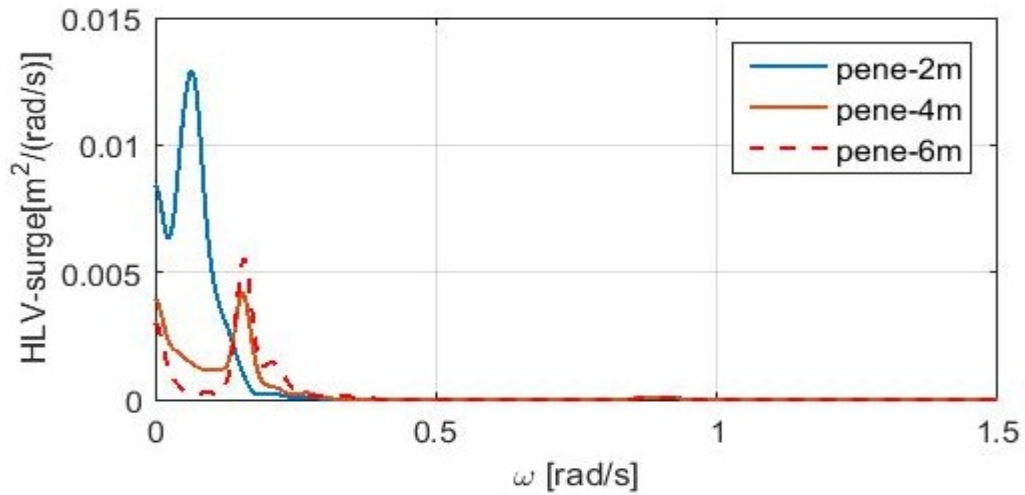
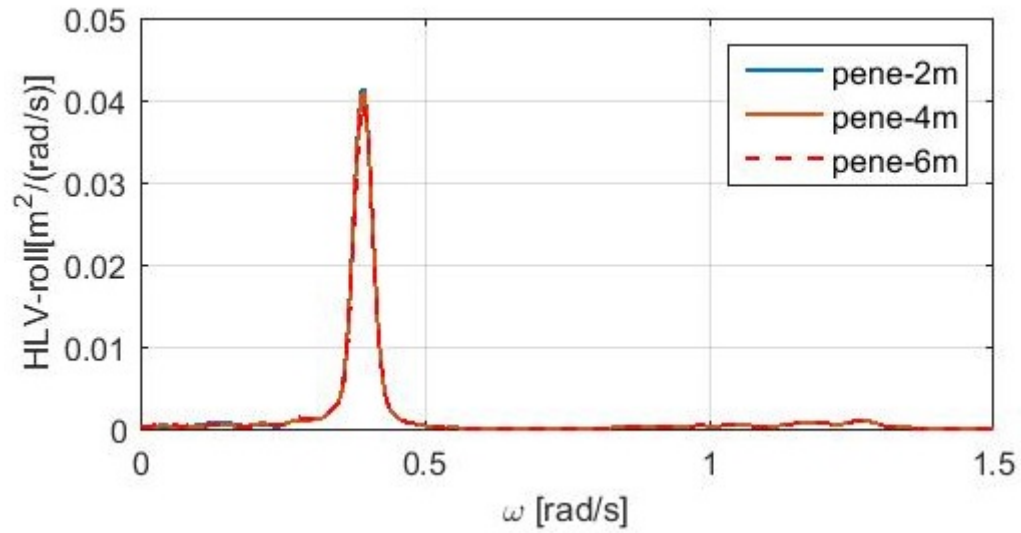
$$\frac{dV}{dx} = p(x)$$

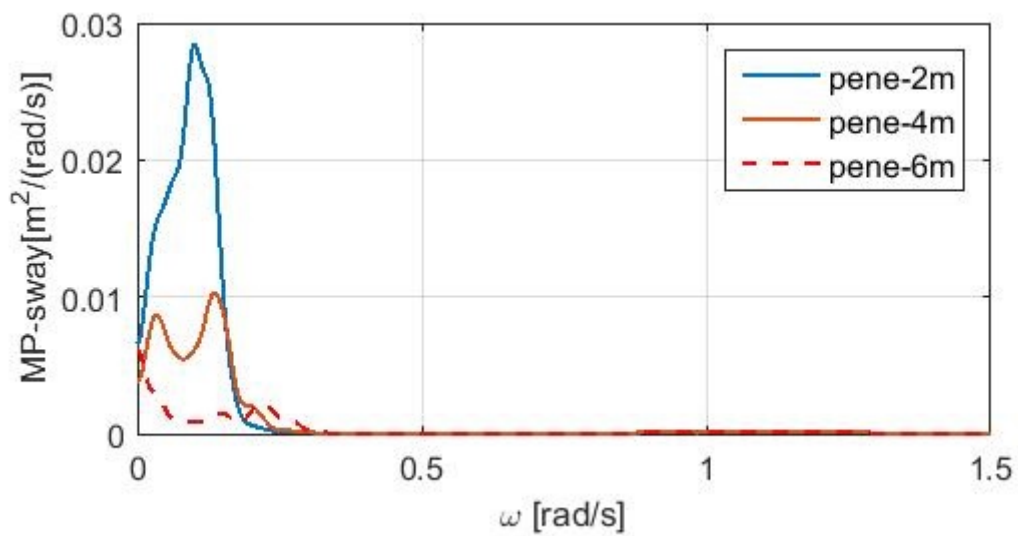
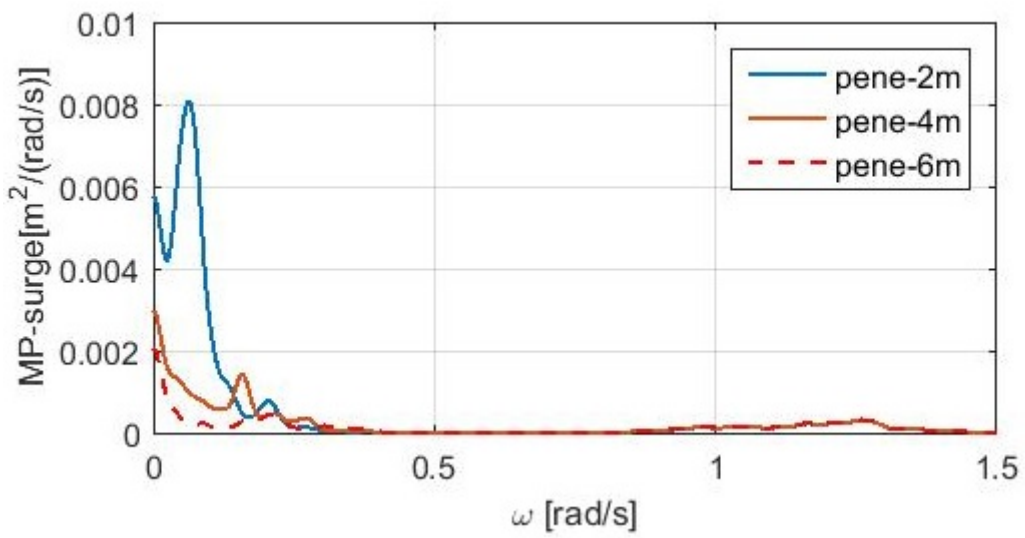
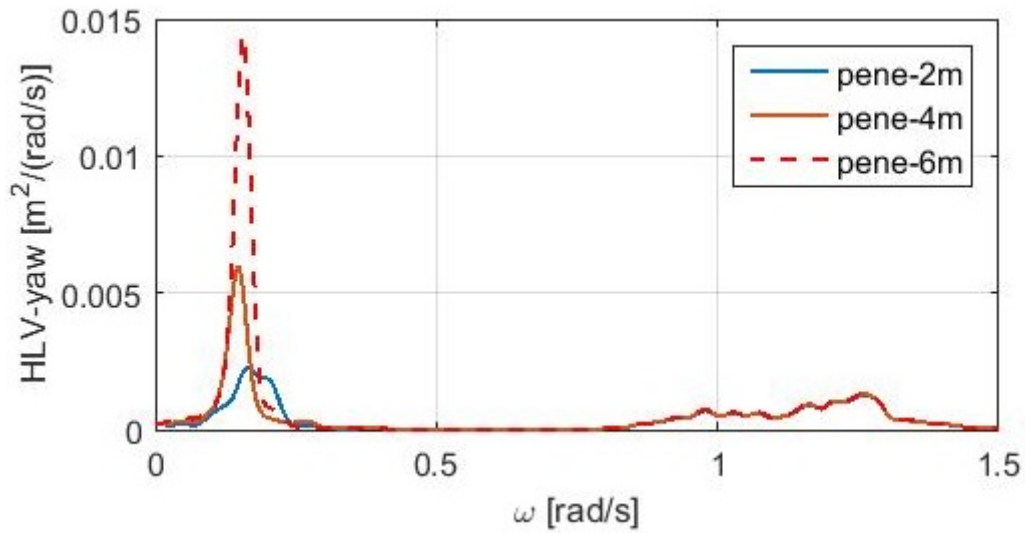
Substituting equation 24 into equation 23, we obtain the following governing differential equation, which is commonly used to analyse piles under lateral loads:

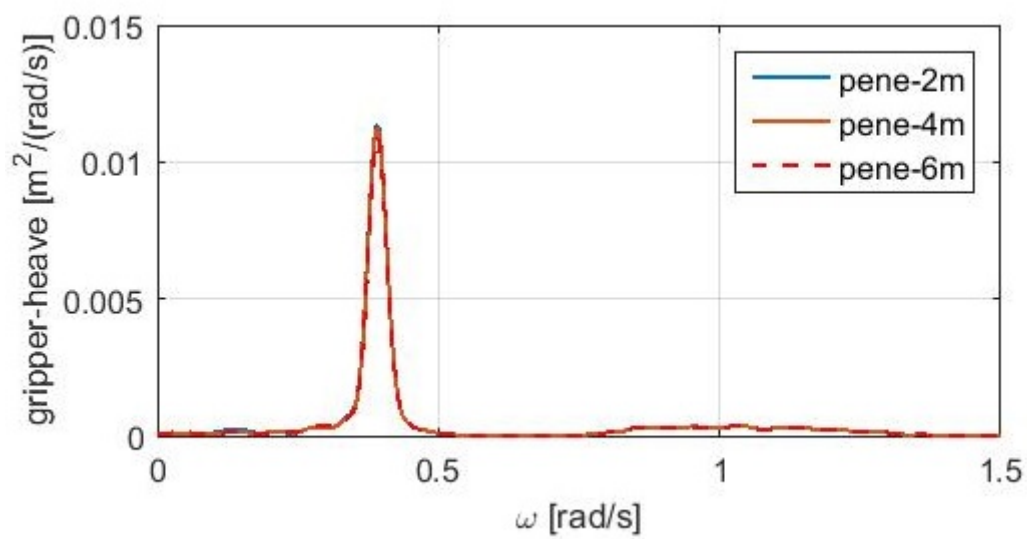
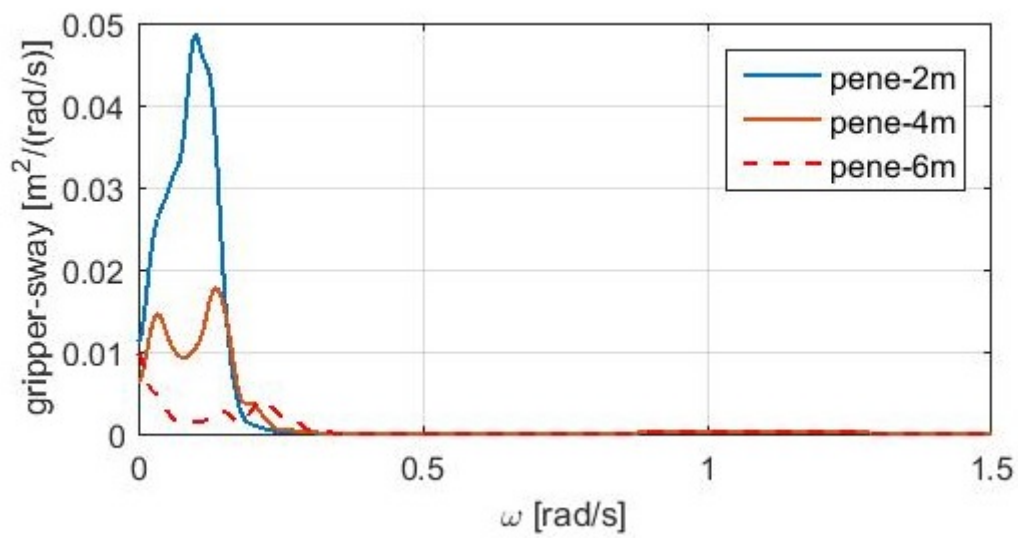
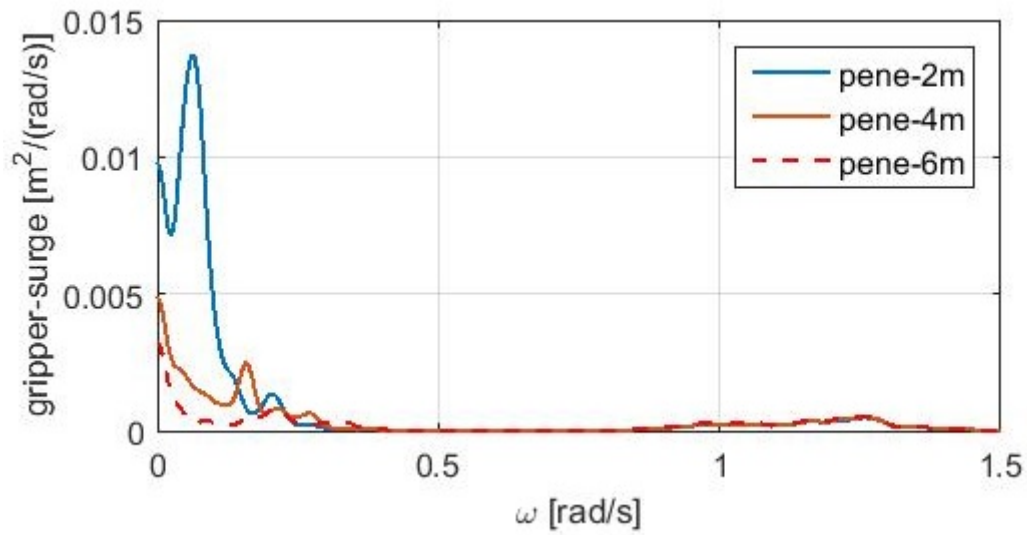
$$E_p I_p \frac{d^4 y}{dx^4} + Q \frac{d^2 y}{dx^2} - p(x) = 0 \quad (25)$$

The variable $p(x)$, in equation Corresponds to the resultant soil resistance force per unit length of the pile that occurs when the unit length of pile is displaced a lateral distance, y , into the soil. The important point for the solution of the differential equation shown above is an adequate representation of the soil reaction, p . If the soil reaction, p , has a linear relationship with lateral pile deflection, y , the equation has a closed-form solution. However, the relationship between the soil reaction (p) and the pile deflection (y) is nonlinear and also varies along the pile depth. [17, 18]

8.2 Appendix 02: Response spectra of the HLV-MP system







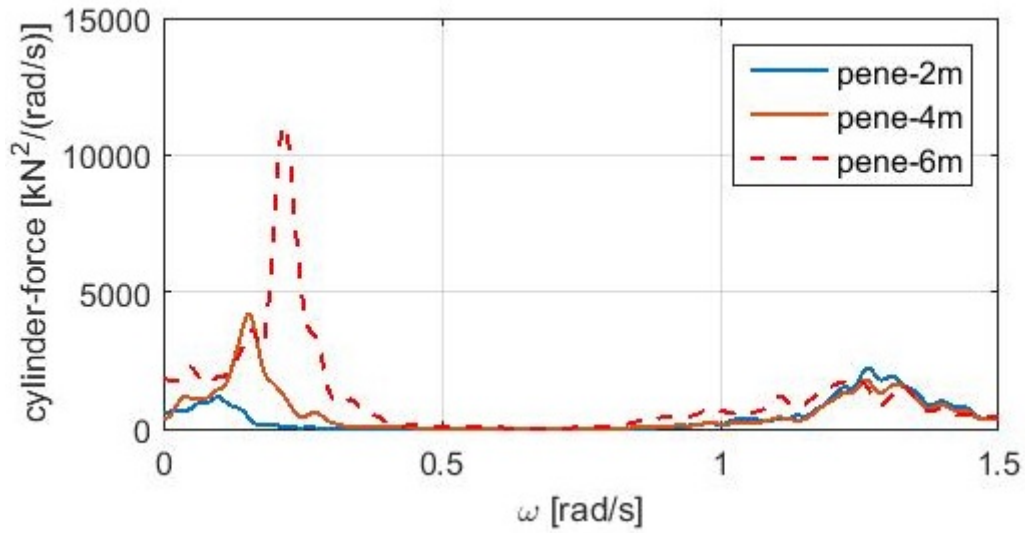
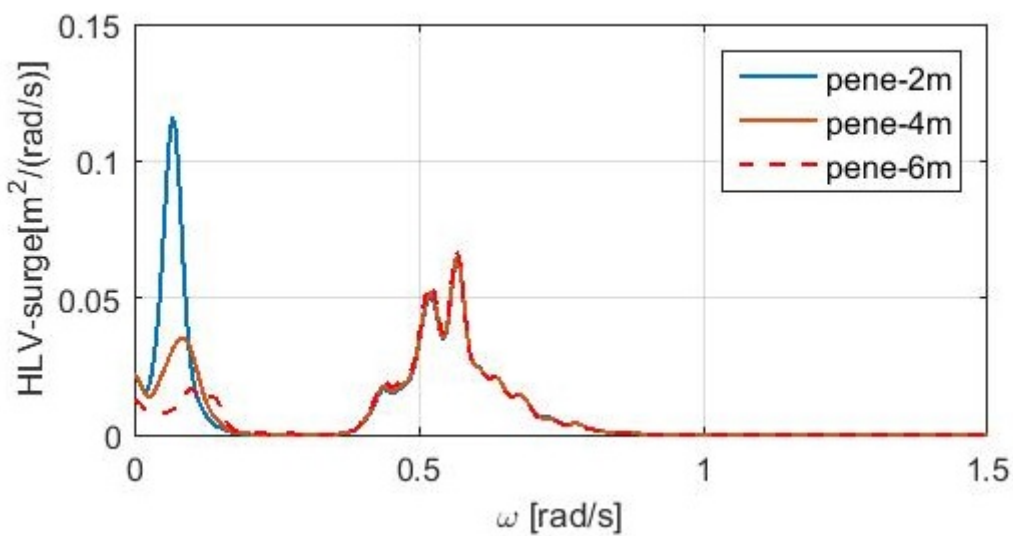
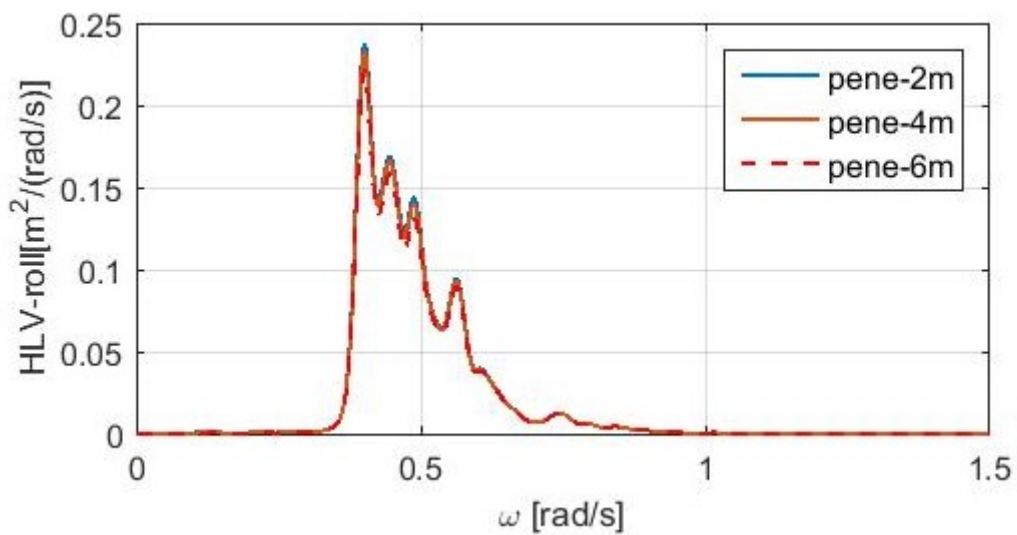
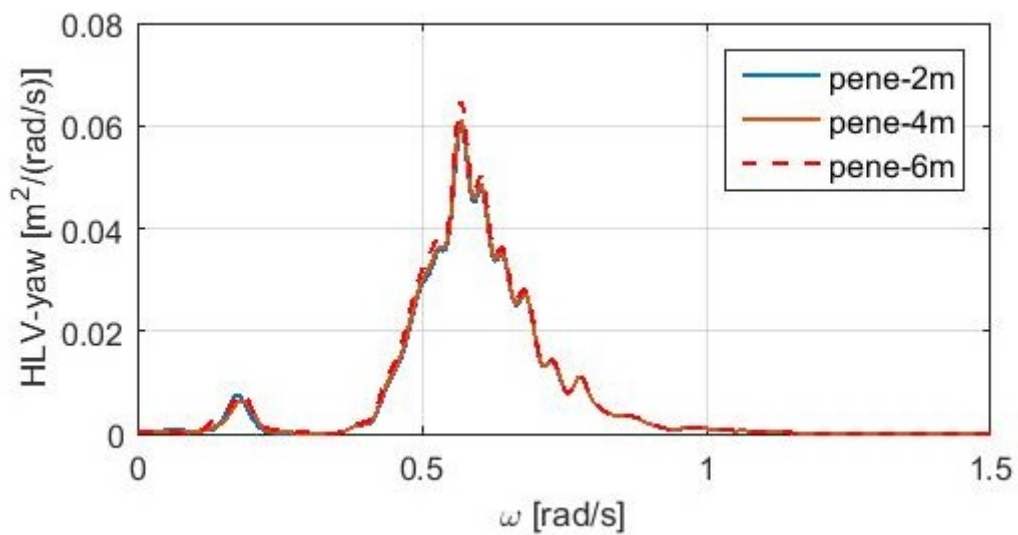
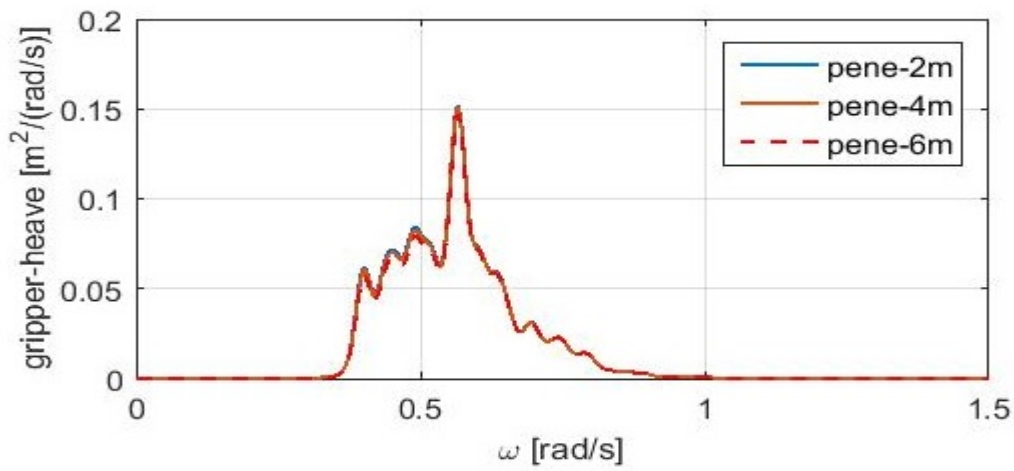
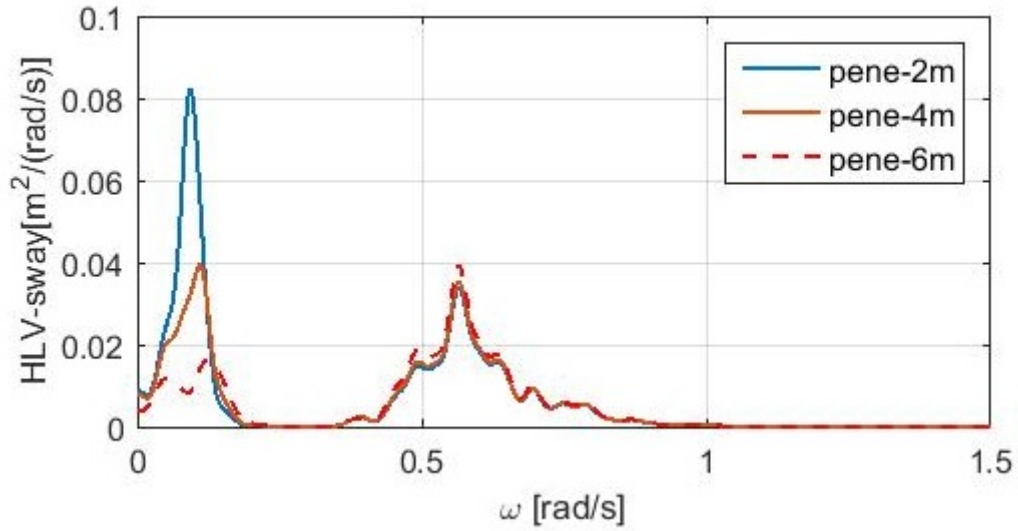
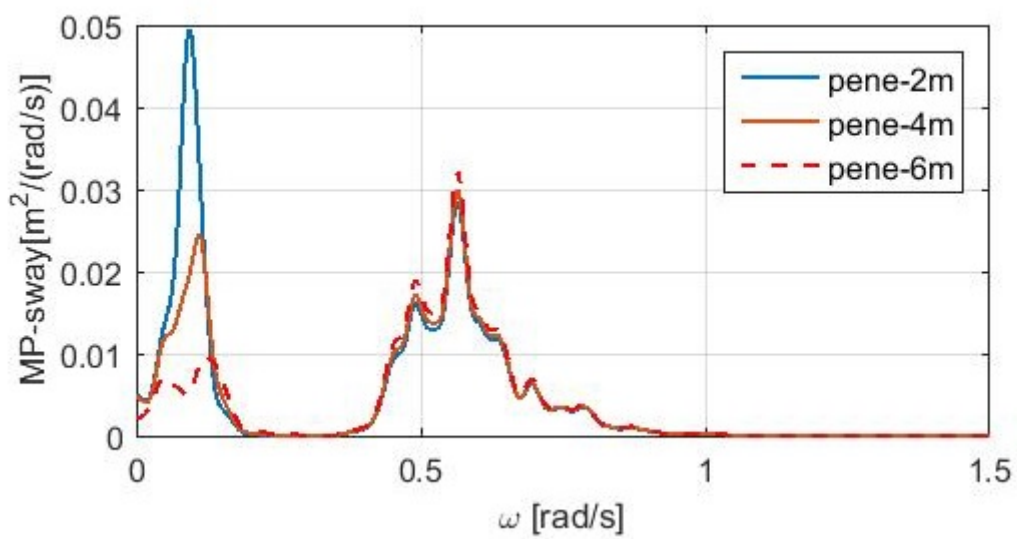
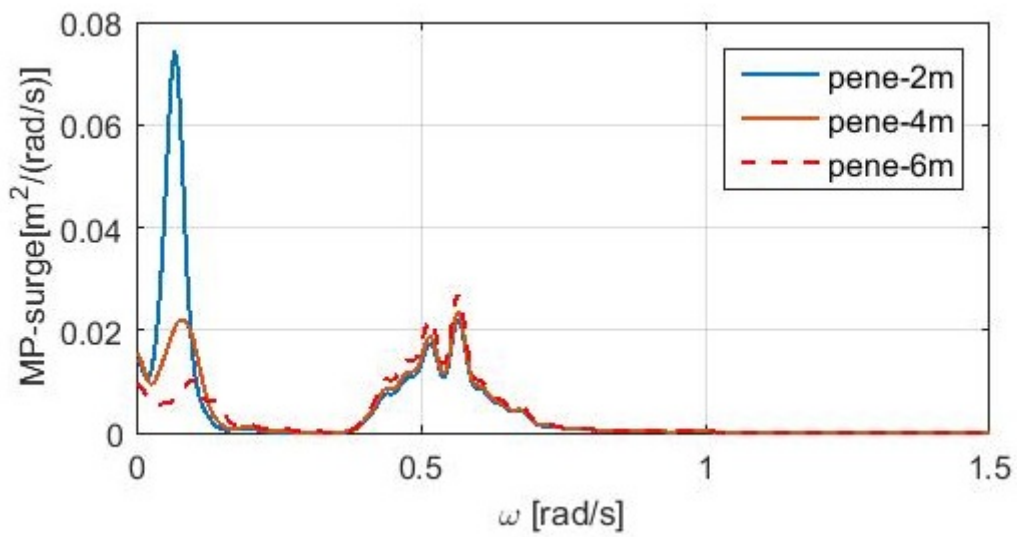
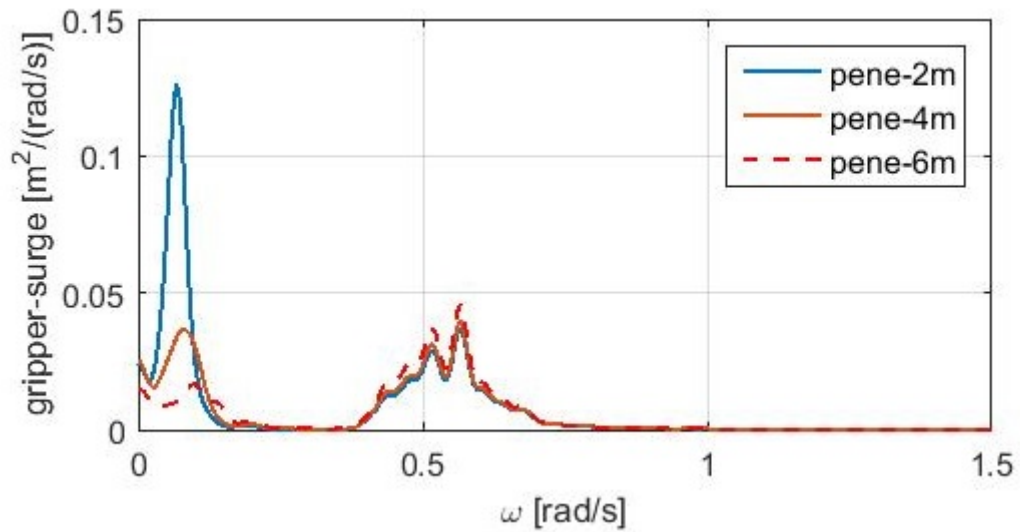


Figure 49 :Response spectra of HLV,MP,Gripper and cylinder force at $H_s=1.5m$, $Dir=150$, $T_p=5s$







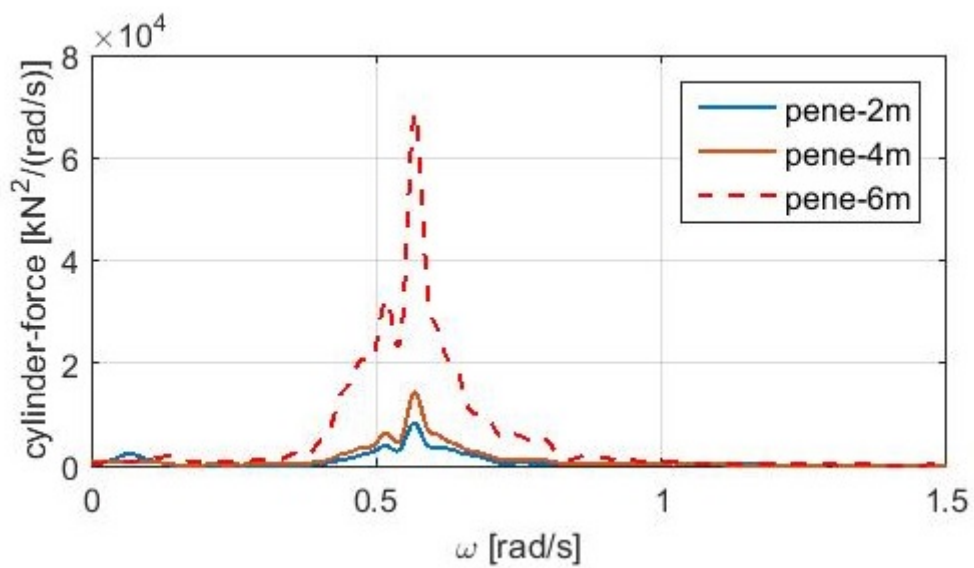
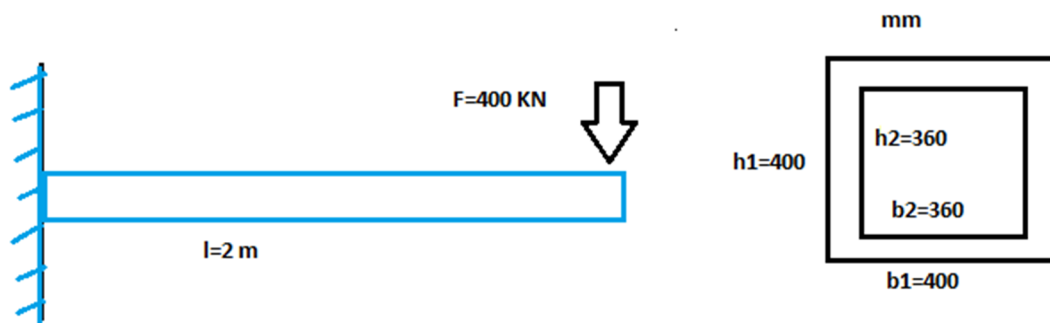


Figure 50: Response spectra of HLV,MP,Gripper and cylinder force at $H_s=1.5m$, $Dir=150$, $T_p=10s$

8.3 Appendix 03: Stiffness Calculation of the Square Arm



For the cantilever beam,

Maximum deflection of the beam can be written as:

$$y = \frac{Fl^3}{3EI} \quad (26)$$

Where:

F = Applied load at the free end

l = Length of the beam

E = Young modulus of Elasticity

I = Second moment of Inertia of the of the beam.

Second moment of Inertia I can be calculated from the equation:

$$I = \frac{bh^3}{12} \quad (27)$$

Where

b = breadth of the beam

h = height of the beam

As the beam is a hollow square section so we can calculate the 2nd moment of inertia of this section by subtracting the value of the inner box from the outer box:

$$I = I_1 - I_2 \quad (28)$$

$$I = \frac{b_1 h_1^3}{12} - \frac{b_2 h_2^3}{12} \quad (29)$$

Where,

$$b_1 = h_1 = 400 \text{ mm}$$

$$b_2 = h_2 = 360 \text{ mm}$$

Now inserting the value of I in the equation 29 we can find the maximum deflection y .

We know that for linear spring:

Applied for force on the spring,

$$F = ky \quad \text{or}$$

$$k = \frac{F}{y} \quad (30)$$

From this equation, we can find the stiffness of the spring. The spring constant K depends on the length and the cross-sectional area of the beam. If we increase the length, then the spring constant will decrease on the other hand if we increase the cross sectional area the stiffness will increase.

8.4 Appendix 04: Dynamic, explicit analysis (Stable time increment calculation)

We have used dynamic explicit step because, an explicit dynamic analysis,

- is computationally efficient for the analysis of large models with relatively short dynamic response times and for the analysis of extremely discontinuous events or processes;
- uses a consistent, large-deformation theory—models can undergo large rotations and large deformation;
- can use a geometrically linear deformation theory—strains and rotations are assumed to be small.
- can be used to perform quasi-static analyses with complicated contact conditions; and
- allows for either automatic or fixed time incrementation to be used—by default, Abaqus/Explicit uses automatic time incrementation with the global time estimator.

The explicit dynamics procedure performs a large number of small time increments efficiently. An explicit central-difference time integration rule is used; each increment is relatively inexpensive (compared to the direct-integration dynamic analysis procedure available in Abaqus/Standard) because there is no solution for a set of simultaneous equations. The explicit central-difference operator satisfies the dynamic equilibrium equations at the beginning of the increment, t ; the accelerations calculated at time t are used to advance the velocity solution to time $t + \Delta t/2$ and the displacement solution to time $t + \Delta t$

The explicit procedure integrates through time by using many small time increments. The central-difference operator is conditionally stable, and the stability limit for the operator (with no damping) is given in terms of the highest frequency of the system as

$$\Delta t \leq \frac{2}{\omega_{max}}.$$

With damping, the stable time increment is given by

$$\Delta t \leq \frac{2}{\omega_{max}}(\sqrt{1 + \xi_{max}^2} - \xi_{max}),$$

where ξ_{max} is the fraction of critical damping in the mode with the highest frequency

An approximation to the stability limit is often written as the smallest transit time of a dilatational wave across any of the elements in the mesh

$$\Delta t \approx \frac{L_{min}}{c_d},$$

where L_{min} is the smallest element dimension in the mesh and c_d is the dilatational wave speed in terms of λ_0 and μ_0 , defined below.

$$c_d = \sqrt{\frac{\hat{\lambda} + 2\hat{\mu}}{\rho}},$$

where ρ is the density of the material.

In an isotropic, elastic material the effective Lamé's constants can be defined in terms of Young's modulus, E , and Poisson's ratio, ν , by

$$\hat{\lambda} = \lambda_0 = \frac{E\nu}{(1 + \nu)(1 - 2\nu)}$$

and

$$\hat{\mu} = \mu_0 = \frac{E}{2(1 + \nu)}.$$

From the above equation we have calculated the minimum time incrementation:

Name	Symbol	Value
Dilation wave speed	c_d	4949.13
smallest element dimension	L_{min}	10
Density of the material	ρ	7850
Young's modulus	E	2E11
Poisson's ratio	ν	0.3
Lame's constant	μ	7.69E10
	λ_0	1.15E11
Minimum time incrementation	Δt	.00221 sec

Table 12: table for calculation minimum stable time incrementation.

The time increment used in an analysis must be smaller than the stability limit of the central-difference operator. Failure to use a small enough time increment will result in an unstable solution. When the solution becomes unstable, the time history response of solution variables such as displacements will usually oscillate with increasing amplitudes. The total energy balance will also change significantly. For that reason, we have chosen automatic time increment with a limit that maximum value can be lower than .001 second which much lower than the minimum value required as calculated in the above table. (From Abaqus theory manual)

8.5 Appendix 05: Coupling

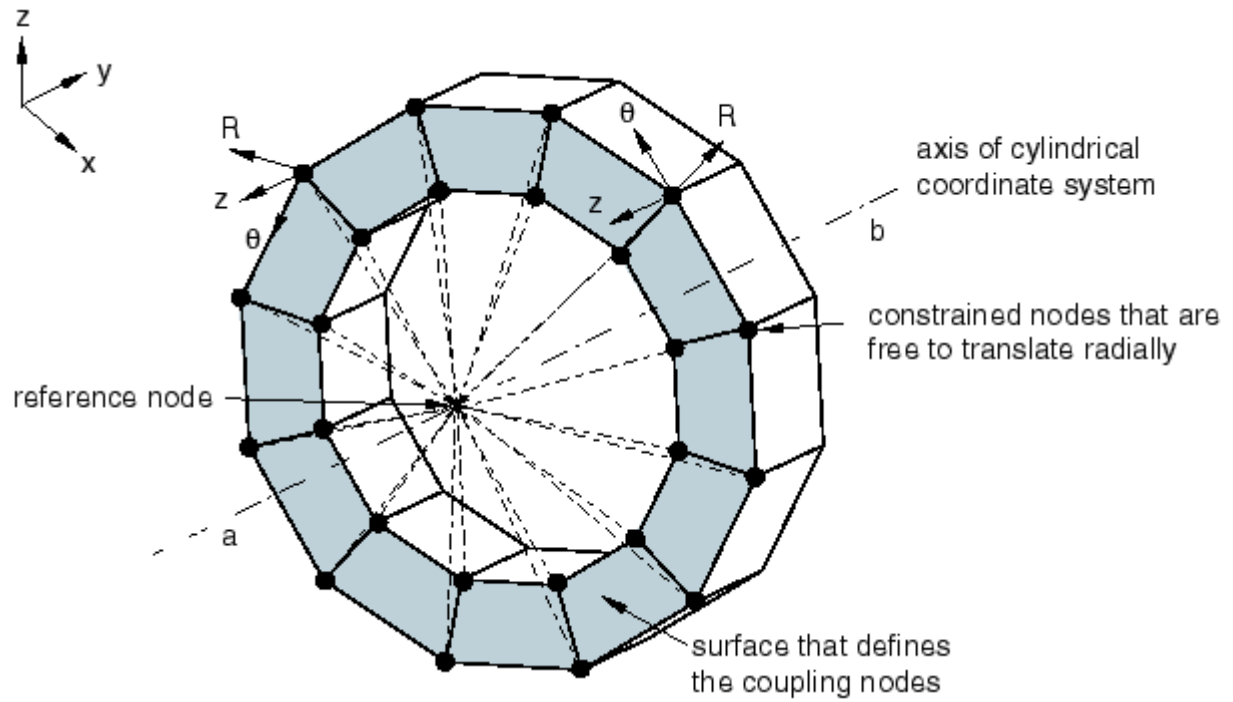


Figure 51: Kinematic coupling constraint.[19]

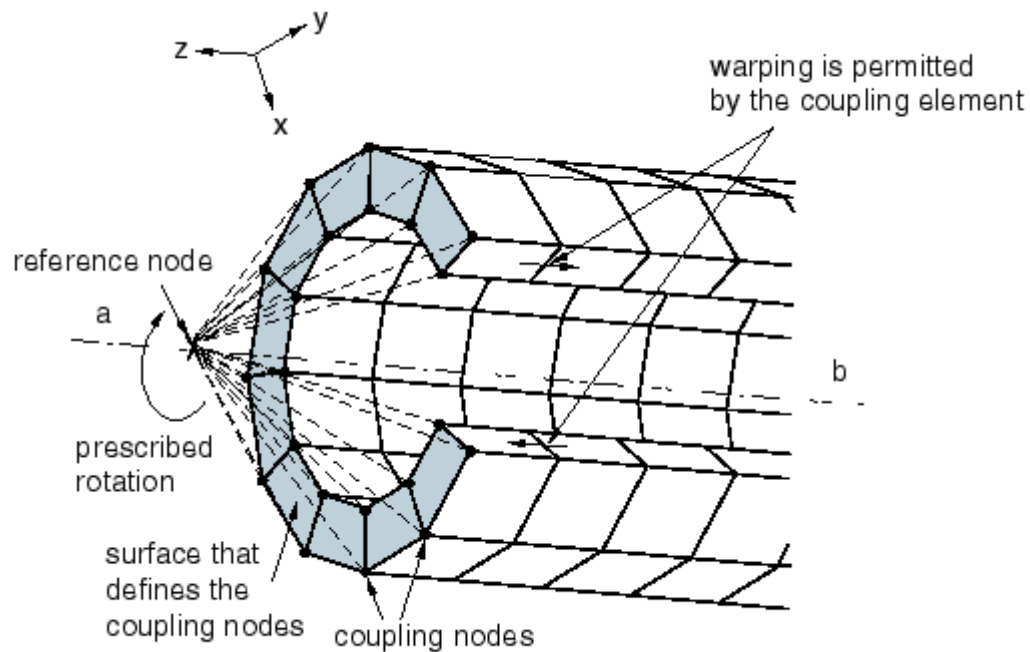


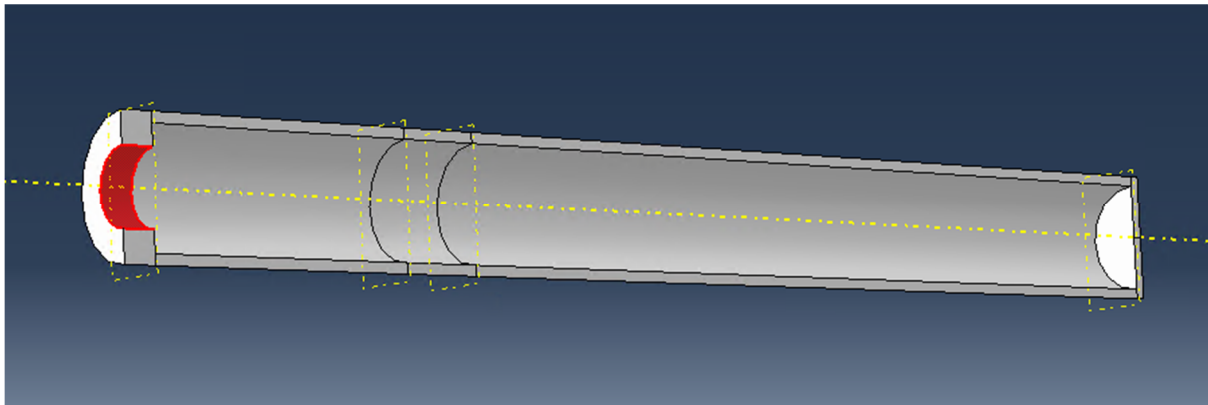
Figure 52: Distributing coupling constraint.[19]

Limitation of Distributed coupling (from Abaqus User's Manual):

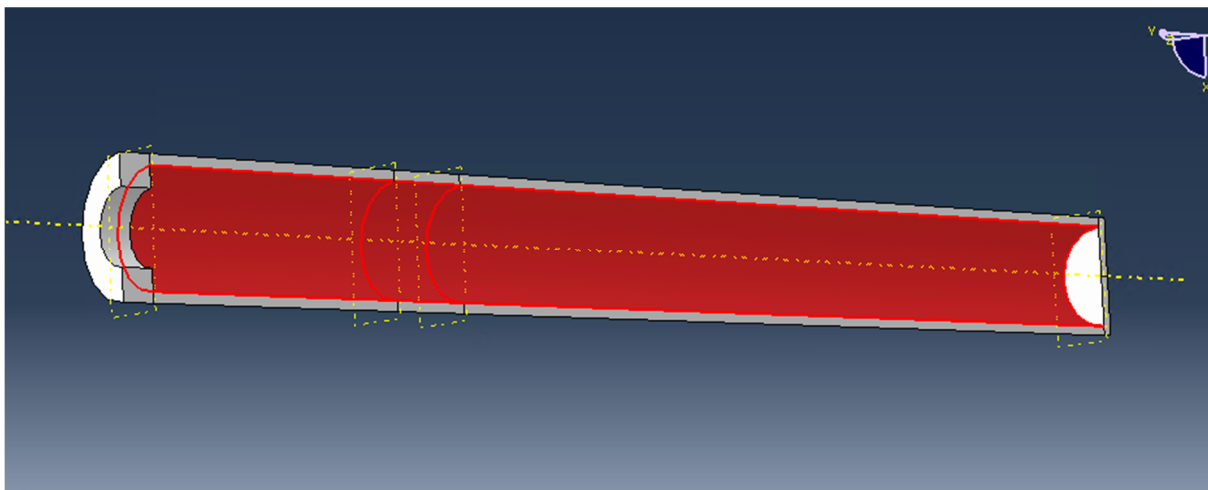
- A distributing coupling constraint cannot be used with axisymmetric elements with asymmetric deformation. This element type is not compatible with the distributing coupling constraint.
- If a distributing coupling constraint is used with axisymmetric elements with twist, the constraint will not include the twist degree of freedom 5 in those elements. It will involve only the displacement degrees of freedom 1 and 2.
- A distributing coupling definition with a large number of coupling nodes produces a large wave front in Abaqus/Standard. This may result in significant memory usage and a long solution time to solve the finite element equilibrium equations.
- A distributing coupling constraint cannot involve more than 46,000 degrees of freedom in Abaqus/Standard, which implies an upper limit of 23,000 nodes per constraint for two-dimensional and axisymmetric cases and an upper limit of 15,333 nodes per constraint for three-dimensional cases.

Though we have tried to run the analysis with distributed coupling but due to those above limitations we received a lot of error message so we have chosen Kinematic coupling instead of distributed coupling. For kinematic coupling, the system uses 6 degrees of freedom while for distributed coupling system use three degrees of freedom.

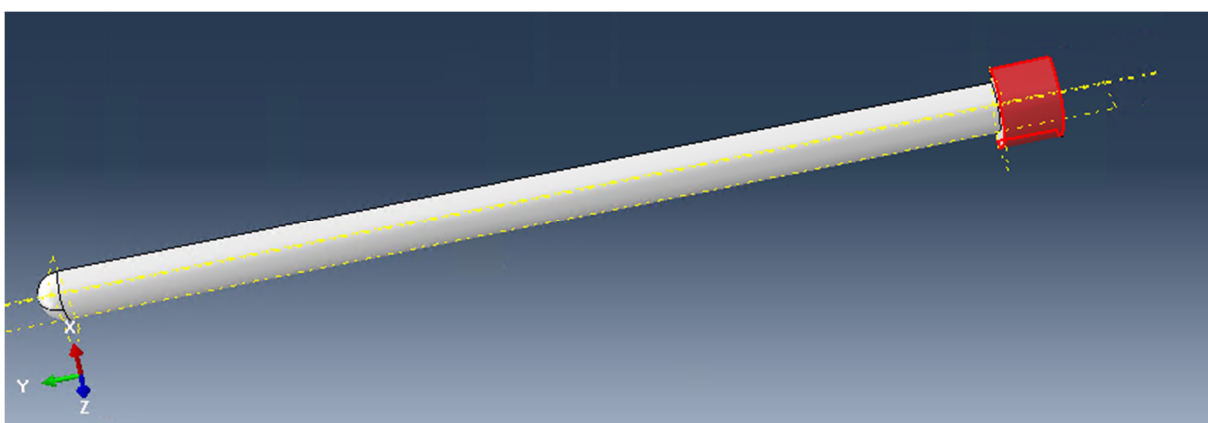
8.6 Appendix 06: Showcase of the Abaqus analysis



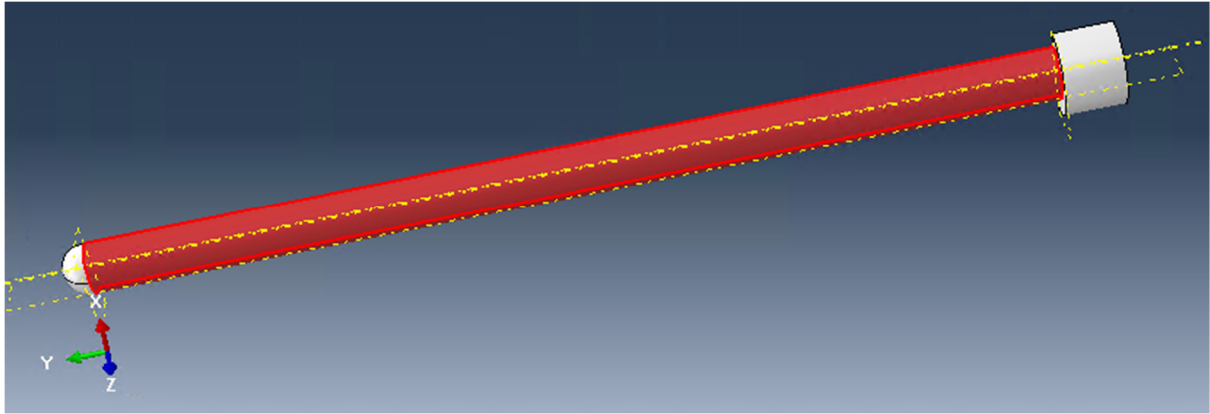
Cylinder neck plus piston rod



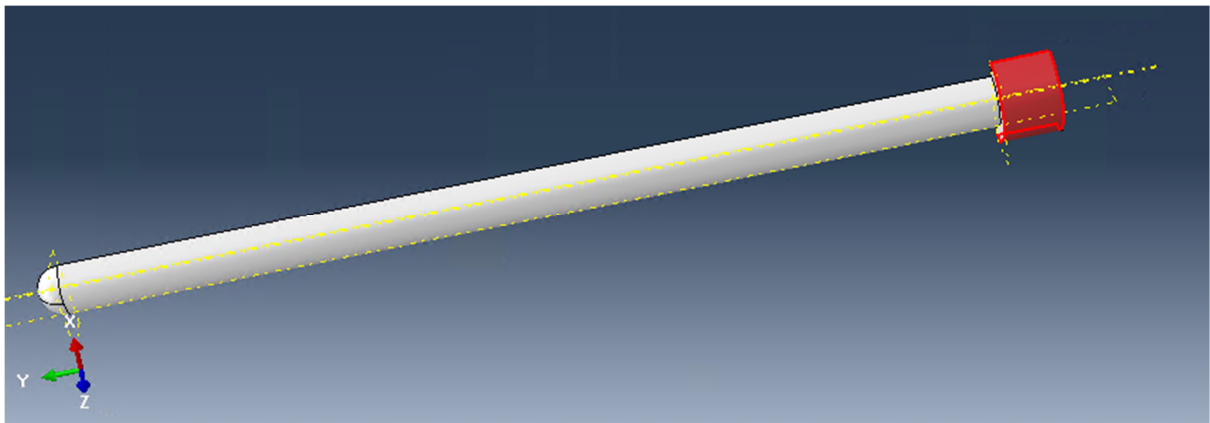
Cylinder plus piston head



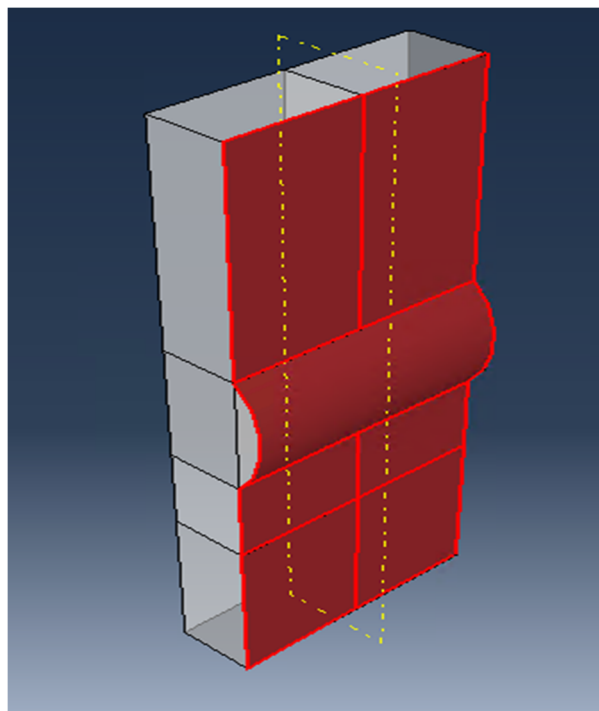
Piston head



Piston Rod



Piston head



MP

Figure 53: Contact surface

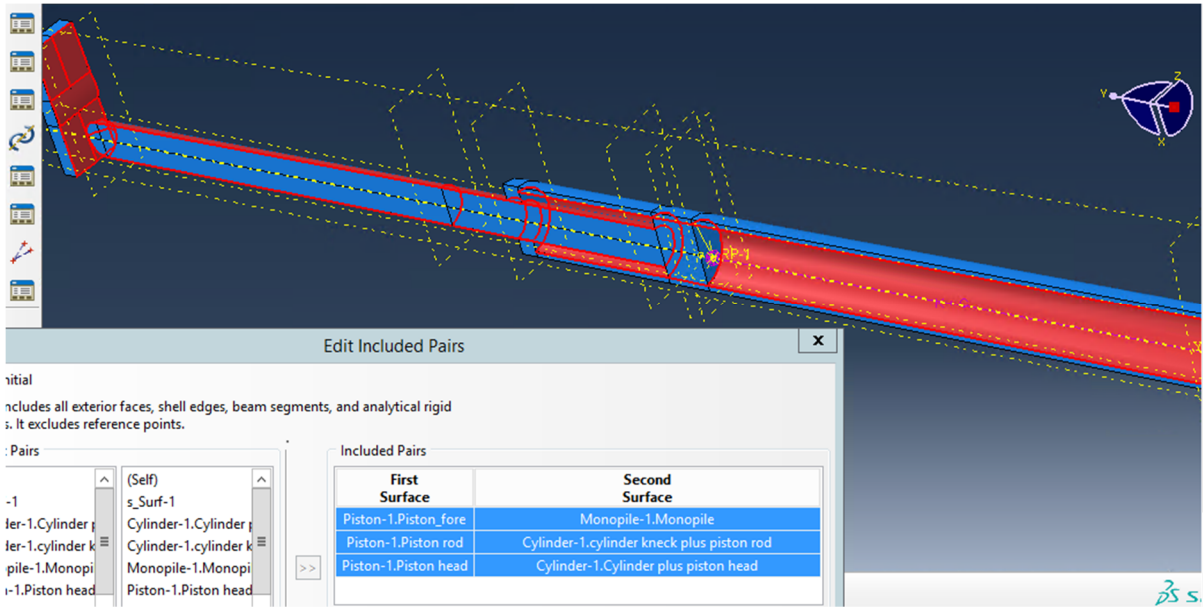
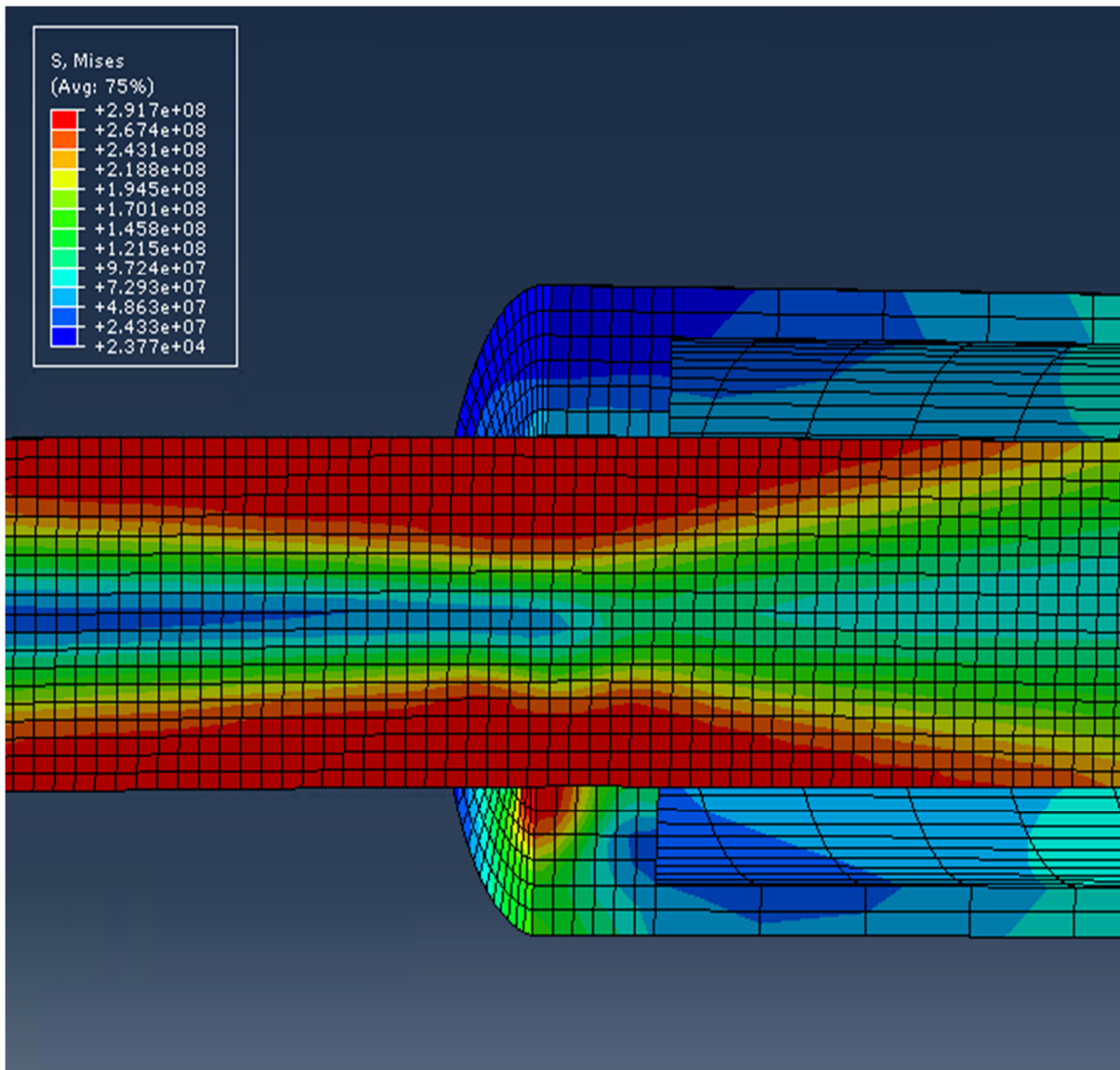


Figure 54:Interaction



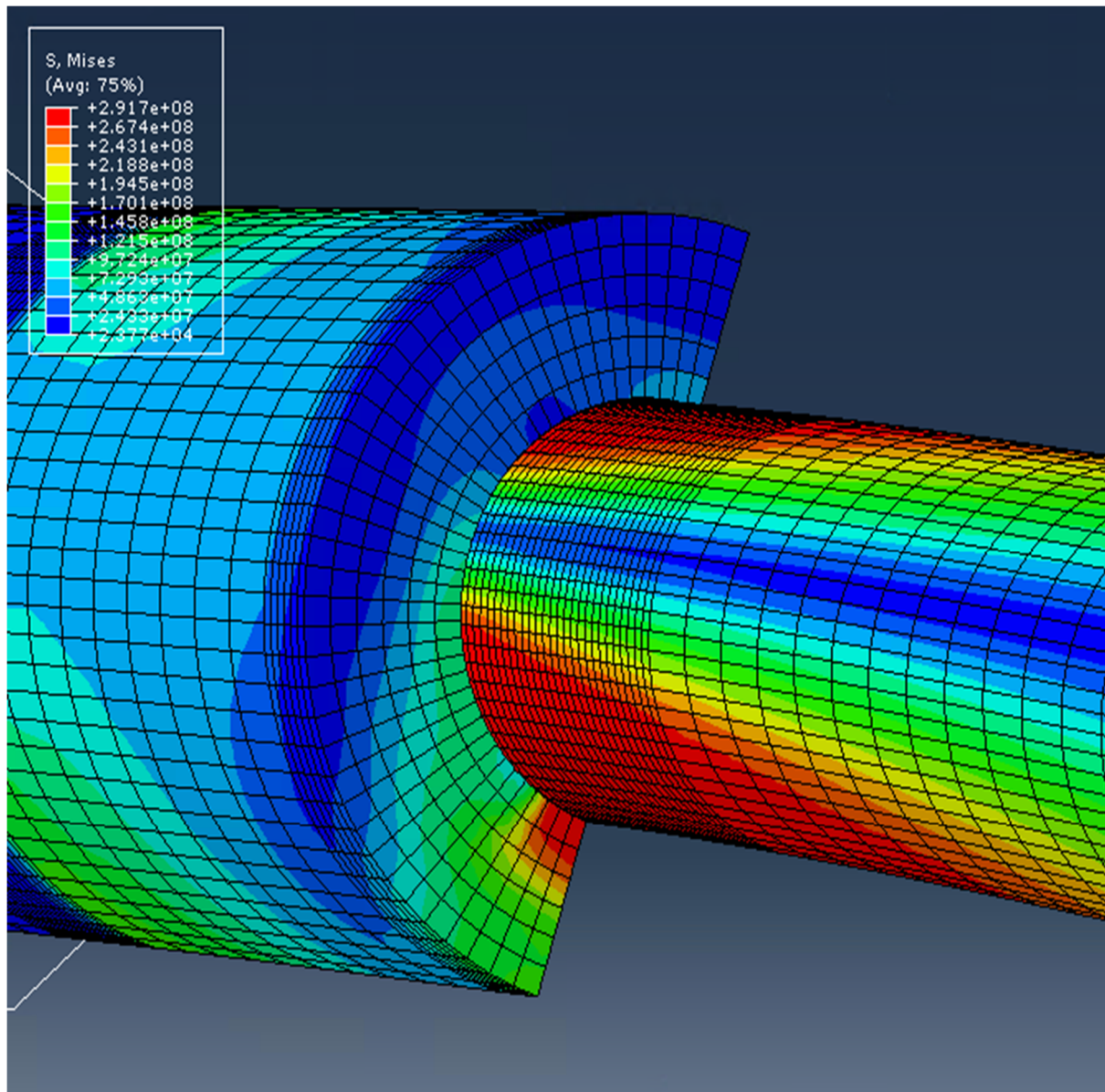


Figure 55: Stress at seal and Piston(roller size:70mm,roller BC at K1, capping 20 mm, speed 0.4 m/s)

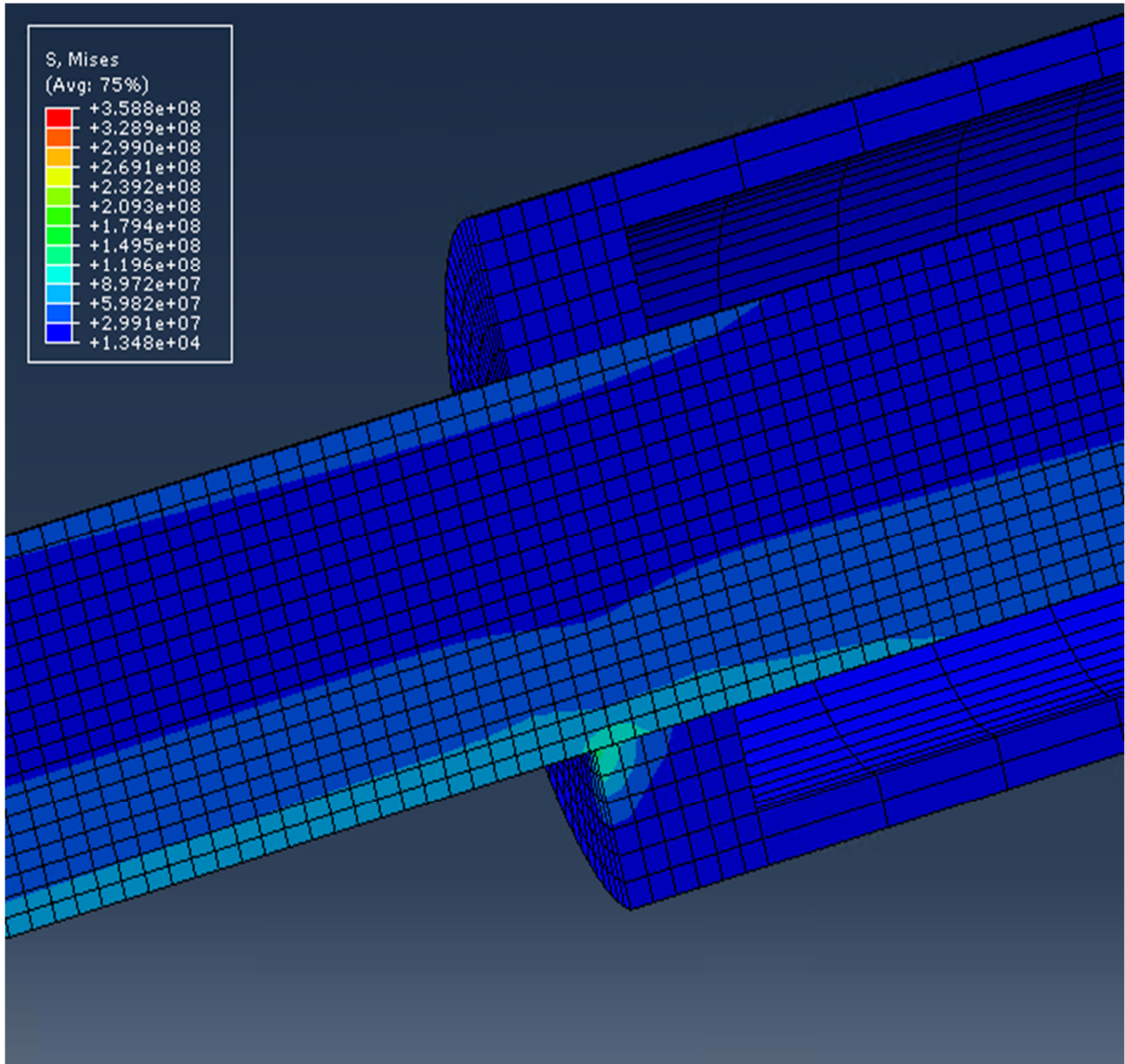


Figure 56: Stress at seal and Piston (roller size: 70mm, fixed BC at K1, capping 10 mm, speed 0.4 m/s)

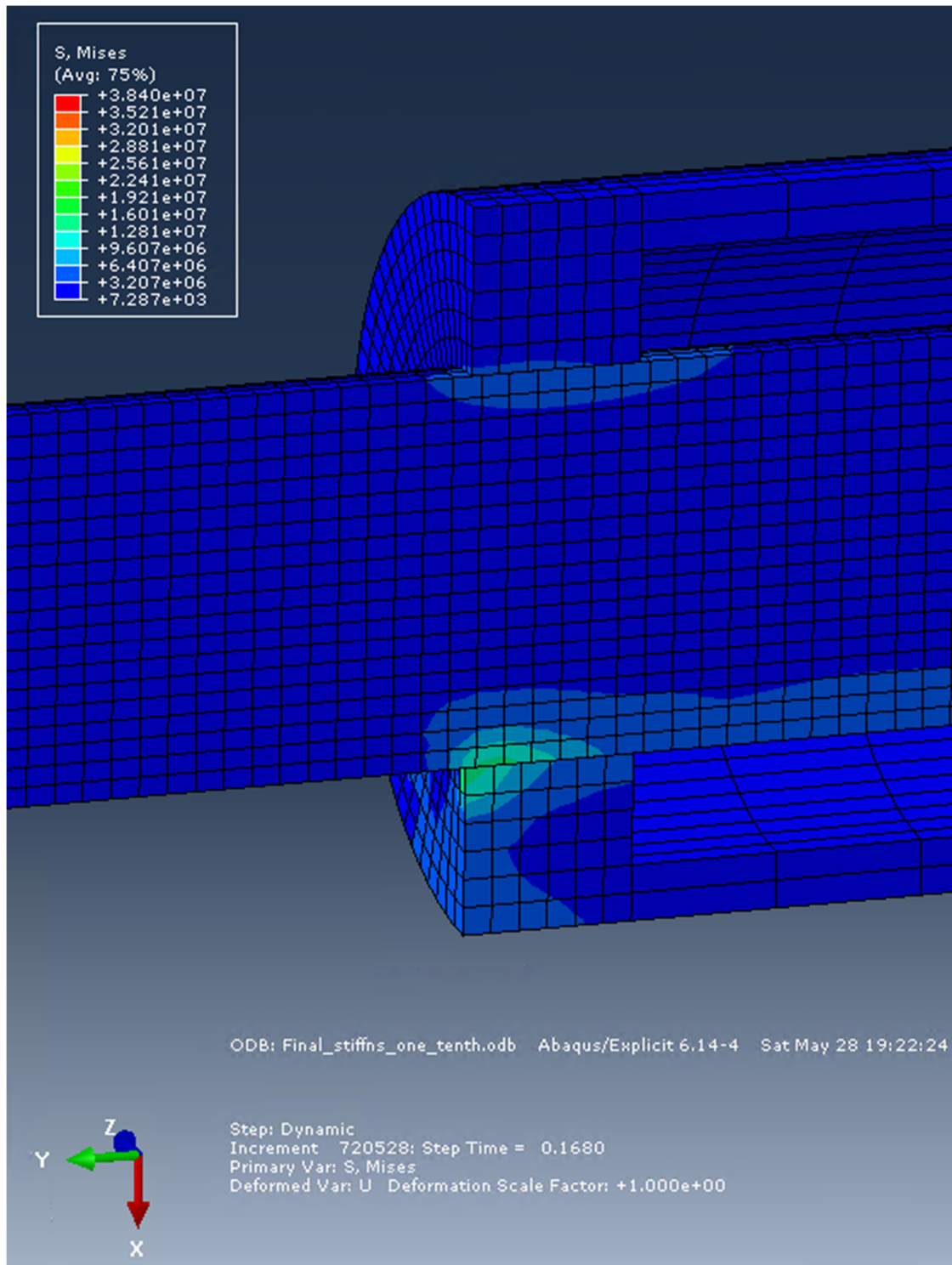
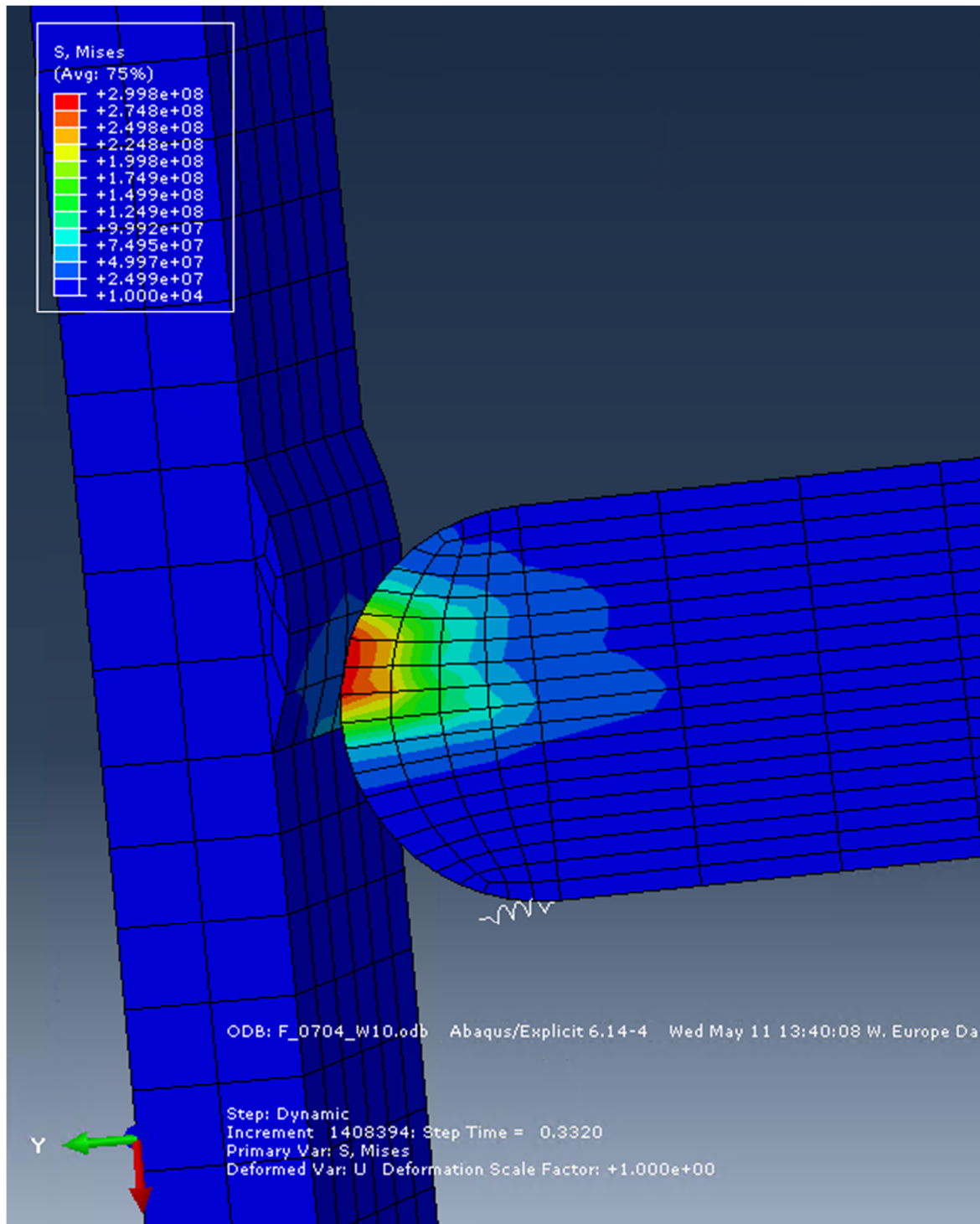
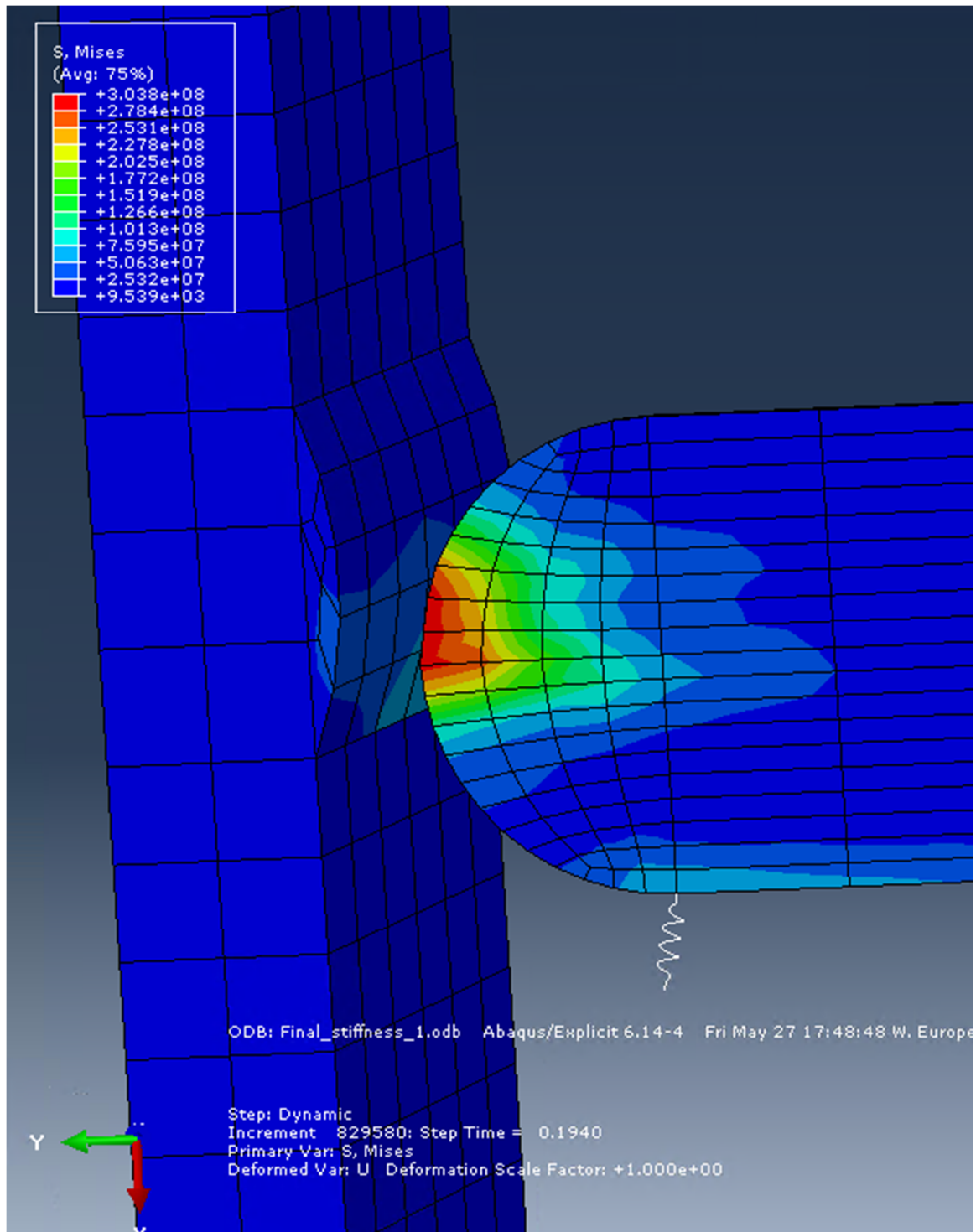


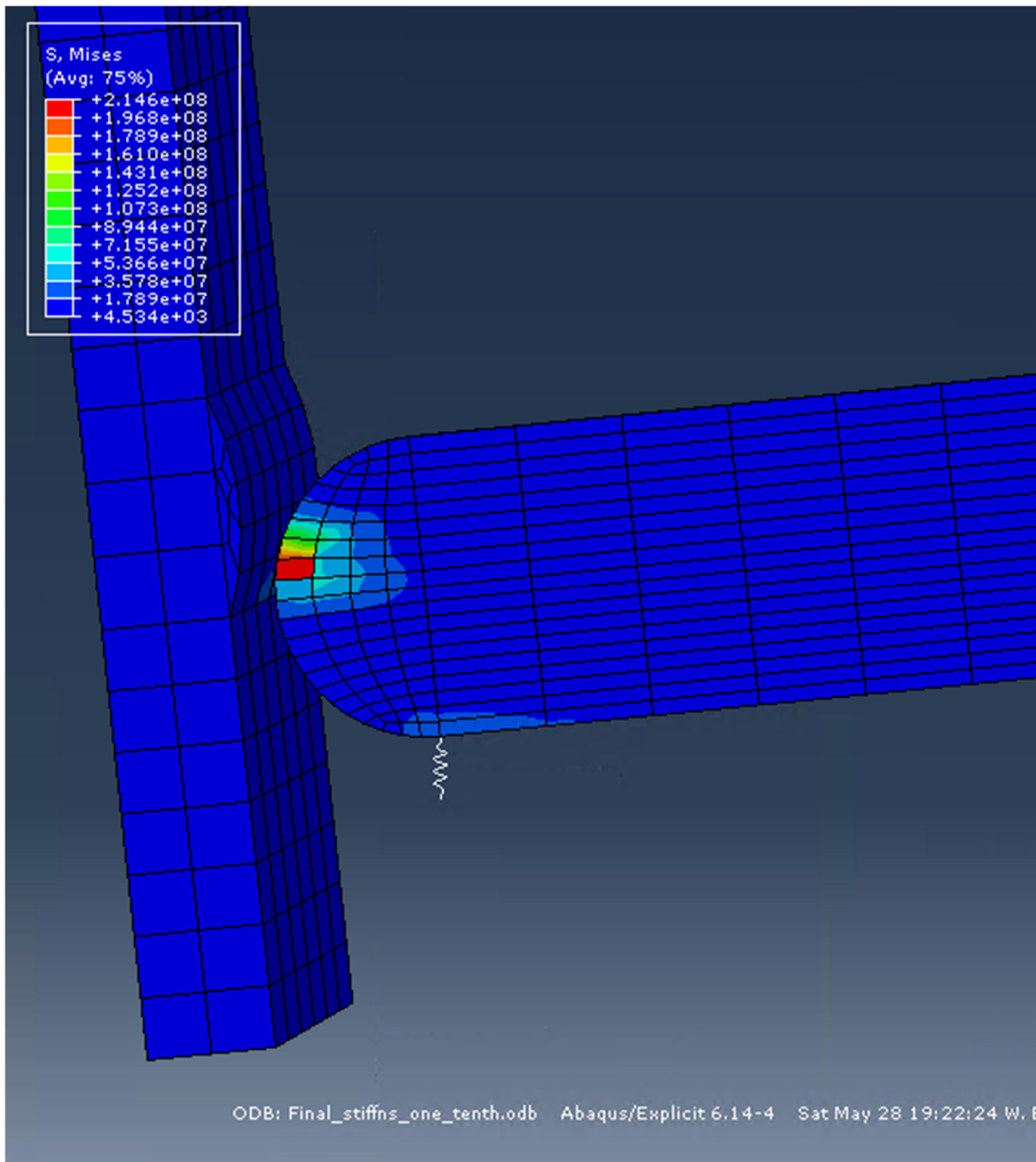
Figure 57: Stress at seal and Piston(roller size:70mm,roller BC at K1, capping 10 mm, speed 0.4 m/s, one tenth stiffness of K2)



Roller BC at K1



Fixed BC K1



Fixed BC at K1 combined with stiffness of K2 is one tenth of the initial

Figure 58: Stress at roller (roller size:70mm,Fixed BC at K1, capping 10 mm, speed 0.4 m/s)